NASA Technical Paper 3446

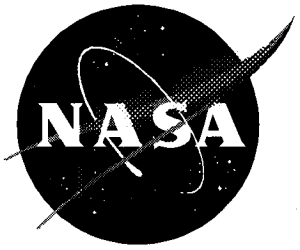


# High-Alpha Research Vehicle (HARV) Longitudinal Controller: Design, Analyses, and Simulation Results

*Aaron J. Ostroff*
*Langley Research Center • Hampton, Virginia*

*Keith D. Hoffler*
*ViGYAN, Inc. • Hampton, Virginia*

*Melissa S. Proffitt*
*Lockheed Engineering & Sciences Company • Hampton, Virginia*

National Aeronautics and Space Administration
Langley Research Center • Hampton, Virginia 23681-0001

July 1994

The use of trademarks or names of manufacturers in this report is for accurate reporting and does not constitute an official endorsement, either expressed or implied, of such products or manufacturers by the National Aeronautics and Space Administration.


## Acknowledgment

The authors wish to acknowledge the following individuals who made important contributions to the research described in this paper:

Philip W. Brown, Michael R. Phillips, and Robert A. Rivers, all from NASA Langley Research Center, who served as test pilots and provided ratings and insightful comments for the piloted simulation tasks.

Michael D. Messina, Lockheed Engineering & Sciences Company, Hampton, VA, who maintained the nonlinear batch simulation and organized test cases for transporting real-time code.

Susan W. Carzoo, Unisys Corporation, who maintained the real-time software for the piloted simulation.

Dr. Barton J. Bacon, NASA Langley Research Center, who constructed and tested the real-$\mu$ algorithms used for robustness analysis.

John V. Foster, NASA Langley Research Center, who performed some engineering-test pilot evaluations.

## Contents

## Summary

This paper describes the design, analysis, and nonlinear simulation results (batch and piloted) for a longitudinal controller scheduled to be flight-tested on the High-Alpha Research Vehicle (HARV). The HARV is an F-18 airplane modified for and equipped with multiaxis thrust vectoring. The longitudinal controller consists of feedback and feed-forward controllers. The paper includes a description of the facilities, a detailed review of the feedback controller design, linear analysis results of the feedback controller, a description of the feed-forward controller design, nonlinear batch simulation results, and piloted simulation results.

Linear analysis shows that the feedback controller meets the stability design guidelines, is highly robust to stability and control derivative parameter changes, has good closed-loop damping ratios, and attenuates the structural modes well below the design guideline.

Batch simulation results include maximum pitch stick agility responses, angle-of-attack $\alpha$ captures, and $\alpha$ regulation for full lateral stick rolls at several $\alpha$'s. The controller meets most of the agility guidelines throughout the $\alpha$ range, has good $\alpha$ regulation, and has consistently good transient response for all altitudes within the design region.

Piloted simulation results include task descriptions for several types of maneuvers, task guidelines, the corresponding Cooper-Harper ratings from three test pilots, and some pilot comments. The ratings show that *desirable* criteria were achieved for almost all of the piloted simulation tasks, most of which had very stringent criteria. The control system was shown to be extremely departure resistant.

## Introduction

Development of the short-to-medium range all-aspect missiles have increased the need for a fighter airplane to rapidly point its nose at an opponent to obtain first shot opportunity during air combat maneuvering. Rapid nose pointing is of particular importance within visual range. Even though long-range missiles are also continually improving, failures and rules of engagement will inevitably produce close-in encounters. During close-in air combat, the need to acquire a position in the opponent's rear quarter has diminished with the continual improvement of short-to-medium range all-aspect missiles. Due to the enhanced capability of these missiles, a great deal of research has gone into developing high-performance airplanes that can rapidly maneuver at angles of attack $\alpha$ greater than the maximum lift, which generates very high nose-turning rates. Simulation studies have shown that operational capability and good controllability in this high-$\alpha$ flight regime provide tactical maneuver advantages during close-in air combat (refs. 1–4) with current missiles and guns. The success in simulated air combat studies have lead to research airplanes that have the capability to maneuver at poststall angles of attack.

In recent years, four high-$\alpha$ flight test airplanes (i.e., X-29, X-31, the High-Alpha Research Vehicle (HARV), and the F-16 Multi-Axis Thrust Vectoring (MATV)) have been maneuvering successfully at poststall angles of attack which was not previously achievable. (See ref. 5.) The X-29 airplane can maintain controlled flight up to $\alpha = 40°$; the X-31 airplane and HARV are designed to maneuver at $\alpha$'s up to 70° with the application of multiaxis thrust vectoring. The F-16 MATV airplane has done sustained maneuvers up to $\alpha = 84°$ with excursions beyond that. Thrust-vectored controls provide the X-31, HARV, and F-16 MATV with the added control power required to maneuver in the high-$\alpha$ flight regime which is not achievable with purely aerodynamic controls.

The HARV is a modified F-18 airplane that began flight evaluation in midyear 1991. The main modification is the addition of thrust-vectored controls in the pitch and yaw axes, which resulted in an airplane that is approximately 4000 lb heavier than an unmodified F-18 airplane. The original thrust-vectored control laws were developed jointly by NASA and McDonnell Aircraft Company and are being used during the initial HARV flight evaluations that include flight envelope expansion and maneuvering capability. Revised controllers based upon modern control design methodologies and processes (ref. 6) will then be installed on the HARV after the initial flights are completed. One of these revised controllers is the longitudinal controller described in this paper.

For completeness, much of the information in reference 7 which pertains to the longitudinal controller design is also contained in this paper. In particular, reference 7 contains the following:

1. An overview of the feedback controller with the application of variable-gain output feedback which generates a feedback gain functional that incorporates optimal gain scheduling
2. A derivation and description of the feed-forward command generator (FFCG) for pilot stick sensitivity and mode selection
3. Formulation of the command generator tracker (CGT), which is a feed-forward control
4. Control system design guidelines

5. Some linear analysis and nonlinear batch simulation analysis

A key part of reference 7 is the design procedure for selection and adjustment of the optimal weights used in the variable-gain output feedback design algorithm. Note that the variable-gain methodology (refs. 7–10) used in the feedback design is an integrated approach for the simultaneous design of the many operating conditions within the flight regime.

This paper contains a detailed description of the longitudinal controller design, analyses, and nonlinear simulation (batch and piloted) results. The longitudinal controller is comprised of a feedback controller and a feed-forward controller. The feedback controller design section includes a description of the modeling and optimal weighting formulation as well as tables of all design weights. The feedback controller is the same design as that described in reference 7 but more specific information is presented in this paper.

Linear analysis results for the feedback controller design are described in another section of this paper. Results for 39 design conditions are shown when practical; however, three example cases (i.e., low-$\alpha$ high-Mach, medium-$\alpha$, and high-$\alpha$) are selected to show results for those analyses that require an extensive amount of data or plots. Linear analysis results include closed-loop eigenvalues, stability margins, robustness to changes in various parameters, and the loop transfer function for a combination rigid-body and servoelastic frequency response. Tables are included to show all variable-gain feedback components and final gains for the three example cases.

The FFCG configuration described in reference 7 has been modified. Key equations for the two command modes of $\alpha$ and load factor have not changed but the implementation is revised to eliminate problems with mode transition. The main implementation change relates to the $\alpha$-trim bias. The modifications, the key equations as derived in reference 7, and implementation are described. A major change is in the CGT, which was described as part of the feedback controller in reference 7. The CGT gain was too sensitive at several flight conditions and variable limits had to be incorporated. The new configuration is described and shown in this paper.

Results for both six-degrees-of-freedom nonlinear batch and piloted simulations are included in this paper. Batch simulation includes selected agility responses for comparison with design guidelines (ref. 11) as well as several capture and regulation maneuvers to illustrate performance capability. The piloted simulation section includes task scenarios, task guidelines, and Cooper-Harper ratings (CHR) for the various maneuvers. Piloted tasks were developed to evaluate the longitudinal control law acquisition capability, tracking capability, and resistance to coupling (regulation of $\alpha$ during rolling maneuvers). Cooper-Harper ratings and pilot comments are given for the version of the control law to be flight tested. Some of the problems encountered with earlier versions during piloted simulations are discussed.

## Symbols

In the following list of symbols, matrices and vectors are shown in boldface; scalars are shown in italics.

| | |
|---|---|
| $\mathbf{A}$ | continuous state matrix |
| $\mathbf{A}_m$ | discrete weighting matrix for cross product of states and controls |
| $\mathbf{A}_p$ | continuous plant state matrix |
| $\mathbf{B}$ | continuous control matrix |
| $\mathbf{B}_p$ | continuous plant control matrix |
| $\mathbf{B}_w$ | continuous plant process noise disturbance matrix |
| $\overline{\mathbf{B}}$ | continuous process noise disturbance matrix |
| $\mathbf{C}$ | plant and controller state to output matrix |
| $C_i$ | steady-state-normalized coefficients, $i = 1$, 2, or 3 |
| $\mathbf{C}_p$ | plant state to output matrix |
| $C_1, C_2, C_3$ | steady-state-normalized coefficients for $\alpha$, $q$, and $n_z$, respectively |
| $\mathbf{D}$ | plant control to output matrix |
| $E$ | expectation operator |
| $E1$ | command-generator-tracker feedforward gain |
| $e$ | exponential function |
| $f$ | scalar weighting for cost function |
| $g$ | gravity, ft/sec$^2$ |
| $\mathbf{H}_{zx}$ | matrix relating plant states to integrator states |
| $\mathbf{H}_{zy}$ | matrix relating measurements to integrator states |
| $\mathbf{I}_u, \mathbf{I}_z$ | identity matrices of appropriate dimension |

| | |
|---|---|
| $I_{xx}, I_{yy}, I_{zz}$ | moments of inertia about the $X$-, $Y$-, and $Z$-axes, respectively, slug-ft$^2$ |
| $I_{xz}$ | product of inertia in $xz$ frame, slug-ft$^2$ |
| $J$ | global cost |
| $J_c$ | continuous local cost |
| $\overline{J}_d$ | discrete local cost |
| $\mathbf{K}$ | feedback-gain matrix |
| $K_{n_z}$ | proportional feedback gain for $n_z$, (deg/sec)/$g$ |
| $K_q$ | proportional feedback gain for $q$ |
| $K_u$ | control filter feedback gain, sec$^{-1}$ |
| $\mathbf{K}_y$ | proportional feedback-gain matrix |
| $K_z$ | integrator feedback gain |
| $K_\alpha$ | proportional feedback gain for $\alpha$, sec$^{-1}$ |
| $\mathbf{K}_0, \mathbf{K}_i$ | variable-gain feedback matrix partitions |
| $k$ | sample time integer |
| $M$ | number of operating conditions |
| $N$ | integer for series summation |
| $n_z$ | load factor, $g$ units |
| $n_{z,c}$ | load factor command, $g$ units |
| $p$ | body-axis roll rate |
| $P_s$ | static pressure, lb/ft$^2$ |
| $\mathbf{p}$ | gain-schedule parameter |
| $\mathbf{Q}$ | discrete state-weighting matrix |
| $\overline{\mathbf{Q}}$ | continuous output-weighting matrix |
| $Q_c$ | impact pressure, lb/ft$^2$ |
| $Q_{n_z}$ | continuous weight for $n_z$ |
| $Q_q$ | continuous weight for $q$ |
| $Q_u$ | continuous weight for control filter |
| $\mathbf{Q}_y$ | continuous-weighting matrix for outputs |
| $Q_z$ | continuous weight for integrator |
| $Q_\alpha$ | continuous weight for $\alpha$ |
| $q$ | pitch rate, deg/sec |
| $\dot{q}$ | pitch acceleration, deg/sec$^2$ |
| $R$ | discrete weight for control |
| $R_v$ | continuous weight for control |
| $r$ | body-axis yaw rate |
| $s$ | Laplace transform variable |
| $t$ | time, sec |
| $u_p$ | plant control input vector |
| $V$ | total airspeed, ft/sec |
| $\overline{\mathbf{V}}$ | covariance matrix for sensor noise |
| $V_0$ | covariance for control input pseudonoise |
| $v_c$ | rate command, deg/sec |
| $\overline{\mathbf{v}}$ | sensor noise vector |
| $v_0$ | control input pseudonoise |
| $\overline{\mathbf{W}}$ | total process noise covariance matrix |
| $\mathbf{W}_0$ | covariance matrix for external disturbance |
| $\overline{\mathbf{w}}$ | process noise vector |
| $\mathbf{w}_p$ | plant process noise vector |
| $\mathbf{w}_0$ | external disturbance noise vector |
| $X_{\text{acc}}$ | distance along $X$-axis from c.g. to accelerometer |
| $\mathbf{X}_0$ | state covariance matrix for initial condition error |
| $\mathbf{x}$ | plant and controller state vector |
| $\dot{\mathbf{x}}$ | time derivative of $\mathbf{x}$ |
| $\mathbf{x}_a$ | actuator state vector |
| $x_{\text{cg}}$ | c.g. location along the $X$-axis, percent of mean aerodynamic chord |
| $\mathbf{x}_m$ | longitudinal state vector |
| $\mathbf{x}_p$ | plant state vector |
| $\dot{\mathbf{x}}_p$ | first derivative of plant state vector |
| $x_q$ | pitch rate state |
| $\mathbf{x}_s$ | sensor state vector |
| $x_u$ | control position state |
| $\dot{x}_u$ | derivative of control position state |
| $x_v$ | airspeed state |
| $x_w$ | washout filter state |
| $x_z$ | integrator state |

| | |
|---|---|
| $\dot{x}_z$ | time derivative of $x_z$ |
| $x_\alpha$ | angle-of-attack state |
| $x_\theta$ | pitch attitude state |
| $\mathbf{x}_0$ | state vector for initial condition errors |
| $\mathbf{y}$ | plant and controller output vector |
| $y_{\text{cmd}}$ | command from feed-forward command generator |
| $y_{n_z}$ | output for load factor |
| $\mathbf{y}_p$ | plant output vector |
| $y_q$ | output for pitch rate |
| $y_u$ | output for controller position command state |
| $y_z$ | output for integrator state |
| $y_\alpha$ | output for angle of attack |
| $z$ | $z$-transform variable |
| $z_{\text{cg}}$ | c.g. location along $Z$-axis, relative to waterline (WL) |
| $\alpha$ | angle of attack, deg |
| $\dot{\alpha}$ | time derivative angle of attack, deg/sec |
| $\alpha_c$ | angle-of-attack command, deg |
| $\alpha_{\text{oc}}$ | angle-of-attack command trim, deg |
| $\alpha_{\text{oc},1g}$ | angle-of-attack command trim for $1g$, deg |
| $\beta$ | sideslip angle, rad |
| $\mathbf{\Gamma}$ | discrete plant and controller control matrix |
| $\mathbf{\Gamma}_p$ | discrete plant control matrix |
| $\mathbf{\Gamma}_w$ | discrete plant and controller process noise matrix |
| $\gamma_w$ | discrete plant process noise |
| $\Delta n_{z,c}$ | perturbation in $n_{z,c}$, $g$ units |
| $\Delta T$ | sampling period, 0.0125 sec |
| $\Delta\alpha_{\text{oc}}$ | incremental bias trim command |
| $\delta_s$ | metric stabilator control, deg |
| $\delta_v$ | pitch thrust vector control, deg |
| $\delta_{ij}$ | Kronecker delta |
| $\delta_{sc}$ | stabilator command, deg |
| $\delta_{sp}$ | pilot stick command, in. |
| $\delta_{vc}$ | pitch thrust-vectoring command, deg |
| $\overline{\boldsymbol{\eta}}$ | plant and controller measurement noise vector |
| $\boldsymbol{\eta}_p$ | plant measurement noise vector |
| $\theta$ | pitch attitude, deg |
| $\mu$ | structured singular value |
| $\boldsymbol{\nu}$ | measured variables used to calculate $\mathbf{p}$ |
| $\mathbf{\Phi}$ | discrete plant and controller state transition matrix |
| $\phi$ | bank angle, deg |
| $\mathbf{\Phi}_p$ | discrete plant state transition matrix |

Subscripts:

| | |
|---|---|
| $c$ | controller or command |
| $i, j$ | series integers |
| $k$ | coefficient for sampling sequence |
| $p$ | plant |

Superscripts:

| | |
|---|---|
| $T$ | transpose |
| $-1$ | inverse |

Special notation:

| | |
|---|---|
| $X(\dots)$ | arguments of variable $X$ |

Abbreviations:

| | |
|---|---|
| A/B | afterburner (maximum thrust) |
| CGI | computer-generated image |
| CGT | command generator tracker |
| CHR | Cooper-Harper rating |
| c.g. | center of gravity |
| DMS | Differential Maneuvering Simulator |
| FFCG | feed-forward command generator |
| HARV | High-Alpha Research Vehicle |
| HUD | heads-up display |
| KCAS | knots, calibrated airspeed |
| PIF | proportional integral filter |
| PIO | pilot-induced oscillation |
| RFCS | Research Flight Control System |

## Description of Facilities

### Airplane

The configuration used for this control law design is an F-18 airplane modified to have multiaxis thrust vectoring for additional pitch and yaw control power. The basic F-18 airplane is a multirole fighter-attack airplane with supersonic dash capability and, by current standards, good low-speed, high-$\alpha$ maneuverability. Thrust-vectoring capability was achieved by removing the secondary (divergent) nozzles and adding three thrust-vectoring vanes per engine. Major dimensions and key features of the F-18 airplane with thrust vectoring are shown in figure 1. The modified airplane, known as the High-Alpha Research Vehicle (HARV), is discussed in reference 12, and is shown in figure 2.

The simulation normally used HARV weight and inertias corresponding to 60-percent internal fuel. Heavy (maximum fuel) and light (minimum landing fuel) configurations were also tested; however, only results from the nominal (60-percent internal fuel) configuration are given in this report. Weights, inertias, and center-of-gravity (c.g.) locations for all configurations are shown in table I.

### Simulation

The HARV simulation was built from the production F-18 airplane nonlinear aerodynamic, engine, and control system models obtained from McDonnell Aircraft Company (McAir). The F-18 airplane simulation on which the HARV model is based is discussed in detail in reference 13. The HARV thrust-vectoring capabilities are discussed in reference 14. The original McAir aerodynamic database covers the $\alpha$ range from $-10°$ to $90°$, the sideslip angle $\beta$ range from $-20°$ to $20°$, altitudes up to 60 000 ft, and speeds up to Mach 2.0. The F-18 airplane simulation was modified to account for the thrust-vectored engine and its effect on the configuration aerodynamics.

The HARV engine model (obtained from McAir who also designed the thrust-vectoring hardware for the airplane) incorporated thrust-vectoring capability, accounted for the effects of Mach number and altitude, and included the dynamic response of engine thrust. The effects of $\alpha$ and vane deflection on thrust were also included. Gross thrust and ram drag were tabulated separately allowing thrust vectoring to affect gross thrust only. The effect of $\alpha$ on engine thrust was obtained with a General Electric engine simulation having a high level of fidelity and the inlet rake survey data from F-18 airplane flight tests. Effects of vane deflection on gross thrust and jet deflection were obtained from ground-based tests. (See ref. 14.)

Aerodynamic increments were added to the database to account for the addition of thrust-vectoring vanes, actuator housings, and spin chute. Jet-induced effects were added to account for the change in airflow over the airframe due to thrust vectoring. This data was obtained from wind tunnel tests described in reference 15.

A Research Flight Control System (RFCS), which consisted of a new lateral-directional control law and the longitudinal control law discussed herein, replaced the existing F-18 airplane control system. The thrust-vectored commands from the RFCS go to a vane control system known as the mixer-predictor. The mixer-predictor converts pitch, yaw, and roll thrust-vectoring commands into commands for the six thrust-vectoring vanes to yield the required jet deflection.

### Piloted Simulator

The piloted simulation portion of the control law design process was conducted with the math model described above in the NASA Langley Differential Maneuvering Simulator (DMS). The DMS is a fixed-base simulator that has the capability of simulating two airplanes as they maneuver relative to each other and the Earth. A wide-angle visual display is provided for each pilot. As illustrated in figure 3, the DMS consists of two 40-ft-diameter projection spheres each enclosing a cockpit, airplane image projection system, and computer-generated image (CGI) sky-Earth-Sun projection system. Each pilot is provided with a projected image of the opposing airplane, which gives range, position, and orientation cues. Reference 16 contains a detailed, although not current, description of the DMS.

The DMS is driven by a real-time digital simulation system built around a CONVEX 3800-series computer[1]. The dynamics of the airplane and control system were calculated using six-degrees-of-freedom rigid-body equations of motion with an 80-Hz frame rate. Input and output to and from the computer, the cockpit, and the displays had a 40-Hz frame rate. Overall transport delay of the system is around 110 msec.

A photograph of a cockpit and target visual display is shown in figure 4. Each cockpit incorporates

[1]Convex Computer Corp., Richardson, TX.

three CRT heads-down displays and a heads-up display (HUD) with a computer-driven gunsight representative of current fighter aircraft equipment. For this study, a fixed reticle projected on the heads-up display was used for tracking. The simulator displays are similar to F-18 airplane displays with some minor modifications to facilitate some of the maneuvers and the tracking tasks.

A movable center stick was provided for pitch and roll commands from the pilot. Longitudinal stick forces and gradients were configured to model those of the F-18 airplane. Longitudinal stick travel was 2.5 in. forward and 5.0 in. aft with a force gradient of 7 lb/in. and a breakout force of 2 lb.

## Feedback Controller Design

This section contains the mathematical equations of the HARV feedback control design. The argument $\mathbf{p}$ shown in the equations represents one or more of the parameters that change during flight. Optimal gain-scheduling is accomplished through the argument $\mathbf{p}$.

For all equations within this report, matrices and vectors are shown in boldface. In the specific design example where a matrix or vector is used as a scalar, the symbol will be shown in italics. Equations presented in reference 7 are general; however, the equations presented in this paper are related to the specific controller and, therefore, some of the symbols will be shown as scalars.

### Modeling

***Continuous model.*** The dynamic process for the plant is represented by

$$\left.\begin{aligned}\dot{\mathbf{x}}_p(\mathbf{p}) &= \mathbf{A}_p(\mathbf{p})\mathbf{x}_p(\mathbf{p}) + \mathbf{B}_p(\mathbf{p})u_p(\mathbf{p}) + \mathbf{B}_w(\mathbf{p})\mathbf{w}_p(\mathbf{p}) \\ \mathbf{y}_p(\mathbf{p}) &= \mathbf{C}_p(\mathbf{p})\mathbf{x}_p(\mathbf{p}) + \boldsymbol{\eta}_p(\mathbf{p})\end{aligned}\right\} \quad (1)$$

in which $\mathbf{x}_p$ and $\mathbf{y}_p$ are the plant state and output vectors; $u_p$ is the scalar plant control; $\mathbf{w}_p$ and $\boldsymbol{\eta}_p$ are plant process and measurement noise vectors; $\mathbf{A}_p$, $\mathbf{B}_p$, and $\mathbf{C}_p$ are the plant state, control, and output matrices, respectively; and $\mathbf{B}_w$ is the plant process noise disturbance matrix. Each noise process is assumed to be white with zero mean; the processes are uncorrelated with each other.

Controller dynamics are also described by state equations

$$\dot{x}_u(\mathbf{p}) = v_c(\mathbf{p}) \quad (2)$$

$$\dot{x}_z(\mathbf{p}) = \mathbf{H}_{zy}(\mathbf{p})\mathbf{y}_p(\mathbf{p}) = \mathbf{H}_{zx}(\mathbf{p})\mathbf{x}_p(\mathbf{p}) + \mathbf{H}_{zy}(\mathbf{p})\boldsymbol{\eta}_p(\mathbf{p}) \quad (3)$$

where $v_c$ is the rate command (control feedback point), $x_u$ is the control position state, $x_z$ is the integrator state, and $\mathbf{H}_{zy}$ and $\mathbf{H}_{zx}$ are matrices that select the feedback measurements and their equivalent states to be integrated. Because there is a single control, only one integrator state is used.

The combination of plant and controller dynamics gives the following general equation

$$\left.\begin{aligned}\dot{\mathbf{x}}(\mathbf{p}) &= \mathbf{A}(\mathbf{p})\mathbf{x}(\mathbf{p}) + \mathbf{B}(\mathbf{p})u(\mathbf{p}) + \overline{\mathbf{B}}(\mathbf{p})\overline{\mathbf{w}}(\mathbf{p}) \\ \mathbf{y}(\mathbf{p}) &= \mathbf{C}(\mathbf{p})\mathbf{x}(\mathbf{p}) + \overline{\boldsymbol{\eta}}(\mathbf{p})\end{aligned}\right\} \quad (4)$$

which can be expanded as

$$\begin{Bmatrix}\dot{\mathbf{x}}_p(\mathbf{p}) \\ \dot{x}_u(\mathbf{p}) \\ \dot{x}_z(\mathbf{p})\end{Bmatrix} = \begin{bmatrix}\mathbf{A}_p(\mathbf{p}) & \mathbf{B}_p(\mathbf{p}) & \mathbf{0} \\ \mathbf{0} & 0 & 0 \\ \mathbf{H}_{zx}(\mathbf{p}) & 0 & 0\end{bmatrix}\begin{Bmatrix}\mathbf{x}_p(\mathbf{p}) \\ x_u(\mathbf{p}) \\ x_z(\mathbf{p})\end{Bmatrix} + \begin{bmatrix}\mathbf{0} \\ \mathbf{I}_u \\ 0\end{bmatrix} v_c(\mathbf{p}) + \begin{bmatrix}\mathbf{B}_w(\mathbf{p}) & \mathbf{0} \\ \mathbf{0} & 0 \\ \mathbf{0} & \mathbf{H}_{zy}(\mathbf{p})\end{bmatrix}\begin{Bmatrix}\mathbf{w}_p(\mathbf{p}) \\ \boldsymbol{\eta}_p(\mathbf{p})\end{Bmatrix} \quad (5a)$$

$$\begin{Bmatrix}\mathbf{y}_p(\mathbf{p}) \\ y_u(\mathbf{p}) \\ y_z(\mathbf{p})\end{Bmatrix} = \begin{bmatrix}\mathbf{C}_p(\mathbf{p}) & \mathbf{0} & \mathbf{0} \\ \mathbf{0} & \mathbf{I}_u & 0 \\ \mathbf{0} & 0 & \mathbf{I}_z\end{bmatrix}\begin{Bmatrix}\mathbf{x}_p(\mathbf{p}) \\ x_u(\mathbf{p}) \\ x_z(\mathbf{p})\end{Bmatrix} + \begin{Bmatrix}\boldsymbol{\eta}_p(\mathbf{p}) \\ 0 \\ 0\end{Bmatrix} \quad (5b)$$

in which the terms $\mathbf{I}_u$ and $\mathbf{I}_z$ represent scalars with magnitude one. In general $\mathbf{I}_u$ and $\mathbf{I}_z$ are identity matrices of appropriate dimension.

The plant state $\mathbf{x}_p$ is partitioned into four states as

$$\mathbf{x}_p(\mathbf{p}) = \begin{bmatrix}\mathbf{x}_m^T(\mathbf{p}) & \mathbf{x}_a^T(\mathbf{p}) & \mathbf{x}_s^T(\mathbf{p}) & x_w(\mathbf{p})\end{bmatrix}^T \quad (6)$$

For the HARV longitudinal control law, $\mathbf{x}_m$ represents four longitudinal states, $\mathbf{x}_a$ represents six actuator states, $\mathbf{x}_s$ represents four sensor (or filter) states, and $x_w$ is a washout filter state. The washout filter is actually part of the controller. However, for design and some types of analysis, the filter is included at the input to the plant because the controller output splits into two signals; one is a direct output signal for the stabilator command and the other is an output signal to the washout filter. The combination of the washout filter and the plant allows design with a single control (dimensions of $x_u$ and $v_c$). The total dimension of $\mathbf{x}_p$ is 15 states and the total dimension of $\mathbf{x}$ is 17 states because of the inclusion of one control and one integrator. The four longitudinal states used in the HARV design are

$$\mathbf{x}_m(\mathbf{p}) = \begin{bmatrix}x_v(\mathbf{p}) & x_\alpha(\mathbf{p}) & x_q(\mathbf{p}) & x_\theta(\mathbf{p})\end{bmatrix}^T \quad (7)$$

which represent total airspeed state $x_v$, angle-of-attack state $x_\alpha$, pitch rate state $x_q$, and pitch attitude state $x_\theta$.

The plant output $\mathbf{y}_p$ has three components, which represent measurements of angle of attack $\alpha$, pitch rate $q$, and load factor $n_z$, and is shown as

$$\mathbf{y}_p(\mathbf{p}) = [\, y_\alpha(\mathbf{p}) \quad y_q(\mathbf{p}) \quad y_{n_z}(\mathbf{p}) \,]^T \tag{8}$$

which means that the dimension of $\mathbf{C}_p$ is $3 \times 15$.

***Discrete model.*** The design approach is to discretize the continuous equations (plant plus controller) to form

$$\begin{Bmatrix} \mathbf{x}_p(\mathbf{p}, k+1) \\ x_u(\mathbf{p}, k+1) \\ x_z(\mathbf{p}, k+1) \end{Bmatrix} = \begin{bmatrix} \mathbf{\Phi}_p(\mathbf{p}) & \mathbf{\Gamma}_p(\mathbf{p}) & \mathbf{0} \\ \mathbf{0} & \mathbf{I}_u & 0 \\ (\Delta T)\mathbf{H}_{zx}(\mathbf{p}) & 0 & \mathbf{I}_z \end{bmatrix} \begin{Bmatrix} \mathbf{x}_p(\mathbf{p}, k) \\ x_u(\mathbf{p}, k) \\ x_z(\mathbf{p}, k) \end{Bmatrix} + \begin{bmatrix} \mathbf{0} \\ (\Delta T)\mathbf{I}_u \\ 0 \end{bmatrix} v_c(\mathbf{p}, k) + \begin{bmatrix} \gamma_{w1}(\mathbf{p}, k) \\ \gamma_{w2}(\mathbf{p}, k) \\ \gamma_{w3}(\mathbf{p}, k) \end{bmatrix} \overline{\mathbf{w}}_k(\mathbf{p}, k) \tag{9a}$$

$$\begin{Bmatrix} \mathbf{y}_p(\mathbf{p}, k) \\ y_u(\mathbf{p}, k) \\ y_z(\mathbf{p}, k) \end{Bmatrix} = \begin{bmatrix} \mathbf{C}_p(\mathbf{p}) & \mathbf{0} & \mathbf{0} \\ \mathbf{0} & \mathbf{I}_u & 0 \\ \mathbf{0} & 0 & \mathbf{I}_z \end{bmatrix} \begin{Bmatrix} \mathbf{x}_p(\mathbf{p}, k) \\ x_u(\mathbf{p}, k) \\ x_z(\mathbf{p}, k) \end{Bmatrix} + \begin{Bmatrix} \boldsymbol{\eta}_p(\mathbf{p}, k) \\ 0 \\ 0 \end{Bmatrix} \tag{9b}$$

in which $\mathbf{\Phi}_p$ and $\mathbf{\Gamma}_p$ are discrete matrices corresponding to $\mathbf{A}_p$ and $\mathbf{B}_p$, respectively, $\gamma_{wi}$ ($i$ = 1, 2, or 3) represents discrete matrices for the process noise, $\Delta T$ is the discrete sampling period (which is 0.0125 sec for this design), integer $k$ represents the present sample time, and the other variables are the same as previously defined. A perfect discrete transformation from equation (5a) to equation (9a) will have slightly different coefficients in the control matrix elements and one term of the state matrix. (See ref. 17.) The terms shown in equation (9a) are incorporated to accurately model the hold function in the digital computer operation.

The control $v_c$ is related to the outputs by the feedback-gain matrix as

$$v_c(\mathbf{p}, k) = -[\, \mathbf{K}_y(\mathbf{p}) \quad K_u(\mathbf{p}) \quad K_z(\mathbf{p}) \,] \begin{Bmatrix} \mathbf{y}_p(\mathbf{p}, k) \\ y_u(\mathbf{p}, k) \\ y_z(\mathbf{p}, k) \end{Bmatrix} \tag{10}$$

in which $\mathbf{K}_y$ is the proportional gain matrix, $K_u$ is the control filter gain, and $K_z$ is the integrator gain. Further partitioning of $\mathbf{K}_y$ gives three terms

$$\mathbf{K}_y(\mathbf{p}) = [\, K_\alpha(\mathbf{p}) \quad K_q(\mathbf{p}) \quad K_{n_z}(\mathbf{p}) \,] \tag{11}$$

for the $\alpha$, $q$, and $n_z$ outputs. A block diagram of the feedback control structure described in equations (9) and (10) is shown in figure 5. This controller is a proportional integral filter (PIF) structure (refs. 17 and 18) that is used for design and linear analysis. Later in this paper, an incremental structure will be shown for the implementation model. The general dynamic form of equations (9) and (10) is

$$\left.\begin{aligned} \mathbf{x}(\mathbf{p}, k+1) &= \mathbf{\Phi}(\mathbf{p})\mathbf{x}(\mathbf{p}, k) + \mathbf{\Gamma}(\mathbf{p})v_c(\mathbf{p}, k) \\ &\quad + \mathbf{\Gamma}_w(\mathbf{p})\overline{\mathbf{w}}(\mathbf{p}, k) \\ \mathbf{y}(\mathbf{p}, k) &= \mathbf{C}(\mathbf{p})\mathbf{x}(\mathbf{p}, k) + \overline{\boldsymbol{\eta}}(\mathbf{p}, k) \end{aligned}\right\} \tag{12}$$

$$v_c(\mathbf{p}, k) = -\mathbf{K}(\mathbf{p})\mathbf{y}(\mathbf{p}, k) \tag{13}$$

## Cost Function

An optimal design process is used in the variable-gain output feedback algorithm. The algorithm requires that a discrete cost function $\overline{J}_d(\mathbf{p}, \mathbf{K}(\mathbf{p}))$ be defined at each operating condition as

$$\overline{J}_d(\mathbf{p}, \mathbf{K}(\mathbf{p})) = \lim_{N \to \infty} \frac{1}{2(N+1)} \sum_{k=0}^{N} E\Big[\mathbf{x}^T(\mathbf{p}, k+1)\mathbf{Q}(\mathbf{p})\mathbf{x}(\mathbf{p}, k+1) + 2\mathbf{x}^T(\mathbf{p}, k)\mathbf{A}_m(\mathbf{p})v_c(\mathbf{p}, k) + v_c^T(\mathbf{p}, k)R(\mathbf{p})v_c(\mathbf{p}, k)\Big] \tag{14}$$

in which $\mathbf{Q}(\mathbf{p})$, $\mathbf{A}_m(\mathbf{p})$, and $R(\mathbf{p})$ are the discrete weighting matrices for the states, cross product of states and controls, and controls, respectively, and $E$ is the expectation operator. The main objective is to minimize a global cost $J(\mathbf{K}(\mathbf{p}))$ expressed by

$$J(\mathbf{K}(\mathbf{p})) = \sum_{j=1}^{M} f_j \overline{J}_{dj}(\mathbf{p}, \mathbf{K}(\mathbf{p})) \qquad (f_j \geq 0) \tag{15}$$

in which each of the local costs are summed and weighted by $f_j$ to assign relative priorities to the $M$ individual operating conditions. For the design in this paper, all $f_j = 1.0$.

The design approach is to first provide optimal weights at each operating condition in the continuous domain and then to discretize these weights (refs. 19 and 20) for use in the design algorithm (eq. (14)). The discrete cost function is the intermediate step to

minimize a continuous cost $J_c(\mathbf{p})$ that is quadratic in outputs and controls and has the form (ref. 9)

$$J_c(\mathbf{p}) = \lim_{t_f \to \infty} \frac{1}{t_f} \int_0^{t_f} E\Big[\mathbf{y}^T(\mathbf{p},t)\overline{\mathbf{Q}}(\mathbf{p})\mathbf{y}(\mathbf{p},t) + v_c^T(\mathbf{p},t)R_v(\mathbf{p})v_c(\mathbf{p},t)\Big]dt \tag{16}$$

in which $t$ is time, $\overline{\mathbf{Q}}$ is the continuous output-weighting matrix, and $R_v$ is the continuous control-weighting matrix, which is a scalar for the HARV design. The outputs are related to the states by equations (12).

The continuous output-weighting matrix has diagonal elements as

$$\overline{\mathbf{Q}}(\mathbf{p}) = \text{diag}[\,\mathbf{Q}_y(\mathbf{p}) \quad Q_u(\mathbf{p}) \quad Q_z(\mathbf{p})\,] \tag{17}$$

for the proportional weight, control filter weight, and integrator weight, respectively. The proportional weight is further partitioned into three terms

$$\mathbf{Q}_y(\mathbf{p}) = \text{diag}[\,Q_\alpha(\mathbf{p}) \quad Q_q(\mathbf{p}) \quad Q_{n_z}(\mathbf{p})\,] \tag{18}$$

for the $\alpha$, $q$, and $n_z$ measurements. The weights for all design cases will be shown later in this paper.

### Stochastic-Weighting Process

The variable-gain algorithm is stochastic and includes adjustments for both process noise and measurement noise. Terms in the process noise calculation can include randomly distributed initial condition errors, control input random pseudonoise, random external disturbances, and integrator noise. The total process noise covariance matrix $\overline{\mathbf{W}}$ is calculated as

$$\overline{\mathbf{W}} = \mathbf{\Phi}(\mathbf{p})\mathbf{X}_0(\mathbf{p})\mathbf{\Phi}^T(\mathbf{p}) + \int_0^{\Delta T} \Big\{e^{A(\mathbf{p})t}\Big[\mathbf{B}(\mathbf{p})\mathbf{V}_0(\mathbf{p})\mathbf{B}^T(\mathbf{p}) + \overline{\mathbf{B}}(\mathbf{p})\mathbf{W}_0(\mathbf{p})\overline{\mathbf{B}}^T(\mathbf{p})\Big]e^{A^T(\mathbf{p})t}\Big\}dt \tag{19}$$

and the noise terms are assumed to be white and have zero mean as

$$\left.\begin{aligned} E\{\mathbf{x}_0(i,\mathbf{p})\} &= \mathbf{0} \qquad E\{\mathbf{x}_0(j,\mathbf{p})\} = \mathbf{0} \\ E\{\mathbf{x}_0(i,\mathbf{p})\mathbf{x}_0^T(j,\mathbf{p})\} &= \mathbf{X}_0(\mathbf{p})\delta_{ij} \end{aligned}\right\} \tag{20}$$

$$\left.\begin{aligned} E\{v_0(i,\mathbf{p})\} &= \mathbf{0} \qquad E\{v_0(j,\mathbf{p})\} = \mathbf{0} \\ E\{v_0(i,\mathbf{p})v_0^T(j,\mathbf{p})\} &= V_0(\mathbf{p})\delta_{ij} \end{aligned}\right\} \tag{21}$$

$$\left.\begin{aligned} E\{\mathbf{w}_0(i,\mathbf{p})\} &= \mathbf{0} \qquad E\{\mathbf{w}_0(j,\mathbf{p})\} = \mathbf{0} \\ E\{\mathbf{w}_0(i,\mathbf{p})\mathbf{w}_0^T(j,\mathbf{p})\} &= \mathbf{W}_0(\mathbf{p})\delta_{ij} \end{aligned}\right\} \tag{22}$$

$$\left.\begin{aligned} E\{\overline{\mathbf{v}}(i,\mathbf{p})\} &= \mathbf{0} \qquad E\{\overline{\mathbf{v}}(j,\mathbf{p})\} = \mathbf{0} \\ E\{\overline{\mathbf{v}}(i,\mathbf{p})\overline{\mathbf{v}}^T(j,\mathbf{p})\} &= \overline{\mathbf{V}}(\mathbf{p})\delta_{ij} \end{aligned}\right\} \tag{23}$$

in which $\mathbf{x}_0$ and $\mathbf{X}_0$ are the initial condition error state vector and state covariance matrix, respectively; $v_0$ and $V_0$ are the control input random pseudonoise and covariance, respectively; $\mathbf{w}_0$ and $\mathbf{W}_0$ are the random external disturbance noise vector and covariance matrix, respectively; $\overline{\mathbf{v}}$ and $\overline{\mathbf{V}}$ are the measurement noise vector and covariance matrix, respectively; and $\delta_{ij}$ is the Kronecker delta. All of the noise terms are assumed to be uncorrelated.

### Design Conditions

Thirty-nine design conditions (table II) are used for the feedback controller: 14 conditions are at 15 000 ft, 13 conditions are at 25 000 ft, and 12 conditions are at 35 000 ft. Nineteen of the design conditions are at $1g$ (Earth axis) flight. The other cases are at various non-$1g$ conditions. The parameters in table II include the design case, altitude, Mach number, $\alpha$, $n_z$, and open-loop short period frequency. Because $n_z$ is referenced to the $Z$-axis of the airplane, the $n_z$ value for $1g$, Earth-axis flight is equal to the cosine of the pitch attitude, which results in a value less than 1.0. Most of the non-$1g$ trim cases are at higher loads; however, design cases such as 13 and 14 are at lower load factors. The appendix contains linear open-loop airplane models for all 39 design conditions plus the transfer functions for actuators, sensors, and antialiasing filters.

### Design Weights

A design procedure for selecting the optimal cost weights is described in reference 7. The optimal cost weights for the HARV longitudinal feedback controller design are shown in table III. The first column contains the design case number, the next five columns of the table contain the continuous model output feedback weights at each operating condition, and the last column contains the continuous model control weights. Table IV contains the stochastic weights for the design. Because all 39 design conditions have the same stochastic weights, weights for only one model are shown. The design model has 17 states and 5 outputs; values of these stochastic weights are arbitrary and most of the small numbers have been incorporated to avoid numerical problems with the design algorithm. The weight on the first output measurement $\alpha$ is an order of magnitude larger than the other weights because $\alpha$ is considered to be a less accurate measurement.

### Feedback-Gain Matrix

Formulation of the feedback-gain matrix is described in references 8–10; only the final equation is included. The feedback-gain matrix, which is used in equation (13), has a linear functional relationship with $\mathbf{p}$ and contains both constant- and variable-gain parts as

$$\mathbf{K}(\mathbf{p}) = \mathbf{K}_0 + \sum_{i=1}^{q} p_i(\boldsymbol{\nu})\mathbf{K}_i \tag{24}$$

where the variable $\boldsymbol{\nu}$ represents a vector of measured variables that the designer selects for the gain-schedule parameters. The relationship between the $p_i$ and $\boldsymbol{\nu}$ may be either linear or nonlinear.

The HARV design has six gain-schedule parameters $p_i(\boldsymbol{\nu})$. These parameters are functions of $\alpha$, impact pressure $Q_c$, and static pressure $P_s$. The $p_i(\boldsymbol{\nu})$ and their limits are as follows:

$$\left.\begin{aligned}
p_1 &= 0.1\alpha && (1.5 \le \alpha \le 65)\\
p_2 &= 0.01Q_c && (10 \le Q_c \le 470)\\
p_3 &= 0.001P_s && (498 \le P_s \le 1200)\\
p_4 &= \frac{Q_c}{P_s} && (0.008 \le p_4 \le 0.4)\\
p_5 &= 0.1\alpha - 3.5 && (\alpha > 35)\\
P_5 &= 0 && (\alpha \le 35)\\
p_6 &= 0.01Q_c - 2.5 && (Q_c > 250)\\
P_6 &= 0 && (Q_c \le 250)
\end{aligned}\right\} \tag{25}$$

The feedback gains change continuously with the measured variables; the function is completely continuous and also smooth except at two points. The first four parameters are used throughout the entire HARV flight envelope. Parameter $p_5$ is used only when $\alpha$ is greater than 35°; parameter $p_6$ is used when $Q_c$ is greater than 250 lb/ft$^2$. Both $p_5$ and $p_6$ have lower limits of zero and are not differentiable at the break points. When any value of $\boldsymbol{\nu}_i$ exceeds the design limit, the variable is limited to the value shown in equations (25). The scale factors have been selected to keep $p_i(\boldsymbol{\nu})$ near unity.

Table V contains the values of the six gain-schedule parameters for the 39 design conditions. These values are input to the variable-gain design algorithm along with the weights described previously to calculate the feedback gains in equation (24). Resultant values for the $\mathbf{K}_i$ matrices ($i$ = 0 to 6) are shown in table VI. Each matrix has five components for which the columns are consistent with the five output measurements.

## Linear Analysis of Feedback Controller

This section presents results of the linear analyses for the feedback controller. Three design conditions have been selected for example cases. The three examples are for design cases 15, 17, and 19 (see table II) corresponding to a low-$\alpha$, high-Mach case (Mach = 0.7, $\alpha$ = 3.58°), an intermediate-$\alpha$ case (Mach = 0.33, $\alpha$ = 20°), and a high-$\alpha$ case (Mach = 0.26, $\alpha$ = 50°), respectively. All three cases were chosen at 25 000 ft because altitude variation has negligible effect. The control structure shown in figure 5 is used in the linear analysis. The configuration in figure 5 is used for most linear analyses but the pitch thrust-vectored washout filter is included at the output of the PIF controller for the servoelastic and control sensitivity robustness analysis. (See discussion in "Continuous model.") Inclusion of the washout filter within the controller allows the single control $y_u$ to be split into two separate controls and the control loop to be broken at the stabilator $\delta_{sc}$ and thrust vector $\delta_{vc}$ commands.

### Feedback Gains

Table VII contains the feedback gains for the three example cases. These gains are computed from equation (24) with the gain-schedule parameters in table V and the variable-gain components in table VI. Figure 6 is a more comprehensive picture which shows the gains at 25 000 ft as a function of $\alpha$. The solid line represents the 1$g$ cases and the crosses represent gains at the other design conditions. At high-$\alpha$ conditions, the gains are essentially linear with $\alpha$, which indicates that $\alpha$ is the dominant gain-schedule variable for this condition. Note that the gain plots are highly nonlinear for the $\alpha$ range and the load factor has a major effect on the gain values. Additional data (not included in this paper) show that for the HARV altitude range of 15 000–35 000 ft, altitude has a minor effect.

### Closed-Loop Eigenvalues

Closed-loop eigenvalues for the three example cases are shown in table VIII. Row 1 in each case corresponds to the normal accelerometer filter, rows 2 and 3 correspond to a second-order pitch rate filter, rows 4–9 correspond to actuator dynamics, and row 10 in design cases 15 and 17 corresponds to an $\alpha$ filter. In design case 19, the $\alpha$ filter state has been combined with another state to form a complex pair (rows 10 and 11). Rows 16 and 17 in each case correspond to the closed-loop phugoid. The closed-loop

phugoid is stable for all 39 design conditions even though the open-loop phugoid is unstable at a few design conditions. All other closed-loop eigenvalues correspond to combinations of short period dynamics and controller dynamics (integrator, control position filter, and washout filter). The other closed-loop eigenvalues have good damping ratios even though the open-loop short period is unstable for design case 19.

### Stability Margins

Single loop stability analysis was done for both the airplane input and outputs. The input analysis was done by opening the control system at the single control loop before the split between the stabilator and pitch thrust-vector washout filter. The plant input during this analysis was augmented by the washout filter. Table IX shows that for the three example cases, the gain and phase margins are much better than the design guidelines of $\pm 6$ dB and $\pm 45°$, respectively. (See ref. 21.) These margins exclude the very low-frequency range of the phugoid mode. Only the pitch rate loop data are shown for the output because analysis of individual output measurement loops shows pitch rate is the most critical loop.

The analysis was made with a database of 177 cases. This data include flight conditions at three altitudes (15 000, 25 000, and 35 000 ft), at various Mach numbers (from Mach 0.9 down to Mach 0.1), at $\alpha$'s up to 65°, and other special cases that include heavyweight airplane, lightweight airplane, and selected conditions at the higher altitude of 40 000 ft. Analysis of the 177 cases shows that the gain and phase margins are within the guidelines for all cases within the HARV flight envelope (Mach $< 0.7$). Results show that the nondesign cases are equally as robust to gain and phase changes as the 39 design cases, which illustrates that the controller is not tuned to any specific design point.

### Robustness

Structured singular value analysis, in which parameters are modeled as uncertain gains, is useful in the assessment of the stability of a linear feedback control system when all parameters vary independently over given intervals. (See ref. 22.) In this paper, the robustness analysis is based upon a new algorithm for real $\mu$. (See ref. 23.) The inverse of $\mu$ is plotted in all figures relating to robustness because the minimum value is indicative of the parameter percentage change for which the control system remains stable.

The first check is for a multiplicative error at the plant output with all three output loops opened. Figure 7 contains the inverse real-$\mu$ frequency plot for the three example cases. For the case of Mach 0.7, the minimum value is slightly less than 1.0, which indicates that the control system will remain stable for almost a 100-percent change in all plant output gains. The cases with an $\alpha$ of 20° and 50° are the most critical with minimum values of approximately 0.6, which indicate that the feedback control system will remain stable for approximately 60-percent changes in plant output gains. Although no established guidelines exist for this type of analysis, these minimum values are considered quite good and indicate a reasonably robust control system. The complex-$\mu$ analyses of 39 design conditions had similar numerical results with the exception of the phugoid and also showed that the worst cases were at an $\alpha$ between 20° and 50°.

A real-$\mu$ analysis also was used to evaluate the sensitivity of the airplane short period stability derivatives and their corresponding control derivatives that affect the $\alpha$ and $q$ accelerations. In the analysis of the four stability derivatives (fig. 8), the minimum values were above 1.0 for the entire frequency range. Results for the four control derivatives show that all minimum values were above 0.9. (See fig. 9.) These results are considered excellent and again indicate a robust feedback control system.

### Loop Transfer and Servoelastic Frequency Response

A singular value loop transfer analysis was made to evaluate the rigid-body control system frequency response and crossover frequency at each design condition and also the servoelastic frequency response at several design conditions. The best location to break the plant input loop is at the single control point before the loop splits into two separate controls. This approach was taken for the rigid-body loop transfer analysis. The servoelastic analysis was more complex but the combination of the servoelastic and rigid-body models made it easier to open the loops at the two control inputs. Each analysis is described below.

To conduct the rigid-body singular value loop transfer analysis, the control loop was opened first at the single plant control input and then at the plant output (three outputs simultaneously). Because there is only one effective control, the Bode response and the singular value response are identical at the plant input. At both input and output locations, the crossover frequencies for all 39 design conditions ranged between 2.4 rad/sec and 10.0 rad/sec, with a slope of approximately 6 dB/octave. The highest crossover frequency is at the highest Mach

number. To obtain lower crossover frequencies at higher $\alpha$ conditions, the feedback controller filter bandwidth was designed to be lower by reducing the filter gain. Figures 10 and 11 show the crossover frequencies and servoelastic response for the three example cases.

The servoelastic analysis was conducted as an extension of the rigid-body analysis; however, the plant input was opened at the two controls. First, a servoelastic modal model was placed in parallel with a series combination of the rigid-body and actuator dynamics; then, the new model was connected in series with the output filters. The unaugmented singular value servoelastic model response for a heavy airplane is shown in figure 10, which shows peaks of approximately $-18$ dB at 75 rad/sec and $-7$ dB at 100 rad/sec. These peaks are mainly the result of the transfer function (not shown) from control input to $q$ output (units of $\sec^{-1}$) which exhibits peaks of $-20$ dB at 75 rad/sec and $-8$ dB at 100 rad/sec. In addition, the transfer function from control input to $n_z$ output (units of $g$/deg) exhibits peaks of $-45$ dB at 37 rad/sec, $-38$ dB at 50 rad/sec, and $-33$ dB at 100 rad/sec. Singular-value control loop transfer analyses at both the plant input and plant output (figs. 10 and 11) show that the structural mode at 100 rad/sec was attenuated to approximately $-20$ dB (worst case is $-19$ dB at Mach 0.7). This attenuation is significantly greater than the guideline of $-8$ dB. (See ref. 21.) The total attenuation is mainly due to a combination of actuator dynamics attenuation and feedback controller attenuation.

## Feed-Forward Controller Design

### Feed-Forward Command Generator (FFCG)

Reference 7 contains a detailed description and derivation of the feed-forward control equations. This section summarizes the controller design and the HARV design changes made after reference 7 was written. The feed-forward command generator (FFCG) converts the pilot stick command into an equivalent command $y_{\text{cmd}}$ that can be interpreted by the feedback controller. The FFCG selects either an $n_{z,c}$ or an $\alpha_c$ command mode and makes a smooth transition between the two modes without any additional work by the pilot.

The FFCG continually generates two solutions. One solution is based upon the $n_{z,c}$ mode with a stick sensitivity of 1.0 $g$/in. (in ref. 7 the sensitivity was 1.3 $g$/in.) and is generated from

$$y_{\text{cmd}} = \frac{\sum_{i=1}^{3} C_i}{C_3}(1.0\delta_{sp}) + \alpha_{\text{oc}} \tag{26}$$

The other solution is based upon the $\alpha_c$ mode with a stick sensitivity of 10°/in. and is generated from

$$y_{\text{cmd}} = \frac{\sum_{i=1}^{3} C_i}{C_1}(10\delta_{sp}) + 20 \tag{27}$$

The $C_i$'s are steady-state-normalized coefficients for $\alpha$, $q$, and $n_z$, respectively, $\delta_{sp}$ is the pilot stick position, and $\alpha_{\text{oc}}$ is a trim that must be estimated. The $\alpha_c$ mode is biased at 20° to yield a maximum command of $\alpha = 70°$ with 5 in. of pitch stick. The $C_i$'s are solved with the functional relationships that are calculated off-line by a least-squares solution. The methodology for derivation of the $C_i$'s is reported in reference 7.

Implementation of the FFCG is illustrated in figure 12 and is modified from the implementation shown in reference 7. This modification eliminated the lockout feature that was installed to minimize a jump between command modes during certain flight conditions with negative $\delta_{sp}$. The slopes of equations (26) and (27) are compared ($\delta_{sp}$ is the same in each equation) and the smallest absolute value of $\Delta y_{\text{cmd}}$ is selected for the linear part of the commanded output. During low-speed, high-$\alpha$ flight the bias is 20°, but during high-speed, low-$\alpha$ flight the bias $\alpha_{\text{oc}}$ must be estimated. The equations and coefficients for estimating $\alpha_{\text{oc}}$ were determined from an off-line least-squares solution. This estimate is a function of impact pressure $Q_c$ and incremental load factor command $\Delta n_{z,c}$; the estimate is separated into a $1g$ bias term as

$$\alpha_{\text{oc},1g} = 14.4773\frac{100}{Q_c} - 14.3764\left(\frac{100}{Q_c}\right)^2 + 12.7386\left(\frac{100}{Q_c}\right)^3 - 2.9491\left(\frac{100}{Q_c}\right)^4 \qquad (Q_c \geq 42.6) \tag{28}$$

and an incremental bias term $\Delta\alpha_{\text{oc}}$ as

$$\Delta\alpha_{\text{oc}} = 6.896806Q_{n_z} + 16.2912Q_{n_z}^2 - 10.09235Q_{n_z}^3 + 2.029378Q_{n_z}^4 \tag{29}$$

where

$$Q_{n_z} = \frac{100\,\Delta n_{z,c}}{Q_c} \qquad (90 \leq Q_c \leq 460;\ \Delta n_{z,c} \geq 0) \tag{30}$$

The $1g$ and incremental bias terms are then summed and limited to 20°. One of the inputs $\Delta n_{z,c}$ for this estimated bias is passed through a 1 rad/sec low-pass filter, which was selected as a compromise between time response and noise bandwidth caused by the pilot moving the pitch stick. By splitting the bias estimate into two parts, a very accurate estimate is obtained at $1g$, which allows the pilot stick to be essentially at null position independent of speed. Very small changes in $\delta_{sp}$ will balance out any residuals. The solution is valid up to approximately $\alpha = 30°$.

### Command Generator Tracker (CGT)

The objective of the CGT is to make the regulated plant outputs optimally track the linear command model outputs. An equation is shown in reference 7 for the calculation of the CGT feed-forward gain defined therein as $E1$. The approach was to calculate $E1$ at each design point and then to use either an interpolation method or an off-line least-squares solution to generate an equation for calculating $E1$ during flight. However, $E1$ was too sensitive to pilot stick commands at several areas of the flight regime, which resulted in saturation of the controls. In the current design, $E1$ has a constant gain of $-40$. The resulting command is then limited to maximize agility by allowing the controls to just reach saturation at maximum $\delta_{sp}$ commands. The gain of $-40$ for $E1$ is representative of the calculated gains at the various design conditions. Adjustment of the variable command limit by trial and error resulted in the special conditions shown in figure 13.

The variable limit is mainly a function of $Q_c$ with various modifications. The limit is maintained between 10 and 60 deg/sec with the upper value of 60 deg/sec chosen to maximize agility at Mach 0.6 and $h = 25\,000$ ft. The lower value of 10 deg/sec is chosen to ensure that some agility can be attained at higher-$\alpha$ flight. Modifications to the limits are outlined below:

1. When static pressure $P_s < 786$ lb/ft$^2$ (altitude $h > 25\,000$ ft) and $\alpha < 30°$, the limit is reduced linearly with $P_s$, which results in a smaller CGT command. At 35 000 ft, the reduction factor is approximately 0.5 because the CGT command was too sensitive at higher altitudes.

2. During any sampling period ($\Delta T = 0.0125$ sec) when the change in filtered $y_{\text{cmd}}$ is less than $-1$ and $\alpha$ is greater than 30°, the limit is increased linearly with $\alpha$. This ensures good agility with a large pitch-down command (forward $\delta_{sp}$ command) when at high $\alpha$. The limit is increased by a factor of 4.5 when $\alpha$ is 60°; a typical scenario is for the limit to increase from 10 to 45. This limit increase occurs only for large and fast forward stick command changes (filtered $y_{\text{cmd}}$ rates more negative than $-80$, which corresponds to nominal $\delta_{sp}$ rates of $-8$ in/sec).

## Nonlinear Configuration

This section briefly describes the controller configuration and puts the various parts into perspective. The incremental implementation for the feedback controller is shown. In addition, special considerations for nonlinear simulation and flight are discussed.

Figure 14 shows a block diagram of the HARV longitudinal controller containing the main components described in previous sections for the feedback and feed-forward controller designs. Pilot commands $\delta_{sp}$ are input to the FFCG, which generates $y_{\text{cmd}}$ based upon the selection of either $\alpha_c$ or $n_{z,c}$. Output $y_{\text{cmd}}$ goes to both the CGT and the variable-gain feedback controller comprised of the PIF control structure and gain functional, which generate feedback-gain matrices $\mathbf{K}(\mathbf{p})$ as a function of parameter $\mathbf{p}$. The thrust-vectoring washout filter is attached to the output of the PIF control structure. Control commands $\delta_{sc}$ and $\delta_{vc}$ are input to the plant and generate airplane responses as measured by the sensors. Measured $\mathbf{y}_p$ signals are fed back to the PIF controller while other measurements are used to calculate $\mathbf{p}$ for both the feedback-gain functional and the FFCG. The $\mathbf{p}$ used for the FFCG is a scaled subset of those used for the feedback controller. An additional part of the controller (not discussed previously) is the flap scheduler, which generates commands for both the leading- and trailing-edge flaps as a function of $\alpha$ and air data measurements $P_s$ and $Q_c$. The flap schedule is the same as used on the F-18 airplane.

The feedback controller uses an incremental implementation (refs. 17 and 18), which is shown in figure 15. In this implementation, $\mathbf{K}_y(\mathbf{p})$ multiplies the incremental change in $\mathbf{y}_p$, $K_z(\mathbf{p})$ multiplies the difference between the sum of the measured feedbacks and $y_{\text{cmd}}$, and $K_u(\mathbf{p})$ is incorporated into the discrete filter loop. One advantage of the incremental approach is that sensor biases are subtracted out in the proportional feedback loop. In the integrator loop, the pilot can move the pitch stick slightly to compensate for biases. Position limiters are incorporated to prevent windup in the rate-to-position integrator. The discrete dynamics in the $\delta_{vc}$ actuator loop represent the Tustin transformation for a low-pass filter with a bandwidth of 1 rad/sec. The implementation from $y_u$ to $\delta_{vc}$ represents a limited washout filter.

Reference 7 contains a derivation for nonlinear pitch rate compensation which has two terms: one term for gravity compensation and the other term for kinematic compensation. The kinematic compensation has been deleted in this paper because it is a function of sideslip angle $\beta$, which is not a readily available airplane measurement. The result of this deletion is a slight deterioration of regulation during 360° stability-axis rolls, mainly at $\alpha$ of 45° or greater. A second modification in the controller is a multirate approach to reduce computation time within the flight computer. Variables that are being computed every other sample period (0.025 sec as opposed to 0.0125 sec) include $\alpha$, $p_i(\nu)$ ($i = 1$ to 6), $\mathbf{K}(\mathbf{p})$, $C_i$ ($i = 1$, 2, or 3), and some trigonometric functions for the nonlinear pitch rate compensation.

## Nonlinear Batch Simulation Results

Several nonlinear batch simulations were conducted to evaluate pitch agility, $\alpha$-capture capability, and $\alpha$ regulation during 360° stability-axis rolls.

### Design Guidelines

Several preliminary open-loop (no pilot) large amplitude design guidelines have been established to assist in the design effort. Most of the guidelines that relate to agility are discussed in reference 11. Agility guidelines include minimum achievable pitch rate $q$ and pitch acceleration $\dot{q}$ criteria for both pitch-up and pitch-down maneuvers at an altitude of 25 000 ft. Pitch-up agility guidelines specify the minimum peak $q$ and $\dot{q}$ values for several initial trim $\alpha$'s based upon maximum aft stick ramp command and full-throttle (afterburner (A/B)) command. The stick command is delayed for approximately 2.0 sec after throttle command to allow thrust to build up. The maximum $\dot{q}$ should be obtained within 1.0 sec from the onset of the pitch stick command and the maximum $q$ should be achieved within 1.75 sec. The pitch-down agility guideline also specifies peak $q$ and $\dot{q}$ values when starting from an initial trim $\alpha$ of 60° with a full-forward stick command. Values for the various guidelines are given in the appropriate section.

The open-loop $\alpha$-regulation tests are used to evaluate how well the longitudinal controller regulates $\alpha$ while rolling about the velocity vector with a full-lateral stick command. The test is made at various initial $\alpha$-trim conditions (low-$\alpha$ to high-$\alpha$) and guidelines (ref. 11) are specified at both the 90° and 360° wind-axis bank angles.

### Pitch-Up Agility

The objective of this maneuver was to evaluate the pitch-up response (fig. 16) to a maximum aft stick input of 5 in. when trimmed at an altitude of 25 000 ft and Mach number of 0.6. In particular, the peak amplitude and corresponding time of the $q$ and $\dot{q}$ responses were compared with design guidelines. To simulate the maneuver, maximum throttle was commanded at time equal to 0.01 sec; 2.0 sec later, after thrust had built up, the pitch stick was ramped to maximum within 0.3 sec to simulate the approximate response time of the pilot. The top plot in figure 16 shows $\alpha$ reaching 60° in less than 2.0 sec and then slowly climbing to 70° after a slight bobble. The sluggish response after $\alpha$ reached 60° was caused by the saturated actuator commands. Although the stabilator remains saturated, the thrust-vectored command came out of saturation at approximately 5.6 sec as the $\alpha$ slowly converged toward 70°. The pitch rate $q$ peaked at the desired guideline of approximately 55 deg/sec, whereas the pitch acceleration $\dot{q}$ was greater than the guideline of 96 deg/sec$^2$. The FFCG started in the $n_z$ mode and made a smooth transition to the $\alpha$ mode at approximately 3.0 sec; based on this, the pilot is unlikely to detect the transition. The smooth time response also indicated good integration between the feedback and feed-forward controllers.

Figures 17 and 18 illustrate $q$ and $\dot{q}$ agility, respectively and their guidelines (ref. 11) for various $\alpha$ at 25 000 ft. The plots show that $q$ meets or exceeds the guideline until initial trim $\alpha$ increases to approximately 45° where $q$ drops slightly below. Similarly, $\dot{q}$ meets or exceeds the guideline until initial trim $\alpha$ increases to 55° where $\dot{q}$ drops slightly below. There is currently no guideline for $\alpha$ greater than 55°.

### Pitch-Down Agility

The objective of this maneuver was to evaluate the pitch-down response (fig. 19) to a full-forward pitch stick input (−2.5 in.) starting from an $\alpha$ trim of 60° and at an altitude of 25 000 ft. The $\alpha$ decreased to 10° in approximately 2.0 sec and crossed 0° at approximately 2.4 sec, which is slightly slower than the pitch-up response. Both $q$ and $\dot{q}$ were significantly better than the tactical guidelines of −24 deg/sec and −14.3 deg/sec$^2$, respectively. (See ref. 11.) Based on these results, the $\alpha$ response is shown to be well damped.

### Angle-of-Attack Capture

Figures 20 and 21 illustrate the $\alpha$ captures for altitudes of 15 000, 25 000, and 35 000 ft. Each figure shows the stick position and the $\alpha$ response for the three altitudes. Figure 20 is for a moderate angle change; the $\alpha$ starts at 20° and passes maximum lift to approximately 45°, which is based upon

a stick position change from 0 to 2.5 in. The initial transient response is very similar for all three altitudes and reaches the desired value in just over 2.0 sec. At $t = 10$ sec (nearly steady-state), the amplitude difference between the upper- and lower-$\alpha$ plots is 2.8°. This small difference in amplitude is due to differences in the command generator feed-forward command gain (eqs. (26) and (27)), which is estimated as a function of four parameters $\alpha$, $Q_c$, $P_s$, and $Q_c/P_s$. A maximum pilot stick position change of 0.28 in. would make the final steady-state amplitude the same at all altitudes. The three time responses have very little overshoot, which indicates a well-damped feedback control system at all altitudes.

Figure 21 contains similar data for a large amplitude change from 5° to nearly 60°, which is based upon a stick position change from 0 to 3.85 in. The initial transient response is again similar for all three $\alpha$ cases but reaches a maximum in approximately 2.5 sec, which is slightly slower than the previous case. When the time equals 10 sec, the $\alpha$ amplitude is 56.2° at 35 000 ft, 58.7° at 25 000 ft, and 62.3° at 15 000 ft. Similarly to the previous case, this amplitude difference is due to $y_{\text{cmd}}$ (not shown but 57.0, 58.4, and 60.8, respectively), which varies with the estimated feed-forward gain as well as stick position. This small difference between $\alpha$ and $y_{\text{cmd}}$ is due mainly to $q$, which is also regulated by the feedback controller. Worst case pilot stick changes of approximately 0.38 in. can make the $\alpha$ amplitude equal to 60° in all cases. All time responses again illustrate a well-damped feedback control system.

Figure 22 is for a pitch-down $\alpha$ response from an initial trim of 60° to a capture at $\alpha = 20°$; the pitch stick is ramped from approximately 4 in. to 0 in. in 0.3 sec. Again, the $\alpha$ response was well damped and similar at all three altitudes. At approximately 5 sec, $\alpha$ began to slowly decrease. The decrease results from the increase in speed ($Q_c$ increases), which causes $\alpha_{\text{oc}}$ (eq. (28)) to decrease below 20°, which in turn causes $y_{\text{cmd}}$ (eqs. (26) and (27)) to decrease by the same amount. The feedback controller was following $y_{\text{cmd}}$ very closely.

### Angle-of-Attack Regulation

The objective of this maneuver was to evaluate the $\alpha$ regulation during full-lateral stick stability-axis rolls. Figure 23 illustrates four $\alpha$-trim cases: 5°, 30°, 45°, and 60°. The dashed vertical lines denote the time in seconds for wind-axis bank angles of 180° and 360°. In all cases, the $\alpha$ regulation is considerably better than the guideline of ±6° for a 90° roll and guideline of ±10° for a 360° roll (ref. 11), although the two high-$\alpha$ cases do not roll fast enough for the bank angle to reach 360° within the 10 sec selected for this illustration.

## Piloted Simulation Results

Pilot-in-the-loop evaluations were conducted with the NASA Langley Differential Maneuvering Simulator (DMS) described earlier. The evaluations included a series of piloted tasks designed to test the longitudinal and lateral-directional control system throughout the flight envelope. Tasks were designed specifically for this effort because no concise set of maneuvers were available to evaluate a configuration with such a large $\alpha$ envelope. Only longitudinal evaluation results are presented herein. However, some of the lateral-directional maneuvers are described to address coupling. The piloted evaluations included $\alpha$ captures, $n_z$ captures, large amplitude rolls, and gross acquisition and tracking tasks. Results from the piloted evaluations are presented in terms of Cooper-Harper ratings (CHR) (ref. 24) and pilot comments. The CHR scale is a numerical scale from 1 to 10, with 1 being the best rating and 10 the worst. (See fig. 24.) In practice, CHR's from 1 to 3 are referred to as level 1, ratings from 4 to 6 are level 2, and ratings from 7 to 9 are level 3.

During initial piloted evaluations of the control law discussed in reference 7, objectionable characteristics were noted because of mode transitions from $n_z$ to $\alpha$. Based on piloted simulation results, modifications of the reference 7 configuration were required primarily in mode transition from $n_z$ to $\alpha$ command and back. These configuration changes are described herein and resulted in transitions from the $n_z$ to $\alpha$ command modes that were nearly undetectable by the pilots. Only results from the final version of the control law to be implemented and flight tested on the HARV are shown. Extensive evaluations were conducted at 15 000, 25 000, 35 000, and 40 000 ft but only the results from the 25 000 ft evaluations are shown herein for space considerations. The results at other altitudes were similar except for the effect of control power deterioration near the maximum $\alpha$ for the higher altitudes. The decrease in control power was due to reduced engine thrust at high altitudes. Altitude effects were barely noticeable below $\alpha = 60°$.

Three NASA test pilots participated in this study. Two have extensive air combat training and experience; all have high-performance airplane experience. One pilot has many years of experience with simulated high-$\alpha$ airplanes and the other two pilots have one to two years of experience with simulated high-$\alpha$ airplanes. All pilots have experience with the use

of simulated within-visual-range air combat scenarios of high-$\alpha$ airplanes versus one or two conventional airplanes.

The first step for each pilot in the task evaluation procedure was to repeat each maneuver to become familiar with the required piloting techniques, flight condition, and configuration. Once the pilots felt proficient, the task was repeated a few times to rate it. Ratings based upon a single good or bad attempt were prevented with this procedure. The drawback is that when flying the configuration in air combat, many flight conditions are encountered that require proper task execution on the first try. Therefore, after the evaluations were completed with all the pilots, limited one-versus-one engagements were flown against a basic F-18 airplane. No problems were found in adjusting between flight conditions; both predictability and controllability remained good. The one-versus-one results are not presented herein.

Note that CHR's from the three pilots varied by only one number for 76 percent of the tasks and by no more than two numbers for any task. This rating spread was considered very good and implies that the tasks were well defined. When wide variations in the ratings are received, Cooper-Harper stated that the problem is usually traceable to poorly defined tasks.

### Nose-Up Angle-of-Attack Capture Tasks

The $\alpha$ captures were conducted from two initial conditions: $1g$ trim at Mach 0.6 and $1g$ trim at $\alpha = 20°$. The captures from Mach 0.6 provided high $q$ and $\dot{\alpha}$ during pull-ups and assessed the effects of mode transition from dominant $n_z$ to dominant $\alpha$ command. The captures from $\alpha = 20°$ produced lower $q$ and $\dot{\alpha}$ values and the system remained in the $\alpha$-command mode for the entire maneuver.

For each maneuver, the configuration was trimmed at the initial condition. When the simulation began, the pilot selected maximum A/B (maximum thrust), rolled to a bank angle $\phi$ of approximately 45°, waited 2.0 sec for the engine to reach maximum power, and then pulled aggressively to capture the target $\alpha$. From the time maximum A/B was applied to the beginning of the maneuver, Mach typically increased $\leq 0.02$. A nonzero $\phi$ was used during the maneuvers to prevent excessive energy loss and the possibility of entering a tail slide during the captures from high speeds to high $\alpha$'s. For consistency, the nonzero bank angle was also used for the lower speed initial condition and smaller $\alpha$ changes.

The Cooper-Harper task tolerance criteria required that the capture be within ±4° for *desirable* and ±7° for *adequate*. No overshoots or undershoots which exceeded the above criteria were allowed. The task tolerance guidelines were intentionally restrictive to make pilot gains high, which would aggrevate any pilot induced oscillation (PIO) tendencies that might exist. The CHR's for each pilot are shown in figures 25 and 26 as a function of target $\alpha$. The stringent *desirable* criterion was met (CHR $\leq 4$) for all but two cases. One pilot gave the 45° capture from Mach 0.6 a CHR of 5; a different pilot gave the 60° capture from Mach 0.6 a CHR of 5.

The $\alpha$ captures at 15° and 30° were conducted with less than maximum aft stick to meter the pitch rates for these relatively small $\alpha$ changes. With full-stick inputs, an $\alpha$ capture without an overshoot outside the *desirable* criterion was not possible. The pilots considered the use of less than maximum aft stick a natural technique that produced good pitch rates and capture times.

The $\alpha$ captures at 45° were accomplished with a technique similar to the procedure used for the lower $\alpha$'s. However, more aft stick and higher rates could be applied. For the Mach 0.6 case, one of the pilots considered the rates required to obtain *desirable* criterion "sluggish." When more aggressive, the pilot could only do the capture within ±5°, which resulted in a CHR of 5 (*adequate* criterion met).

At $\alpha = 60°$, very little pitch control power remains and the high rates obtained from the Mach 0.6 pull-up made the *desirable* criterion difficult to meet. Two of the pilots were able to meet the *desirable* criterion consistently; the other pilot was only able to meet the *adequate* criterion.

For the FFCG described in reference 7, the $\alpha$ captures of 30° and 45° from Mach 0.6 presented a problem. For a capture of $\alpha = 30°$, the $n_z$ to $\alpha$ transition occurred at 30°; for a capture of $\alpha = 45°$, the transition occurred just before 45°. The FFCG stick gains of reference 7 changed noticeably when the mode transitions occurred, which resulted in a commanded $\alpha$ change. This problem was not discovered in batch simulation runs. The new implementation of the CGT described herein works smoothly and causes no problems for these tasks. Transition is almost undetectable by the pilot.

### Nose-Down Angle-of-Attack Capture Tasks

One nose-down capture maneuver was used to evaluate the nose-down rate, nose-down handling qualities, and transition from $\alpha$ command to $n_z$ command. The configuration was trimmed at $1g$ and $\alpha = 60°$. When the task began, the pilot pushed

over aggressively to momentarily capture $\alpha = 10°$ and then recover to $1g$ level flight at 250 KCAS. The CHR's primarily reflect the $\alpha$ capture of 10°. A recovery to $1g$ level flight was done to assure that no problems occurred with the $\alpha$ to $n_z$ mode transition. This maneuver was designed to evaluate nose-down pointing capability from a poststall initial condition. However, the maneuver was not intended to address minimum altitude loss, which is attained by a pushover to maximum lift $\alpha = 37°$.

The Cooper-Harper task tolerance criteria required that the $\alpha$ capture be within $\pm 4°$ for *desirable* and $\pm 7°$ for *adequate*. The resulting CHR's are shown in figure 27. With the FFCG from reference 7, this task received CHR's of 7 from all pilots because of some problems not detected during the batch simulation runs. During batch runs, the stick motion was exact, which resulted in good captures for the original system. However, during piloted simulation, the initial stick position for the capture was not as precise. Small errors in initial stick position set up large amplitude oscillations induced by mode transitions caused by small correcting motions of the stick during the capture attempt. The FFCG discussed herein solved this problem and yielded CHR's of 3 or 4. The pilots still approached the task with caution because the available very high nose-down rates were difficult to arrest within the *desirable* criterion. The technique that was finally settled upon incorporated slightly less than maximum forward stick to make the capture more predictable. The resulting workload was high but the task was repeatable with the intentionally reduced nose-down rate. All of the pilots liked the nose-down rate capability, thought they could meter the rate as needed, and liked the reassurance that $\alpha$ could be rapidly decreased for a quick recovery from poststall if necessary.

The transition from $\alpha$ to $n_z$ command during the acceleration to 250 KCAS caused a very slight pitch bobble, which the pilots did not consider to be a problem.

### $g$-Heading Capture Task

Maneuvers were also conducted to evaluate the $n_z$ mode of the control system. These maneuvers started with the configuration trimmed at $1g$ and Mach 0.6. When the simulation started, the pilot rolled to an appropriate bank angle (approximately 60° for $2g$ and 85° for $3g$) and pulled to capture the target $n_z$. The $g$ and Mach number were held for 90° of heading change and followed by a heading capture. The pilots were requested to rate the longitudinal and lateral-directional task separately. Only longitudinal results are given here.

Cooper-Harper longitudinal task tolerance criteria required that the $g$ capture be made and the $g$ held within $\pm 0.2g$ for *desirable* and $\pm 0.3g$ for *adequate*. As shown in figure 28, the CHR's given for both the $2g$ and $3g$ captures were 4 or better, which indicated *desirable* criterion was met in all cases. Two pilots had generally favorable comments about the $g$ captures; one of the two pilots noted a slight overshoot tendency. One pilot commented that there was a tendency to overshoot and to drift away from the target $g$ but did not consider this a serious problem, just somewhat annoying. The overshoot and drift tendency may not exist in the $g$ environment of the real airplane when compared with the fixed base simulator. One pilot had difficulty deciding between a 3 and 4 CHR for the $3g$ task. The pilot considered handling qualities very good but thought the system could be improved.

### Coupling-During-Roll Evaluation Tasks

Two sets of roll maneuvers were conducted to evaluate the lateral-directional control law (not discussed herein) and coupling to the longitudinal axis during rolls. Changes in $\alpha$ during rolls can significantly alter airplane roll performance and energy state as well as lead to departures (airplane not responsive to pilot commands). Also, during gross acquisition tasks (pointing) at high $\alpha$, both the lateral-directional and longitudinal axes directly affect the capture. To augment target acquisition and prevent departures, $\alpha$ must be controllable. Therefore, during the roll tasks, the pilots were required to give CHR's on $\alpha$ regulation.

The Cooper-Harper $\alpha$-control criteria during rolls required that $\alpha$ be maintained within $\pm 2°$ for *desirable* and within $\pm 6°$ for *adequate*. The *desirable* criterion is extremely stringent, which makes the pilot gains high and potential problems with the controller more noticeable. The stringent criterion would also produce less favorable CHR's. The two maneuvers were $1g$ and loaded rolls. In both rolls, the pilots used maximum lateral stick. The $1g$ rolls started from a trimmed condition at the desired $\alpha$ and rolled through 360° to capture wings level ($\phi = 0°$) after the roll. The loaded rolls were more difficult. They required an initial nonzero $\phi$ at the desired $\alpha$ and Mach followed by a roll to capture $\phi = 90°$ on the opposite side. Bank angle changes from 120° to 180° were noted during loaded rolls. The loaded rolls at $\alpha = 5°$ and Mach 0.6 and at $\alpha = 15°$ and Mach 0.4 were at or near $1g$ to give a comparison between the $1g$ and loaded maneuver types. Results from the two types of rolls were very similar. The CHR's from the

$\alpha$ regulation are shown in figure 29 for the $1g$ rolls and in figures 30 and 31 for the loaded rolls.

For all but one pilot at one $\alpha$, *desirable* criterion was met (CHR $\leq$ 4) even with the very stringent $\alpha$ regulation requirement. With the exception of $\alpha$'s of 5° and 15°, difficulty in controlling $\alpha$ occurred only at the beginning of the rolls where small excursions in $\alpha$ were noted. These excursions were caused by slight longitudinal stick inputs associated with the lateral stick input and kinematic coupling ($\alpha$ changes which resulted from small $\beta$ changes at the roll onset). Roll rate is automatically limited by the lateral-directional control law to prevent inertial coupling pitchout. Therefore, pitch surface saturation was not seen and regulation of $\alpha$ was very good with a low workload once the roll was established for $\alpha$'s $> 15°$.

At $\alpha = 5°$, the roll occurred so fast that the pilots had no time to react to $\alpha$ changes. However, if there was no longitudinal stick input associated with the lateral input, $\alpha$ did not change much, which resulted in good CHR's.

The rolls conducted at $\alpha = 15°$ produced the highest workload, particularly for the $1g$ rolls. At $\alpha = 15°$, changes in Mach number during the rolls produced changes in $\alpha$ since the control law was in the $n_z$ mode. During the loaded rolls, these changes meant that small pilot stick corrections were required as the Mach number changed. During the $1g$ rolls at $\alpha = 15°$, small stick inputs caused mode transitions back and forth between the $\alpha$ and $n_z$ commands, which made the task difficult. However, most pilots were consistently able to maintain the very strict *desirable* $\alpha$-control criterion during the rolls.

Overall, the pilots commented that the ability to control $\alpha$ during rolls exceeded their expectations and was superior to anything they had previously flown. The task required very little attention except at the very beginning of the roll and at $\alpha = 15°$.

### Tracking Evaluation Tasks

Two tracking tasks were performed using a prerecorded target. The tasks were both done at approximately $3g$, with one task at Mach 0.45 ($\alpha$'s from 15° to 25°) and one at Mach 0.6 ($\alpha$'s from 10° to 20°). These tasks provided an evaluation of the acquisition and tracking capability of the configuration in the moderate-$\alpha$ range. During the low-speed (Mach 0.45) task, the effect of mode transitions between the $\alpha$ and $n_z$ commands on tracking were evaluated. The target was set 600 ft directly ahead of the test configurations at the start of the run. When the maneuver started, the target rolled into a $3g$ turn while holding a constant Mach number. Thirty seconds after the run began, the target reversed to a $3g$ turn in the opposite direction. From there, reversals were done at 40 and 50 sec and the run ended at 70 sec. For the run to be considered valid, the range to the target could not exceed 1800 ft at any time and the Mach number could not vary by more than $\pm 0.05$.

The Cooper-Harper task criteria were to keep the target within a 12.5-mrad-diameter pipper 50 percent of the time for *desirable*, and 10 percent of the time for *adequate* tracking. The tracking criteria were not to include the time during reversals. The longitudinal axis CHR's for both Mach numbers are shown in figure 32. *Desirable* criterion was achieved by all pilots for both tasks.

When these same tasks were performed with the control system described in reference 7, ratings were in the 5 to 6 region for the Mach 0.45 case due to PIO's induced by mode transitions. With the current FFCG implementation, the pilots were unable to detect mode transitions. However, level 2 ratings were still given by two of the three pilots because of a tendency for the nose to drift above the target while tracking in the $n_z$ mode; the tendency for the nose to drift increased the pilot workload. The pilot that gave a level 1 rating did not consider the gradual correction for the nose-up drift to be a problem. The nose-up drift was caused by the change in $\alpha_{oc}$ in response to a change in the $n_z$ command. Without a change in $\alpha_{oc}$, undetectable transitions between modes would not be possible.

The Mach 0.6 tracking tasks did not include mode transitions and the pilot comments were good overall. However, the configuration was considered a little sensitive in pitch and the nose-up drift tendency was again noted. One pilot gave a CHR of 4 because a slight PIO tendency increased the workload, which caused a reaction to "consciously get out of the loop."

### Departure Resistance

The pilots attempted to depart the airplane with a series of predetermined inputs and other inputs of their choice. The system was proven to be extremely departure resistant. The only resemblance to departure occurred during high-rate rolls at either low or high $\alpha$ with attempts to make large changes in $\alpha$ either with or without a reversal of the roll rate. For coordinated rolls (by neglecting gravity effects and setting $\beta \cong 0$), the relationship between body-axis roll rate $p$ and body-axis yaw rate $r$ is

$$r = p \tan \alpha \tag{31}$$

Therefore, when rapid changes in $\alpha$ occurred during rolls, $p$ and $r$ changes are required to maintain coordination. The changes could not be done fast enough, which resulted in large $\alpha$ and $\beta$ excursions due to kinematic coupling. Recovery from these excursions was always immediate.

## Conclusions

This paper describes the design, analysis, and simulation of a longitudinal controller for the F-18 HARV. The following list contains the main conclusions and additional explanation where required:

1. The output feedback gains are highly nonlinear for the range of angle of attack $\alpha$. Load factor $n_z$ has a major effect on the gains, whereas altitude has a minor effect for the HARV altitude range of 15 000–35 000 ft.

2. The closed-loop control system has good damping characteristics (as illustrated in the three example cases) even though the high-$\alpha$ example design case has an unstable open-loop short period. Also, the closed-loop phugoid is stable for all 39 design conditions even though the open-loop phugoid is unstable at a few design conditions.

3. The closed-loop control system meets the gain and phase margin guidelines of $\pm 6$ dB and $\pm 45°$, respectively, at both the plant input and output for the entire HARV flight regime. Results from 177 flight conditions show that nondesign cases are as equally robust to gain and phase changes as the 39 design cases, which illustrates that the controller is not sensitive to off-design conditions.

4. The closed-loop control system has good robustness to changes in plant output gains and changes to stability and control derivatives. A real-$\mu$ analysis for a multiplicative error at the plant output with all three output loops opened shows that gain changes of 60 percent are needed to drive the closed-loop system unstable. For the $\mu$ analysis of four stability derivatives that affect the short period, gain changes greater than 100 percent are required for instability; results for four control derivatives show that gain changes of at least 90 percent are required for instability. Although no established guidelines exist for this type of analysis, all of these results are considered quite good and indicate a reasonably robust control system.

5. The controller has good structural mode attenuation and greatly exceeds the guideline. Singular-value loop transfer analysis at both the plant input and plant output showed that a structural mode at 100 rad/sec was attenuated to approximately $-20$ dB. This attenuation is significantly greater than the guideline of $-8$ dB.

6. Nonlinear batch simulation analysis shows that the controller exhibits good agility and meets most of the guidelines for the entire $\alpha$ range. Pitch-up agility results show that $q$ meets or exceeds the guidelines until initial trim $\alpha$ increases to approximately 45° where $q$ drops slightly below the guideline. Similarly, $\dot{q}$ meets or exceeds the guideline until initial trim $\alpha$ increases to 55° where $\dot{q}$ drops slightly below. There is currently no guideline above $\alpha = 55°$. In addition, pitch-down results show that both $q$ and $\dot{q}$ are significantly better than their tactical guidelines.

7. During the pitch-up agility maneuver, the control system will make a smooth transition from an $n_z$-command mode to an $\alpha$-command mode. The smooth time response indicates good integration between the feedback and feed-forward controllers.

8. Based upon nonlinear batch simulation analysis, the $\alpha$ regulation during full-lateral stick stability-axis rolls is considerably better than the $\pm 6°$ guideline for a 90° roll and $\pm 10°$ guideline for a 360° roll, which indicates a tight control system.

9. Nonlinear batch simulation analysis shows that the controller has good $\alpha$-capture capability and consistency for the design altitude range. Several $\alpha$ captures illustrate similar transient responses at all altitudes within the HARV flight envelope. Small differences in steady-state values result from variations in the feed-forward gains within the command generator; these differences can be corrected by small changes in pilot stick position. All plots show very little overshoot, which indicates a highly damped feedback control system at all altitudes.

10. Piloted simulation uncovered problems with an earlier control law design. The modified control law discussed herein receives good Cooper-Harper ratings (CHR) with *desirable* criteria pilot responses for most tasks. The flying qualities are mostly level 1 or close to the level 1 to level 2 boundary. Piloted simulation shows the following:

    A. Almost all (19 of 21) CHR's for the nose-up $\alpha$ captures meet the stringent *desirable* criterion of $\pm 4°$, which is considered good for this task.

    B. All pilots like the nose-down pitch rate capability and the reassurance that $\alpha$ can be rapidly decreased for a quick recovery from

poststall if necessary. Maximum pitch rate makes meeting the *desirable* capture criterion of $\pm 4^\circ$ difficult; *desirable* criterion is attainable by using less than the maximum rate.

C. Cooper-Harper ratings for both the $2g$ and $3g$ captures show that *desirable* criterion was met by all pilots.

D. A very stringent *desirable* criterion of $\pm 2^\circ$ was used for the $\alpha$ regulation during full lateral stick rolls at several different $\alpha$'s and $g$'s. The two maneuvers were $1g$ rolls and loaded rolls. Overall, pilots commented that the ability to control $\alpha$ during rolls exceed their expectations and the controller is superior to anything they had previously flown. This is reflected by the CHR's of mostly level 1.

E. Tracking evaluation tasks have CHR's of either 3 or 4. Pilot comments for the Mach 0.6 tracking tasks were good overall but the configuration was considered a little sensitive in pitch. During the Mach 0.45 task, there is a tendency for the nose to drift above the target while tracking in the $n_z$ mode, which resulted in level 2 ratings because of increased pilot workload. The nose-up drift is caused by a change in $\alpha$ bias that is estimated in the feed-forward command generator.

F. With this control system, the airplane is extremely departure resistant.

NASA Langley Research Center
Hampton, VA 23681-0001
May 25, 1994

# Appendix

## Open-Loop Models

This appendix contains the 39 longitudinal open-loop airplane models for the operating conditions described in table II. In addition, transfer functions for the longitudinal actuators, sensor, and antialiasing filters are included.

### Open-Loop Airplane Models

The following are state-transition matrices **A** and the control matrices **B** for the 39 airplane models. Each model has four states and two controls in the following order:

1. $V$ total velocity, ft/sec
2. $\alpha$ angle of attack, deg
3. $q$ pitch rate, deg/sec
4. $\theta$ pitch attitude, deg
5. $\delta_s$ symmetric stabilator control, deg
6. $\delta_v$ pitch thrust vector control, deg

All numbers smaller than 1.0E−10 are shown as 0. Models 7, 20, and 33 have the $\delta_s$ control elements set to zero because $\delta_s$ is in saturation at those operating conditions.

**A1**

| | | | |
|---|---|---|---|
| −1.3820E−02 | 8.7773E−02 | 2.0660E−03 | −5.6184E−01 |
| −7.8960E−03 | −1.0817E+00 | 9.8815E−01 | 0 |
| −5.4849E−03 | −7.5943E+00 | −5.9355E−01 | 0 |
| 0 | 0 | 1.0 | 0 |

**B1**

| | |
|---|---|
| −2.0803E−01 | −9.2081E−03 |
| −1.7612E−01 | −1.7350E−02 |
| −1.2839E+01 | −1.5944E+00 |
| 0 | 0 |

**A2**

| | | | |
|---|---|---|---|
| −1.4508E−02 | 9.5986E−03 | 1.4572E−03 | −5.6184E−01 |
| −9.9970E−03 | −8.7803E−01 | 9.8797E−01 | 0 |
| −3.1497E−03 | −4.5764E+00 | −4.7959E−01 | 0 |
| 0 | 0 | 1.0000E+00 | 0 |

**B2**

| | |
|---|---|
| −1.5206E−01 | −9.6873E−04 |
| −1.5669E−01 | −1.6548E−02 |
| −9.4529E+00 | −1.3096E+00 |
| 0 | 0 |

**A3**

| | | | |
|---|---|---|---|
| −1.6234E−02 | −1.8176E−01 | −1.2164E−05 | −5.6184E−01 |
| −1.5100E−02 | −6.7351E−01 | 9.8873E−01 | 0 |
| −1.5360E−02 | −1.8918E+00 | −3.6678E−01 | 0 |
| 0 | 0 | 1.0000E+00 | 0 |

**B3**

| | |
|---|---|
| −1.3552E−01 | 1.0202E−02 |
| −1.2994E−01 | −2.2488E−02 |
| −6.1738E+00 | −1.4189E+00 |
| 0 | 0 |

**A4**

| | | | |
|---|---|---|---|
| −5.6223E−02 | −3.5131E−01 | 6.8777E−07 | −5.6184E−01 |
| −4.2307E−02 | −2.4410E−01 | 9.9043E−01 | 5.7095E−09 |
| −4.3225E−03 | −3.5517E−01 | −1.8620E−01 | 0 |
| 0 | 0 | 1.0000E+00 | 0 |

**B4**

| | |
|---|---|
| −1.3776E−01 | −9.1970E−02 |
| −5.4475E−02 | −5.2898E−02 |
| −1.4900E+00 | −1.9423E+00 |
| 0 | 0 |

**A5**

| | | | |
|---|---|---|---|
| −1.1579E−01 | −2.2796E−01 | 0 | −5.6184E−01 |
| −5.5977E−02 | −1.0120E−01 | 9.8545E−01 | 1.0403E−08 |
| −7.9017E−03 | −3.3627E−01 | −3.1355E−01 | 0 |
| 0 | 0 | 1.0000E+00 | 0 |

**B5**

| | |
|---|---|
| −1.3844E−01 | −1.2089E−01 |
| −4.1732E−02 | −5.5345E−02 |
| −8.3743E−01 | −1.6899E+00 |
| 0 | 0 |

**A6**

| | | | |
|---|---|---|---|
| −1.7673E−01 | −8.4210E−02 | 0 | −5.4781E−01 |
| −4.6829E−02 | −1.2849E−02 | 9.8455E−01 | 3.4351E−02 |
| −1.4699E−02 | −7.2936E−01 | 6.3096E−02 | −1.8667E−08 |
| 0 | 0 | 1.0000E+00 | 0 |

**B6**

| | |
|---|---|
| −1.6849E−01 | −1.6234E−01 |
| −3.5964E−02 | −4.4747E−02 |
| −9.0676E−01 | −1.5776E+00 |
| 0 | 0 |

**A7**

| | | | |
|---|---|---|---|
| −2.1712E−01 | 1.7024E−02 | 0 | −4.8505E−01 |
| −3.3469E−02 | 1.9644E−03 | 9.9217E−01 | 7.1098E−02 |
| −1.8319E−01 | −1.6056E+00 | −1.4794E−01 | 0 |
| 0 | 0 | 1.0000E+00 | 0 |

**B7**

| | |
|---|---|
| 0 | −1.5970E−01 |
| 0 | −6.1952E−02 |
| 0 | −1.6731E+00 |
| 0 | 0 |

**A8**

| | | | |
|---|---|---|---|
| −1.6154E−01 | −5.3571E+00 | 1.1041E−05 | −5.2796E−01 |
| −1.8867E−02 | −4.8992E−01 | 9.9270E−01 | 1.4839E−02 |
| −1.2463E−01 | −3.0092E+00 | −5.6551E−01 | −2.3512E−03 |
| 0 | 0 | 1.0000E+00 | 0 |

**B8**

| | |
|---|---|
| −7.4320E−01 | −8.5983E−02 |
| −1.3302E−01 | −1.7313E−02 |
| −1.1481E+01 | −1.6478E+00 |
| 0 | 0 |

**A9**

| | | | |
|---|---|---|---|
| −1.3529E−01 | −3.7725E+00 | 8.4638E−06 | −5.2796E−01 |
| −2.3634E−02 | −4.5269E−01 | 9.9120E−01 | 1.7294E−02 |
| −5.6183E−02 | −2.5589E+00 | −5.1387E−01 | −2.5570E−03 |
| 0 | 0 | 1.0000E+00 | 0 |

**B9**

| | |
|---|---|
| −5.5771E−01 | −8.2526E−02 |
| −1.2017E−01 | −1.9626E−02 |
| −8.2145E+00 | −1.6084E+00 |
| 0 | 0 |

**A10**

| | | | |
|---|---|---|---|
| −3.5560E−01 | −5.2092E+00 | 9.2728E−06 | −4.6023E−01 |
| −2.6876E−02 | −1.2073E−01 | 9.9055E−01 | 2.9005E−02 |
| −1.1284E−01 | −3.0182E+00 | −7.2036E−01 | −5.5447E−03 |
| 0 | 0 | 1.0000E+00 | 0 |

**B10**

| | |
|---|---|
| −1.1147E+00 | −1.3829E−01 |
| −1.2122E−01 | −1.8472E−02 |
| −7.289E+00 | −1.5717E+00 |
| 0 | 0 |

**A11**

| | | | |
|---|---|---|---|
| −8.3637E−02 | −1.4968E+00 | 3.0657E−06 | −5.2796E−01 |
| −2.9880E−02 | −3.7019E−01 | 9.9074E−01 | 2.5934E−02 |
| −9.8652E−03 | −1.0042E+00 | −3.0333E−01 | −2.1694E−03 |
| 0 | 0 | 1.0000E+00 | 0 |

**B11**

| | |
|---|---|
| −2.8741E−01 | −8.9009E−02 |
| −8.1484E−02 | −3.3312E−02 |
| −3.4843E+00 | −1.8354E+00 |
| 0 | 0 |

**A12**

| | | | |
|---|---|---|---|
| −2.3270E−01 | −2.1267E+00 | 3.4749E−06 | −4.6023E−01 |
| −3.2597E−02 | −1.4597E−01 | 9.8796E−01 | 4.3511E−02 |
| −2.1477E−03 | −1.1324E+00 | −5.4560E−01 | −4.2250E−03 |
| 0 | 0 | 1.0000E+00 | 0 |

**B12**

| | |
|---|---|
| −5.1037E−01 | −1.4977E−01 |
| −8.1249E−02 | −3.0518E−02 |
| −3.2163E+00 | −1.7783E+00 |
| 0 | 0 |

**A13**

| | | | |
|---|---|---|---|
| −3.3181E−03 | 2.8017E−01 | 5.0069E−04 | −5.5970E−01 |
| −2.4662E−02 | −4.4944E−01 | 9.8834E−01 | 8.7995E−03 |
| −8.4316E−03 | −6.3550E−01 | −2.4997E−01 | −6.5673E−04 |
| 0 | 0 | 1.0000E+00 | 0 |

**B13**

| | |
|---|---|
| −5.5619E−02 | −1.7506E−02 |
| −8.0847E−02 | −4.5433E−02 |
| −2.4145E+00 | −1.8266E+00 |
| 0 | 0 |

**A14**

| | | | |
|---|---|---|---|
| −8.5408E−02 | 2.0597E−02 | 0 | −3.9728E−01 |
| −7.7199E−02 | −2.8976E−01 | 9.7760E−01 | 2.1499E−01 |
| −2.7813E−02 | −1.6733E−01 | 3.7533E−03 | −1.5131E−03 |
| 0 | 0 | 1.0000E+00 | 0 |

**B14**

| | |
|---|---|
| −2.8710E−02 | −1.3626E−01 |
| −9.9186E−03 | −8.8371E−02 |
| −1.1328E−01 | −1.5340E+00 |
| 0 | 0 |

**A15**

| | | | |
|---|---|---|---|
| −9.7850E−03 | −5.7081E−02 | 1.5858E−04 | −5.6184E−01 |
| −8.5016E−03 | −7.3240E−01 | 9.9172E−01 | 0 |
| −1.0039E−02 | −4.5444E+00 | −4.0645E−01 | 0 |
| 0 | 0 | 1.0000E+00 | 0 |

**B15**

| | |
|---|---|
| −1.4961E−01 | −1.4081E−02 |
| −1.2498E−01 | −1.8662E−02 |
| −8.7086E+00 | −1.6570E+00 |
| 0 | 0 |

**A16**

| | | | |
|---|---|---|---|
| −1.2892E−02 | −2.1418E−01 | −3.7871E−04 | −5.6184E−01 |
| −1.1163E−02 | −5.8328E−01 | 9.9204E−01 | 0 |
| −1.2438E−02 | −2.2707E+00 | −2.9286E−01 | 0 |
| 0 | 0 | 1.0000E+00 | 0 |

**B16**

| | |
|---|---|
| −1.3355E−01 | 1.3123E−02 |
| −1.0916E−01 | −2.3759E−02 |
| −6.0317E+00 | −1.7385E+00 |
| 0 | 0 |

**A17**

| | | | |
|---|---|---|---|
| −4.7573E−02 | −3.4273E−01 | 1.3207E−06 | −5.6184E−01 |
| −3.0705E−02 | −2.0042E−01 | 9.9325E−01 | −2.5008E−08 |
| −5.96180E−03 | −4.1837E−01 | −1.6415E−01 | 1.1045E−09 |
| 0 | 0 | 1.0000E+00 | 0 |

**B17**

| | |
|---|---|
| −1.3713E−01 | −1.0277E−01 |
| −4.6247E−02 | −5.0505E−02 |
| −1.5134E+00 | −2.1825E+00 |
| 0 | 0 |

**A18**

| | | | |
|---|---|---|---|
| −1.0177E−01 | −2.4735E−01 | 3.1883E−07 | −5.5799E−01 |
| −3.9980E−02 | −8.6942E−02 | 9.9013E−01 | 1.4028E−02 |
| −6.7700E−03 | −3.5285E−01 | −2.6703E−01 | −4.8352E−04 |
| 0 | 0 | 1.0000E+00 | 0 |

**B18**

| | |
|---|---|
| −1.4826E−01 | −1.3222E−01 |
| −3.6851E−02 | −4.6204E−02 |
| −9.1317E−01 | −1.7296E+00 |
| 0 | 0 |

**A19**

| | | | |
|---|---|---|---|
| −1.5425E−01 | −8.4298E−02 | 2.0793E−07 | −5.1488E−01 |
| −3.4121E−02 | −1.4329E−02 | 9.8976E−01 | 4.9099E−02 |
| −6.7871E−03 | −8.3303E−01 | 5.6289E−02 | −2.9045E−08 |
| 0 | 0 | 1.0000E+00 | 0 |

**B19**

| | |
|---|---|
| −1.9471E−01 | −1.7359E−01 |
| −3.2122E−02 | −3.8558E−02 |
| −1.0246E+00 | −1.6324E+00 |
| 0 | 0 |

**A20**

| | | | |
|---|---|---|---|
| −1.9607E−01 | 1.8325E−02 | −1.6409E−06 | −4.1903E−01 |
| −2.4170E−02 | −1.4411E−03 | 9.9445E−01 | 7.4421E−02 |
| −1.8499E−01 | −1.8167E+00 | −1.3313E−01 | 0 |
| 0 | 0 | 1.0000E+00 | 0 |

**B20**

| | |
|---|---|
| 0 | −1.3378E−01 |
| 0 | −6.0197E−02 |
| 0 | −1.5525E+00 |
| 0 | 0 |

**A21**

| | | | |
|---|---|---|---|
| −1.0807E−01 | −3.3520E+00 | 2.4961E−05 | −5.2796E−01 |
| −1.5263E−02 | −3.5068E−01 | 9.9473E−01 | 1.5453E−02 |
| −8.8227E−02 | −2.1792E+00 | −3.9173E−01 | −1.6769E−03 |
| 0 | 0 | 1.0000E+00 | 0 |

**B21**

| | |
|---|---|
| −4.8658E−01 | −1.1236E−01 |
| −9.3115E−02 | −2.3958E−02 |
| −7.7126E+00 | −2.1991E+00 |
| 0 | 0 |

**A22**

| | | | |
|---|---|---|---|
| −9.0217E−02 | −2.3089E+00 | 1.0059E−05 | −5.2796E−01 |
| −1.8762E−02 | −3.2189E−01 | 9.9368E−01 | 1.8015E−02 |
| −4.2194E−02 | −1.8691E+00 | −3.5513E−01 | −1.8242E−03 |
| 0 | 0 | 1.0000E+00 | 0 |

**B22**

| | |
|---|---|
| −3.6674E−01 | −1.0256E−01 |
| −8.3857E−02 | −2.7735E−02 |
| −5.4902E+00 | −2.1717E+00 |
| 0 | 0 |

**A23**

| | | | |
|---|---|---|---|
| −2.4062E−01 | −3.2907E+00 | 1.0574E−05 | −4.6023E−01 |
| −2.1200E−02 | −9.6559E−02 | 9.9322E−01 | 3.0214E−02 |
| −8.3068E−02 | −2.0079E+00 | −4.9663E−01 | −3.9556E−03 |
| 0 | 0 | 1.0000E+00 | 0 |

**B23**

| | |
|---|---|
| −7.3373E−01 | −1.7643E−01 |
| −8.4626E−02 | −2.5778E−02 |
| −4.8796E+00 | −2.1050E+00 |
| 0 | 0 |

**A24**

| | | | |
|---|---|---|---|
| −5.5589E−02 | −8.0799E−01 | 3.0757E−06 | −5.2796E−01 |
| −2.4970E−02 | −2.6540E−01 | 9.9336E−01 | 2.7017E−02 |
| −8.0941E−03 | −7.0241E−01 | −2.0921E−01 | −1.5478E−03 |
| 0 | 0 | 1.0000E+00 | 0 |

**B24**

| | |
|---|---|
| −1.8889E−01 | −9.0045E−02 |
| −5.6406E−02 | −3.8613E−02 |
| −2.3135E+00 | −2.0235E+00 |
| 0 | 0 |

**A25**

| | | | |
|---|---|---|---|
| −1.5769E−01 | −1.2464E+00 | 3.3212E−06 | −4.6023E−01 |
| −2.6517E−02 | −1.1676E−01 | 9.9138E−01 | 4.5323E−02 |
| −4.9043E−03 | −7.5576E−01 | −3.7520E−01 | −3.0141E−03 |
| 0 | 0 | 1.0000E+00 | 0 |

**B25**

| | |
|---|---|
| −3.3591E−01 | 1.5702E−01 |
| −5.6241E−02 | −3.5324E−02 |
| −2.1366E+00 | −1.9487E+00 |
| 0 | 0 |

**A26**

| | | | |
|---|---|---|---|
| −1.4799E−03 | 3.7474E−01 | 3.4523E−04 | −5.5970E−01 |
| −2.4318E−02 | −3.1274E−01 | 9.9165E−01 | 9.1706E−03 |
| −5.7837E−03 | −4.2394E−01 | −1.7267E−01 | −4.7388E−04 |
| 0 | 0 | 1.0000E+00 | 0 |

**B26**

| | |
|---|---|
| −3.7089E−02 | −1.2182E−02 |
| −5.5740E−02 | −4.8642E−02 |
| −1.5990E+00 | −1.8719E+00 |
| 0 | 0 |

**A27**

| | | | |
|---|---|---|---|
| −5.8649E−02 | 1.4562E−01 | 0 | −3.9728E−01 |
| −9.7055E−02 | −2.7542E−01 | 9.8401E−01 | 2.2381E−01 |
| −2.0472E−02 | −1.0391E−01 | 2.3766E−03 | −1.0788E−03 |
| 0 | 0 | 1.0000E+00 | 0 |

**B27**

| | |
|---|---|
| −1.8896E−02 | −1.3304E−01 |
| −6.8075E−03 | −9.1693E−02 |
| −7.4668E−02 | −1.5150E+00 |
| 0 | 0 |

**A28**

| | | | |
|---|---|---|---|
| −8.8257E−03 | −2.7677E−01 | −9.4246E−04 | −5.6184E−01 |
| −9.0749E−03 | −4.7549E−01 | 9.9486E−01 | 0 |
| −1.8778E−02 | −2.3763E+00 | −2.4379E−01 | 0 |
| 0 | 0 | 1.0000E+00 | 0 |

**B28**

| | |
|---|---|
| −1.3431E−01 | 9.7489E−03 |
| −8.3626E−02 | −2.1907E−02 |
| −5.4646E+00 | −1.8154E+00 |
| 0 | 0 |

**A29**

| | | | |
|---|---|---|---|
| −1.3503E−02 | −3.4369E−01 | −1.3901E−03 | −5.6184E−01 |
| −1.1684E−02 | −3.8144E−01 | 9.9544E−01 | 0 |
| −1.5311E−02 | −1.1206E+00 | −1.4936E−01 | 0 |
| 0 | 0 | 1.0000E+00 | 0 |

**B29**

| | |
|---|---|
| −1.3362E−01 | 2.3442E−03 |
| −7.4738E−02 | −2.7580E−02 |
| −3.8958E+00 | −1.9604E+00 |
| 0 | 0 |

**A30**

| | | | |
|---|---|---|---|
| −3.6378E−02 | −3.3058E−01 | 1.3543E−06 | −5.6178E−01 |
| −2.1764E−02 | −1.6148E−01 | 9.9540E−01 | 1.1630E−03 |
| −9.9397E−03 | −5.0165E−01 | −1.4496E−01 | −4.5991E−05 |
| 0 | 0 | 1.0000E+00 | 0 |

**B30**

| | |
|---|---|
| −1.2523E−01 | −1.1121E−01 |
| −3.8871E−02 | −4.1541E−02 |
| −1.5783E+00 | −2.1698E+00 |
| 0 | 0 |

**A31**

| | | | |
|---|---|---|---|
| −8.8703E−02 | −2.6830E−01 | 7.5841E−07 | −5.4041E−01 |
| −2.7580E−02 | −7.2754E−02 | 9.9365E−01 | 2.6327E−02 |
| −3.3416E−03 | −3.6790E−01 | −2.2129E−01 | −9.0744E−04 |
| 0 | 0 | 1.0000E+00 | 0 |

**B31**

| | |
|---|---|
| −1.5815E−01 | −1.7097E−01 |
| −3.2152E−02 | −4.3409E−02 |
| −9.9877E−01 | −2.0099E+00 |
| 0 | 0 |

**A32**

| | | | |
|---|---|---|---|
| −1.3235E−01 | −8.0098E−02 | 7.6752E−07 | −4.7441E−01 |
| −2.3482E−02 | −1.3921E−02 | 9.9361E−01 | 5.2846E−02 |
| −3.4882E−03 | −9.0622E−01 | 4.7900E−02 | −3.3557E−08 |
| 0 | 0 | 1.0000E+00 | 0 |

**B32**

| | |
|---|---|
| −2.1363E−01 | −2.1852E−01 |
| −2.7498E−02 | −3.6346E−02 |
| −1.0958E+00 | −1.8787E+00 |
| 0 | 0 |

**A33**

| | | | |
|---|---|---|---|
| −1.5347E−01 | 1.2320E−02 | −7.5442E−07 | −4.0696E−01 |
| −1.8737E−02 | 9.2665E−04 | 9.9604E−01 | 6.4489E−02 |
| −7.6505E−02 | −2.4306E+00 | −4.2878E−02 | 0 |
| 0 | 0 | 1.0000E+00 | 0 |

**B33**

| | |
|---|---|
| 0 | −1.0623E−01 |
| 0 | −3.6799E−02 |
| 0 | −1.2328E+00 |
| 0 | 0 |

**A34**

| | | | |
|---|---|---|---|
| −6.7577E−02 | −1.9369E+00 | 1.7594E−05 | −5.2796E−01 |
| −1.2335E−02 | −2.4196E−01 | 9.9631E−01 | 1.6141E−02 |
| −5.8820E−02 | −1.4745E+00 | −2.6241E−01 | −1.1617E−03 |
| 0 | 0 | 1.0000E+00 | 0 |

**B34**

| | |
|---|---|
| −3.0812E−01 | −1.1210E−01 |
| −6.2776E−02 | −2.5575E−02 |
| −4.9817E+00 | −2.2365E+00 |
| 0 | 0 |

**A35**

| | | | |
|---|---|---|---|
| −5.7268E−02 | −1.2721E+00 | 6.2707E−06 | −5.2796E−01 |
| −1.5078E−02 | −2.2124E−01 | 9.9559E−01 | 1.8821E−02 |
| −2.8420E−02 | −1.2731E+00 | −2.3747E−01 | −1.2640E−03 |
| 0 | 0 | 1.0000E+00 | 0 |

**B35**

| | |
|---|---|
| −2.3273E−01 | −1.1296E−01 |
| −5.6403E−02 | −2.9213E−02 |
| −3.5338E+00 | −2.2052E+00 |
| 0 | 0 |

**A36**

| | | | |
|---|---|---|---|
| −1.5707E−01 | −1.9160E+00 | 6.5864E−06 | −4.6023E−01 |
| −1.6732E−02 | −7.5129E−02 | 9.9527E−01 | 3.1566E−02 |
| −5.7006E−02 | −1.3094E+00 | −3.3135E−01 | −2.7408E−03 |
| 0 | 0 | 1.0000E+00 | 0 |

**B36**

| | |
|---|---|
| −4.6614E−01 | −1.8737E−01 |
| −5.6943E−02 | −2.7026E−02 |
| −3.1451E+00 | −2.1272E+00 |
| 0 | 0 |

**A37**

| | | | |
|---|---|---|---|
| −7.7855E−04 | 3.4732E−01 | 1.3703E−04 | −5.5970E−01 |
| −1.5770E−02 | −2.6909E−01 | 9.9428E−01 | 7.1889E−03 |
| −4.6668E−03 | −4.4189E−01 | −1.4684E−01 | −3.0138E−04 |
| 0 | 0 | 1.0000E+00 | 0 |

**B37**

| | |
|---|---|
| −4.0356E−02 | −3.1748E−02 |
| −4.9997E−02 | −4.4093E−02 |
| −1.8130E+00 | −2.1694E+00 |
| 0 | 0 |

**A38**

| | | | |
|---|---|---|---|
| −1.5736E−01 | −3.7928E−01 | 1.3581E−06 | −3.6114E−01 |
| −1.7558E−02 | −1.2968E−02 | 9.9421E−01 | 6.3349E−02 |
| −3.0896E−03 | −1.3071E+00 | 5.7023E−02 | 0 |
| 0 | 0 | 1.0000E+00 | 0 |

**B38**

| | |
|---|---|
| −3.0976E−01 | −2.3194E−01 |
| −3.2469E−02 | −3.2199E−02 |
| −1.5525E+00 | −1.9473E+00 |
| 0 | 0 |

**A39**

| | | | |
|---|---|---|---|
| −7.1927E−02 | 8.7245E−02 | 0 | −3.9728E−01 |
| −3.9744E−02 | −1.1375E−01 | 9.8892E−01 | 1.1686E−01 |
| −5.2789E−03 | −2.9716E−01 | 2.9038E−03 | −7.4713E−04 |
| 0 | 0 | 1.0000E+00 | 0 |

**B39**

| | |
|---|---|
| −6.3100E−02 | −1.6850E−01 |
| −2.0587E−02 | −5.5758E−02 |
| −3.8539E−01 | −1.7212E+00 |
| 0 | 0 |

### Actuator, Sensor, and Filter Transfer Functions

The stabilator transfer function is

$$\left[\frac{(36.4)^2}{s^2+2(0.41)(36.4)s+(36.4)^2}\right]\left[\frac{(105)^2}{s^2+2(0.59)(105)s+(105)^2}\right]$$

The pitch thrust-vectoring transfer function is

$$\left[\frac{(75)^2}{s^2+2(0.59)(75)s+(75)^2}\right]$$

The angle-of-attack probe transfer function is

$$\frac{14}{s+14}$$

The normal acceleration $n_z$ state-space output equation is

$$n_z=\left[\frac{V}{g}(q-\dot{\alpha})+\frac{X_{\text{acc}}}{g}\dot{q}\right]\frac{\pi}{180}$$

where true airspeed $V$ can be calculated from the Mach number (table II) and the speed of sound at the appropriate altitude, $g$ is gravity (also a function of altitude), and $X_{\text{acc}}$ is the distance of the sensor (12.35 ft) forward of the center of gravity. The $\dot{\alpha}$ and $\dot{q}$ equations are calculated from the second and third rows of the appropriate $\mathbf{A}_i$ and $\mathbf{B}_i$ matrices.

Antialiasing filter transfer functions include the following:

1. Angle of attack: $\left[\frac{(209)^2}{s^2+2(0.74)(209)s+(209)^2}\right]$
2. Pitch rate: $\left[\frac{(78.5)^2}{s^2+2(0.89)(78.5)s+(78.5)^2}\right]$
3. Load factor: $\left[\frac{(200)^2}{s^2+2(0.89)(200)s+(200)^2}\right]$

For control system analysis, all the transfer functions were included; for design, the $\alpha$ antialiasing filter was not included and the load factor antialiasing filter was approximated by a first-order filter with a 200-rad/sec bandwidth. The latter generates an extra state to eliminate the $\mathbf{D}_i$ terms in the $n_z$ output equation because the design algorithm cannot accept $\mathbf{D}_i$ terms.

## References


1. Doane, P. M.; and Gay, C. H.: *Multi-System Integrated Control (MUSIC) Program.* WRDC-TR-90-6001, U.S. Air Force, June 1990.

2. Ogburn, Marilyn E.; Nguyen, Luat T.; Wunschel, Alfred J.; Brown, Philip W.; and Carzoo, Susan W.: *Simulation Study of Flight Dynamics of a Fighter Configuration With Thrust-Vectoring Controls at Low Speeds and High Angles of Attack.* NASA TP-2750, 1988.

3. Lynch, Urban H. D.; Ettinger, Robert C.; Pelt, Jay Van; and Skow, Andrew M.: *Tactical Evaluation of the Air-to-Air Combat Effectiveness of Supermaneuverability.* WRDC-TR-90-3035, U.S. Air Force, 1990.

4. Hoffler, Keith D.; Ogburn, Marilyn E.; Nguyen, Luat T.; Brown, Philip W.; and Phillips, Michael R.: Utilization and Benefits of Advanced Aerodynamic and Propulsive Controls: A Simulator Study. *High Angle of Attack Technology–Volume II*, NASA CP-3150, 1992, pp. 87–119.

5. Matheny, Neil W., compiler: *High-Angle-of-Attack Projects and Technology Conference*, Volume 1. NASA CP-3137, 1992.

6. Davidson, J. B.; Foster, J. V.; Ostroff, A. J.; Lallman, F. R.; Murphy, P. C.; Hoffler, K. D.; and Messina, M. D.: Development of a Control Law Design Process Utilizing Advanced Synthesis Methods With Application to the NASA F-18 HARV. *The Compton Observatory Science Workshop*, Chris R. Shrader, Neil Gehrels, and Brian Dennis, eds., NASA CP-3137, vol. 4, 1992, pp. 111–157.

7. Ostroff, Aaron J.; and Proffitt, Melissa S.: *Longitudinal-Control Design Approach for High-Angle-of-Attack Aircraft.* NASA TP-3302, 1993.

8. Ostroff, Aaron J.: High-Alpha Application of Variable-Gain Output Feedback Control. *J. Guid., Control, & Dyn.*, vol. 15, Mar.–Apr. 1992, pp. 491–497.

9. Haylo, Nesim; Moerder, Daniel D.; Broussard, John R.; and Taylor, Deborah B.: *A Variable-Gain Output Feedback Control Design Methodology.* NASA CR-4226, 1989.

10. Halyo, Nesim: A Variable-Gain Output Feedback Control Design Approach. *A Collection of Technical Papers, Part 2—AIAA Guidance, Navigation and Control Conference*, Aug. 1989, pp. 1238–1248. (Available as AIAA-89-3575.)

11. Foster, John V.; Bundick W. T.; and Pahle, Joseph W.: Controls for Agility Research in the NASA High-Alpha Technology Program. SAE Paper 912148, Sept. 1991.

12. Gilbert, William P.; and Gatlin, Donald H.: Review of the NASA High-Alpha Technology Program. *High-Angle-of-Attack Technology—Volume 1*, NASA CP-3149, Part 1, 1992, pp. 23–59.

13. Buttrill, Carey S.; Arbuckle, P. Douglas; and Hoffler, Keith D.: *Simulation Model of a Twin-Tail, High Performance Airplane.* NASA TM-107601, 1992.

14. Mason, Mary L.; Capone, Francis J.; and Asbury, Scott C.: *A Static Investigation of the Thrust Vectoring System of the F/A-18 High-Alpha Research Vehicle.* NASA TM-4359, 1992.

15. Bowers, Albion H.; Noffz, Gregory K.; Grafton, Sue B.; Mason, Mary L.; and Peron, Lee R.: Multiaxis Thrust Vectoring Using Axisymmetric Nozzles and Postexit Vanes on an F/A-18 Configuration Vehicle. *High-Angle-of-Attack Technology—Volume 1*, NASA CP-3149, Part 2, 1992, pp. 829–861.

16. Ashworth, B. R.; and Kahlbaum, W. M., Jr.: *Description and Performance of the Langley Differential Maneuvering Simulation.* NASA TN D-7304, 1973.

17. Broussard, John R.: *Design, Implementation and Flight Testing of PIF Autopilots for General Aviation Aircraft.* NASA CR-3709, 1983.

18. Maybeck, Peter S.: *Stochastic Models, Estimation, and Control*, Volume 3. Academic Press, 1982.

19. Halyo, Nesim; and Caglayan, Alper K.: A Separation Theorem for the Stochastic Sampled-Data LQG Problem. *Int. J. Control*, vol. 23, no. 2, Feb. 1976, pp. 237–244.

20. Armstrong, Ernest S.: *ORACLS—A Design System for Linear Multivariable Control.* Marcel Dekker, Inc., 1980.

21. *Military Specification—Flight Control System, General Specification For.* MIL-F-87242 (USAF), Mar. 31, 1986.

22. Doyle, John: Analysis of Feedback Systems With Structured Uncertainties. *IEE Proc.*, vol. 129, pt. D, no. 6, Nov. 1982, pp. 242–250.

23. Dailey, R. Lane: A New Algorithm For the Real Structured Singular Value. *Proceedings of the 1990 American Control Conference, American Automatic Control Council*, Volume 3, May 1990, pp. 3036–3040.

24. Cooper, George E.; and Harper, Robert P., Jr.: *The Use of Pilot Rating in the Evaluation of Aircraft Handling Qualities.* NASA TN D-5153, 1969.

Table I. Mass Properties

| State | Weight, lbf | $x_{cg}$, percent $\bar{c}$ | $z_{cg}$, relative to WL | $I_{xx}$, slug-ft$^2$ | $I_{yy}$, slug-ft$^2$ | $I_{zz}$, slug-ft$^2$ | $I_{xz}$, slug-ft$^2$ |
|---|---|---|---|---|---|---|---|
| Light | 31 618 | 26.6 | 103.4 | 22 163 | 172 238 | 186 823 | −2043 |
| Nominal | 35 765 | 23.3 | 105.4 | 22 633 | 174 246 | 189 336 | −2132 |
| Heavy | 37 619 | 23.3 | 105.9 | 22 938 | 179 130 | 194 003 | −2507 |

Table II. Design Conditions

| Design case | Mach | $\alpha$, deg | $n_z$, $g$ units | Short-period frequency, rad/sec |
|---|---|---|---|---|
| Altitude = 15 000 ft | | | | |
| 1 | 0.70 | 2.52 | 1.0 | 2.7 |
| 2 | .60 | 3.37 | 1.0 | 2.1 |
| 3 | .49 | 5 | 1.0 | 1.4 |
| 4 | .27 | 20 | .94 | .57 |
| 5 | .21 | 35 | .82 | .54 |
| 6 | .20 | 50 | .80 | .83 |
| 7 | .22 | 65 | .82 | 1.3 |
| 8 | .70 | 20 | 6.3 | 1.7 |
| 9 | .60 | 20 | 4.9 | 1.6 |
| 10 | .60 | 35 | 6.9 | 1.7 |
| 11 | .40 | 20 | 2.1 | .97 |
| 12 | .40 | 35 | 3.1 | .97 |
| 13 | .30 | 5 | .37 | .79 |
| 14 | .10 | 45 | .22 | .35 |
| Altitude = 25 000 ft | | | | |
| 15 | 0.70 | 3.58 | 1.0 | 2.1 |
| 16 | .59 | 5 | 1.0 | 1.5 |
| 17 | .33 | 20 | .94 | .63 |
| 18 | .26 | 35 | .88 | .56 |
| 19 | .26 | 50 | .90 | .90 |
| 20 | .28 | 65 | .92 | 1.3 |
| 21 | .70 | 20 | 4.2 | 1.5 |
| 22 | .60 | 20 | 3.2 | 1.4 |
| 23 | .60 | 35 | 4.5 | 1.4 |
| 24 | .40 | 20 | 1.4 | .82 |
| 25 | .40 | 35 | 2.0 | .83 |
| 26 | .30 | 5 | .24 | .64 |
| 27 | .10 | 45 | .14 | .27 |
| Altitude = 35 000 ft | | | | |
| 28 | 0.70 | 5.34 | 1.0 | 1.5 |
| 29 | .60 | 7.24 | .99 | 1.0 |
| 30 | .41 | 20 | .94 | .70 |
| 31 | .34 | 35 | .94 | .60 |
| 32 | .34 | 50 | .95 | .94 |
| 33 | .35 | 60 | .95 | 1.6 |
| 34 | .70 | 20 | 2.7 | 1.2 |
| 35 | .60 | 20 | 2.0 | 1.2 |
| 36 | .60 | 35 | 2.9 | 1.1 |
| 37 | .40 | 5 | .28 | .66 |
| 38 | .40 | 50 | 1.4 | 1.1 |
| 39 | .20 | 45 | .34 | .53 |

Table III. Optimal Cost Weights

| Design case | $Q_\alpha$ | $Q_q$ | $Q_{n,z}$ | $Q_u$ | $Q_z$ | $R_v$ |
|---|---|---|---|---|---|---|
| 1 | 94.6876 | 91.4846 | 14.7383 | 2.4387 | 11.8359 | 0.0038 |
| 2 | 116.0329 | 75.9189 | 8.9587 | 4.0312 | 14.5041 | .0063 |
| 3 | 138.2935 | 58.1897 | 4.4272 | 9.0703 | 17.2867 | .0142 |
| 4 | 722.7099 | 79.3696 | 1.5625 | 10.0000 | 22.5847 | .0214 |
| 5 | 762.9073 | 40.3961 | .3387 | 10.0000 | 23.8409 | .0238 |
| 6 | 800.0000 | 3.6249 | .0171 | 3.2258 | 25.0000 | .0403 |
| 7 | 200.0657 | .8319 | .0129 | 2.0000 | 25.0082 | .0164 |
| 8 | 126.5197 | 66.6656 | 7.7252 | 6.1515 | 15.8150 | .0096 |
| 9 | 150.7106 | 44.8945 | 5.3054 | 6.9444 | 18.8388 | .0109 |
| 10 | 177.6644 | 20.3447 | 2.9014 | 1.5379 | 22.2081 | .0096 |
| 11 | 684.2341 | 112.5526 | 6.8553 | 4.7236 | 21.3823 | .0295 |
| 12 | 782.2292 | 17.6359 | 3.7769 | 4.7236 | 24.4447 | .0295 |
| 13 | 167.6470 | 32.3296 | .9339 | 1.7803 | 20.9559 | .0445 |
| 14 | 803.2323 | .3282 | .0815 | 18.1406 | 25.1010 | .1134 |
| 15 | 132.2815 | 59.7755 | 8.8535 | 4.0312 | 16.5352 | 0.0063 |
| 16 | 150.2881 | 45.8563 | 4.7661 | 7.9012 | 18.7860 | .0123 |
| 17 | 756.2476 | 46.1103 | 1.2841 | 10.0000 | 23.6327 | .0350 |
| 18 | 787.4826 | 15.8949 | .2646 | 10.0000 | 24.6088 | .0443 |
| 19 | 799.4125 | 4.2137 | .0158 | 10.0000 | 24.9816 | .0343 |
| 20 | 797.1861 | 6.3590 | .0969 | 10.0000 | 12.4560 | .0164 |
| 21 | 158.9245 | 37.8135 | 4.1725 | 7.9012 | 19.8656 | .0123 |
| 22 | 174.8601 | 23.4588 | 2.5917 | 9.0703 | 21.8575 | .0142 |
| 23 | 189.7631 | 9.8827 | 1.2646 | 2.2676 | 23.7204 | .0142 |
| 24 | 743.9655 | 56.5155 | 3.1610 | 6.6098 | 23.2489 | .0413 |
| 25 | 793.8685 | 8.2248 | 1.5487 | 6.4515 | 24.8084 | .0403 |
| 26 | 183.1379 | 17.3183 | .4543 | 2.7127 | 22.8922 | .0678 |
| 27 | 799.6596 | 3.9695 | .0128 | 20.0000 | 24.9894 | .0953 |
| 28 | 163.5634 | 32.9563 | 4.3908 | 31.6049 | 20.4454 | 0.0123 |
| 29 | 173.6166 | 24.9270 | 2.3669 | 40.0000 | 21.7021 | .0278 |
| 30 | 775.2657 | 27.3099 | 1.0665 | 36.2812 | 24.2271 | .0567 |
| 31 | 799.5079 | 3.9247 | .2094 | 40.0000 | 24.9846 | .0772 |
| 32 | 799.9307 | 3.6961 | .0152 | 40.0000 | 12.4989 | .0314 |
| 33 | 795.0167 | 8.4284 | .1969 | 40.0000 | 6.2111 | .0109 |
| 34 | 180.8571 | 18.1610 | 1.8924 | 40.0000 | 22.6071 | .0193 |
| 35 | 189.2436 | 10.5712 | 1.0957 | 40.0000 | 23.6555 | .0193 |
| 36 | 196.5172 | 3.9141 | .4792 | 14.6924 | 24.5647 | .0230 |
| 37 | 187.4423 | 12.9098 | .5585 | 10.2030 | 23.4303 | .0638 |
| 38 | 798.2298 | 5.4121 | .0001 | 40.0000 | 24.9447 | .0230 |
| 39 | 802.7795 | .8515 | .0110 | 40.0000 | 25.0869 | .0494 |

Table IV. Stochastic Weights[a]

| State | $\mathbf{x}_0$ weight | State | $\mathbf{x}_0$ weight | Output | $\bar{\mathbf{v}}$ weight |
|---|---|---|---|---|---|
| 1 | 0.01 | 10 | 0 | 1 | 0.10 |
| 2 | .01 | 11 | .05 | 2 | .01 |
| 3 | .01 | 12 | .05 | 3 | .01 |
| 4 | .01 | 13 | .05 | 4 | .01 |
| 5 | 0 | 14 | .01 | 5 | .01 |
| 6 | 0 | 15 | 0 | | |
| 7 | 0 | 16 | .01 | | |
| 8 | 0 | 17 | 0 | | |
| 9 | 0 | | | | |

[a]Stochastic weights for $v_0$ and $\mathbf{w}_0$ are set equal to 0. All 39 design cases have the same weights.

Table V. Gain-Schedule Design Parameters

| Design case | $p_1$ | $p_2$ | $p_3$ | $p_4$ | $p_5$ | $p_6$ |
|---|---|---|---|---|---|---|
| 1 | 0.2515 | 4.6232 | 1.1943 | 0.3871 | 0.0000 | 2.1232 |
| 2 | .3370 | 3.2904 | 1.1943 | .2755 | .0000 | .7904 |
| 3 | .5000 | 2.0866 | 1.1943 | .1747 | .0000 | .0000 |
| 4 | 2.0000 | .6131 | 1.1943 | .0513 | .0000 | .0000 |
| 5 | 3.5000 | .3581 | 1.1943 | .0300 | .0000 | .0000 |
| 6 | 5.0000 | .3271 | 1.1943 | .0274 | 1.5000 | .0000 |
| 7 | 6.5000 | .3951 | 1.1943 | .0331 | 3.0000 | .0000 |
| 8 | 2.0000 | 4.6232 | 1.1943 | .3871 | .0000 | 2.1232 |
| 9 | 2.0000 | 3.2904 | 1.1943 | .2755 | .0000 | .7904 |
| 10 | 3.5000 | 3.2904 | 1.1943 | .2755 | .0000 | .7904 |
| 11 | 2.0000 | 1.3920 | 1.1943 | .1166 | .0000 | .0000 |
| 12 | 3.5000 | 1.3920 | 1.1943 | .1166 | .0000 | .0000 |
| 13 | .5000 | .7695 | 1.1943 | .0644 | .0000 | .0000 |
| 14 | 4.5000 | .0838 | 1.1943 | .0070 | 1.0000 | .0000 |
| 15 | 0.3580 | 3.0402 | 0.7854 | 0.3871 | 0.0000 | 0.5402 |
| 16 | .5000 | 2.0819 | .7854 | .2651 | .0000 | .0000 |
| 17 | 2.0000 | .6120 | .7854 | .0779 | .0000 | .0000 |
| 18 | 3.5000 | .3884 | .7854 | .0495 | .0000 | .0000 |
| 19 | 5.0000 | .3729 | .7854 | .0475 | 1.5000 | .0000 |
| 20 | 6.5000 | .4512 | .7854 | .0575 | 3.0000 | .0000 |
| 21 | 2.0000 | 3.0402 | .7854 | .3871 | .0000 | .5402 |
| 22 | 2.0000 | 2.1637 | .7854 | .2755 | .0000 | .0000 |
| 23 | 3.5000 | 2.1637 | .7854 | .2755 | .0000 | .0000 |
| 24 | 2.0000 | .9154 | .7854 | .1166 | .0000 | .0000 |
| 25 | 3.5000 | .9154 | .7854 | .1166 | .0000 | .0000 |
| 26 | .5000 | .5060 | .7854 | .0644 | .0000 | .0000 |
| 27 | 4.5000 | .0551 | .7854 | .0070 | 1.0000 | .0000 |
| 28 | 0.5344 | 1.9278 | 0.4980 | 0.3871 | 0.0000 | 0.0000 |
| 29 | .7246 | 1.3720 | .4980 | .2755 | .0000 | .0000 |
| 30 | 2.0000 | .6171 | .4980 | .1239 | .0000 | .0000 |
| 31 | 3.5000 | .4226 | .4980 | .0849 | .0000 | .0000 |
| 32 | 5.0000 | .4032 | .4980 | .0810 | 1.5000 | .0000 |
| 33 | 6.0000 | .4498 | .4980 | .0903 | 2.5000 | .0000 |
| 34 | 2.0000 | 1.9278 | .4980 | .3871 | .0000 | .0000 |
| 35 | 2.0000 | 1.3720 | .4980 | .2755 | .0000 | .0000 |
| 36 | 3.5000 | 1.3720 | .4980 | .2755 | .0000 | .0000 |
| 37 | .5000 | .5804 | .4980 | .1166 | .0000 | .0000 |
| 38 | 5.0000 | .5804 | .4980 | .1166 | 1.5000 | .0000 |
| 39 | 4.5000 | .1408 | .4980 | .0283 | 1.0000 | .0000 |

Table VI. Variable-Gain Components

| | $y_\alpha$ | $y_q$ | $y_{n,z}$ | $y_u$ | $y_z$ |
|---|---|---|---|---|---|
| $\mathbf{K}_0$ | −10.6285 | −25.4721 | −5.3189 | 21.9340 | −30.8027 |
| $\mathbf{K}_1$ | −1.2185 | −1.0865 | −10.2974 | −.0423 | −4.5770 |
| $\mathbf{K}_2$ | −3.5173 | −12.7954 | −18.7768 | 12.7372 | 14.6450 |
| $\mathbf{K}_3$ | 4.4277 | .8839 | .2946 | −6.7833 | −16.0592 |
| $\mathbf{K}_4$ | 33.5886 | 51.6908 | 38.9416 | 9.9597 | −37.4526 |
| $\mathbf{K}_5$ | −1.5707 | −.6439 | 50.1606 | 1.7770 | 19.0618 |
| $\mathbf{K}_6$ | 4.5668 | 9.1496 | 24.2615 | 1.5378 | −8.7858 |

Table VII. Feedback Gains

| Design case | $K_\alpha$ | $K_q$ | $K_{n,z}$ | $K_u$ | $K_z$ |
|---|---|---|---|---|---|
| 15 | −2.8113 | −39.1150 | −37.6789 | 60.0010 | −19.7742 |
| 17 | −9.1233 | −30.7536 | −34.1390 | 25.0931 | −46.5250 |
| 19 | −15.3165 | −33.4935 | 13.5122 | 24.2836 | −34.0246 |

Table VIII. Closed-Loop Eigenvalues

| Number | Real | Imaginary | Damping ratio |
|---|---|---|---|
| Design case 15 | | | |
| 1 | −195.5 | 0 | 1.0000 |
| 2 | −106.9 | 30.47 | .9617 |
| 3 | −106.9 | −30.47 | .9619 |
| 4 | −61.28 | 86.62 | .5776 |
| 5 | −61.28 | −86.62 | .5776 |
| 6 | −44.47 | 62.50 | .5797 |
| 7 | −44.47 | −62.50 | .5797 |
| 8 | −24.18 | 33.38 | .5866 |
| 9 | −24.18 | −33.38 | .5866 |
| 10 | −13.89 | 0 | 1.0000 |
| 11 | −11.49 | 11.52 | .7061 |
| 12 | −11.49 | −11.52 | .7061 |
| 13 | −1.266 | .3584 | .9622 |
| 14 | −1.266 | −.3584 | .9622 |
| 15 | −.5100 | 0 | 1.0000 |
| 16 | −.003157 | .04924 | .0640 |
| 17 | −.003157 | −.04924 | .0640 |
| Design case 17 | | | |
| 1 | −199.3 | 0 | 1.0000 |
| 2 | −76.52 | 38.21 | .8947 |
| 3 | −76.52 | −38.21 | .8947 |
| 4 | −61.96 | 85.09 | .5887 |
| 5 | −61.96 | −85.09 | .5887 |
| 6 | −43.12 | 62.09 | .5705 |
| 7 | −43.12 | −62.09 | .5705 |
| 8 | −16.09 | 33.73 | .4306 |
| 9 | −16.09 | −33.73 | .4306 |
| 10 | −13.27 | 0 | 1.0000 |
| 11 | −8.941 | 2.004 | .9758 |
| 12 | −8.941 | −2.004 | .9758 |
| 13 | −1.096 | 1.213 | .6706 |
| 14 | −1.096 | −1.213 | .6706 |
| 15 | −.3913 | 0 | 1.0000 |
| 16 | −.01082 | .1175 | .0917 |
| 17 | −.01082 | −.1175 | .0917 |
| Design case 19 | | | |
| 1 | −200.1 | 0 | 1.0000 |
| 2 | −75.29 | 37.82 | .8936 |
| 3 | −75.29 | −37.82 | .8936 |
| 4 | −62.00 | 85.07 | .5890 |
| 5 | −62.00 | −85.07 | .5890 |
| 6 | −43.35 | 62.10 | .5724 |
| 7 | −43.35 | −62.10 | .5724 |
| 8 | −15.80 | 33.59 | .4258 |
| 9 | −15.80 | −33.59 | .4258 |
| 10 | −13.81 | 1.890 | .9908 |
| 11 | −13.81 | −1.890 | .9908 |
| 12 | −4.417 | 0 | 1.0000 |
| 13 | −.8716 | .9895 | .6610 |
| 14 | −.8716 | −.9895 | .6610 |
| 15 | −.3045 | 0 | 1.0000 |
| 16 | −.09067 | .1351 | .5571 |
| 17 | −.09067 | −.1351 | .5571 |

Table IX. Single Loop Margins

| Design case | Gain margin, dB | Phase margin, deg |
|---|---|---|
| Plant input | | |
| 15 | 8.8 | 57.9 |
| 17 | 12.8 | 53.0 |
| 19 | −23.7<br>14.4 | 56.1 |
| Plant output—pitch rate loop | | |
| 15 | 8.8 | −130.0<br>58.0 |
| 17 | −10.1<br>12.6 | −83.2<br>52.0 |
| 19 | −10.4<br>14.5 | −66.5<br>57.0 |

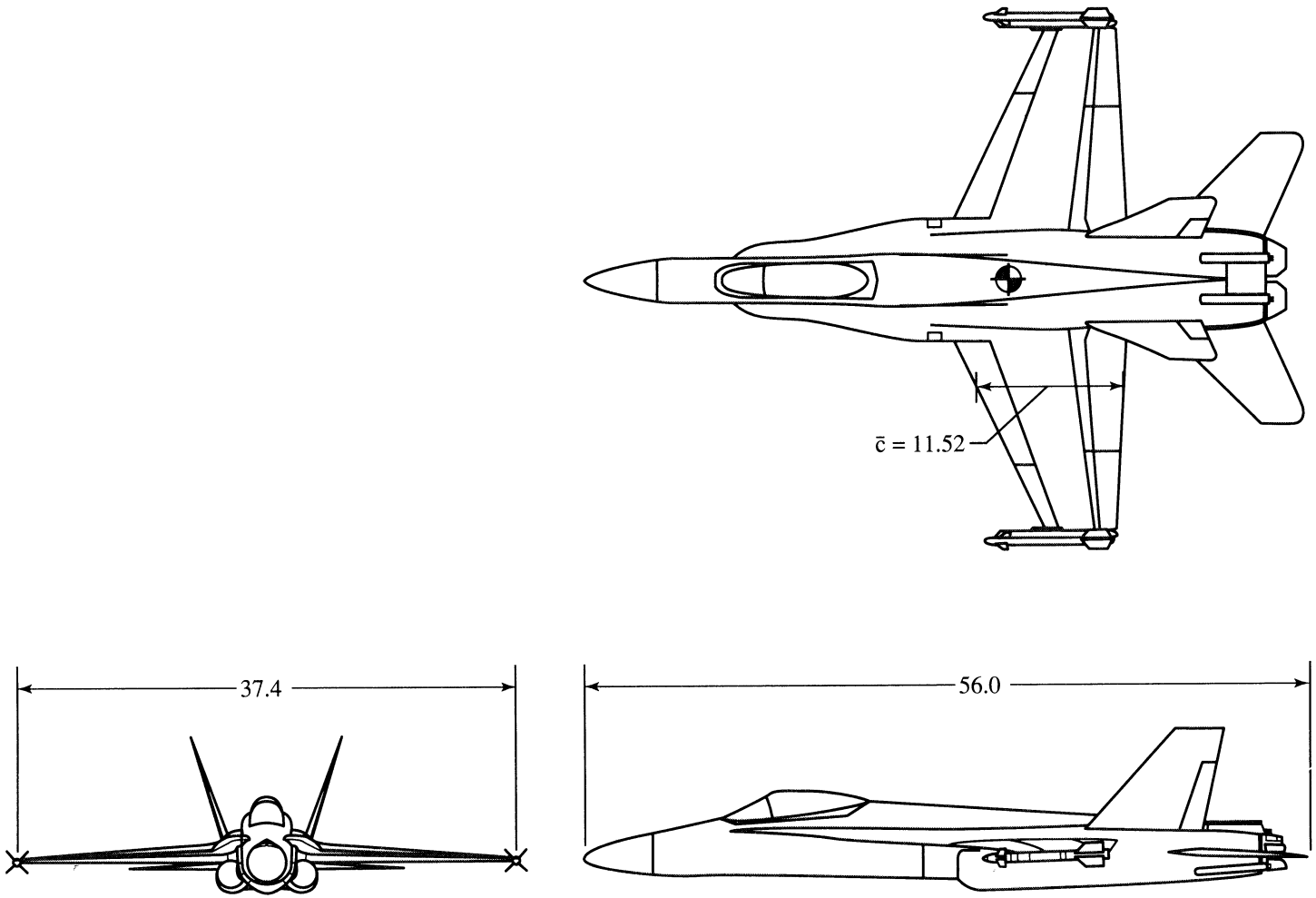


Figure 1. High-Alpha Research Vehicle. All dimensions in feet.

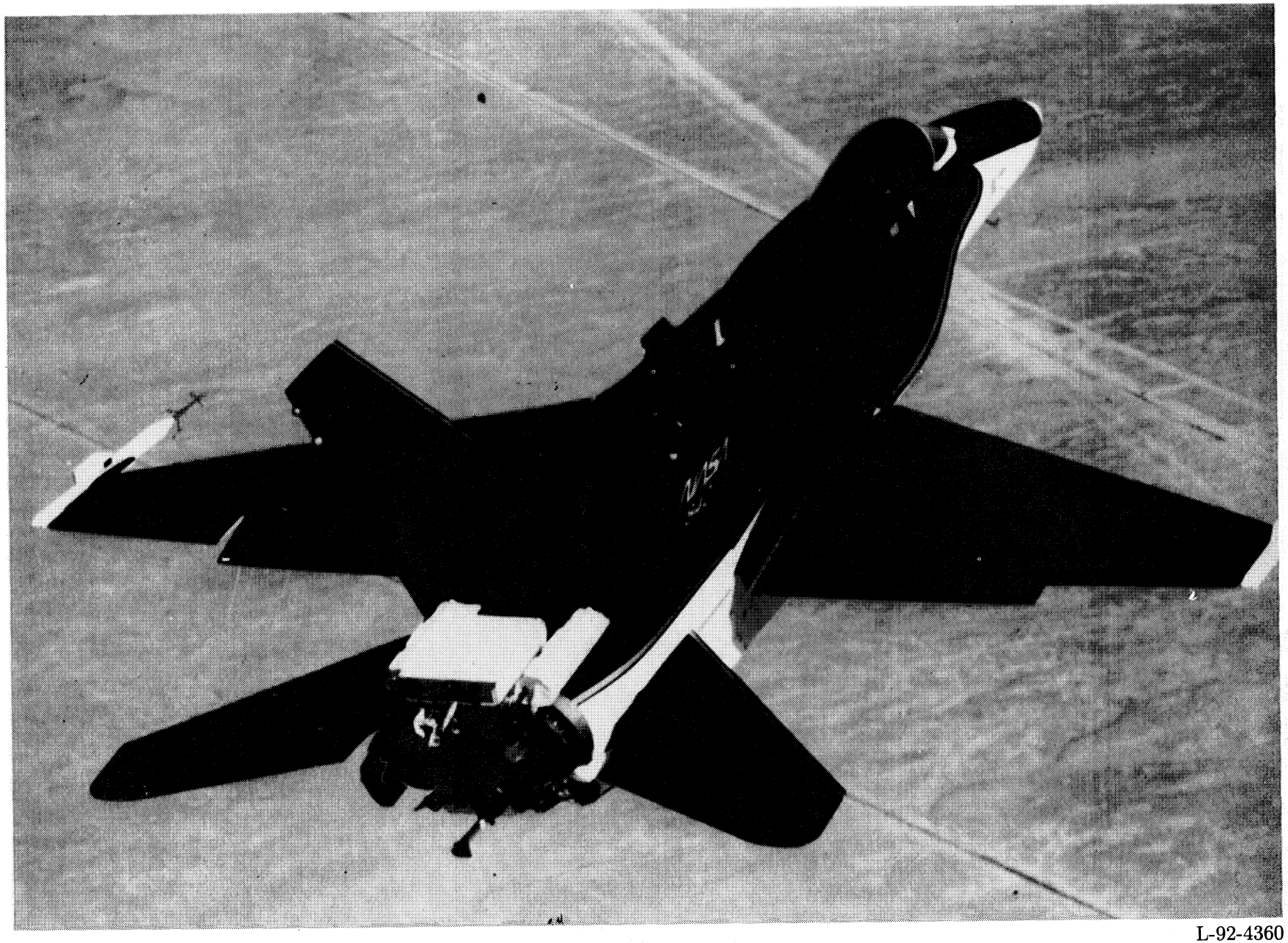

L-92-4360

Figure 2. High-Alpha Research Vehicle.

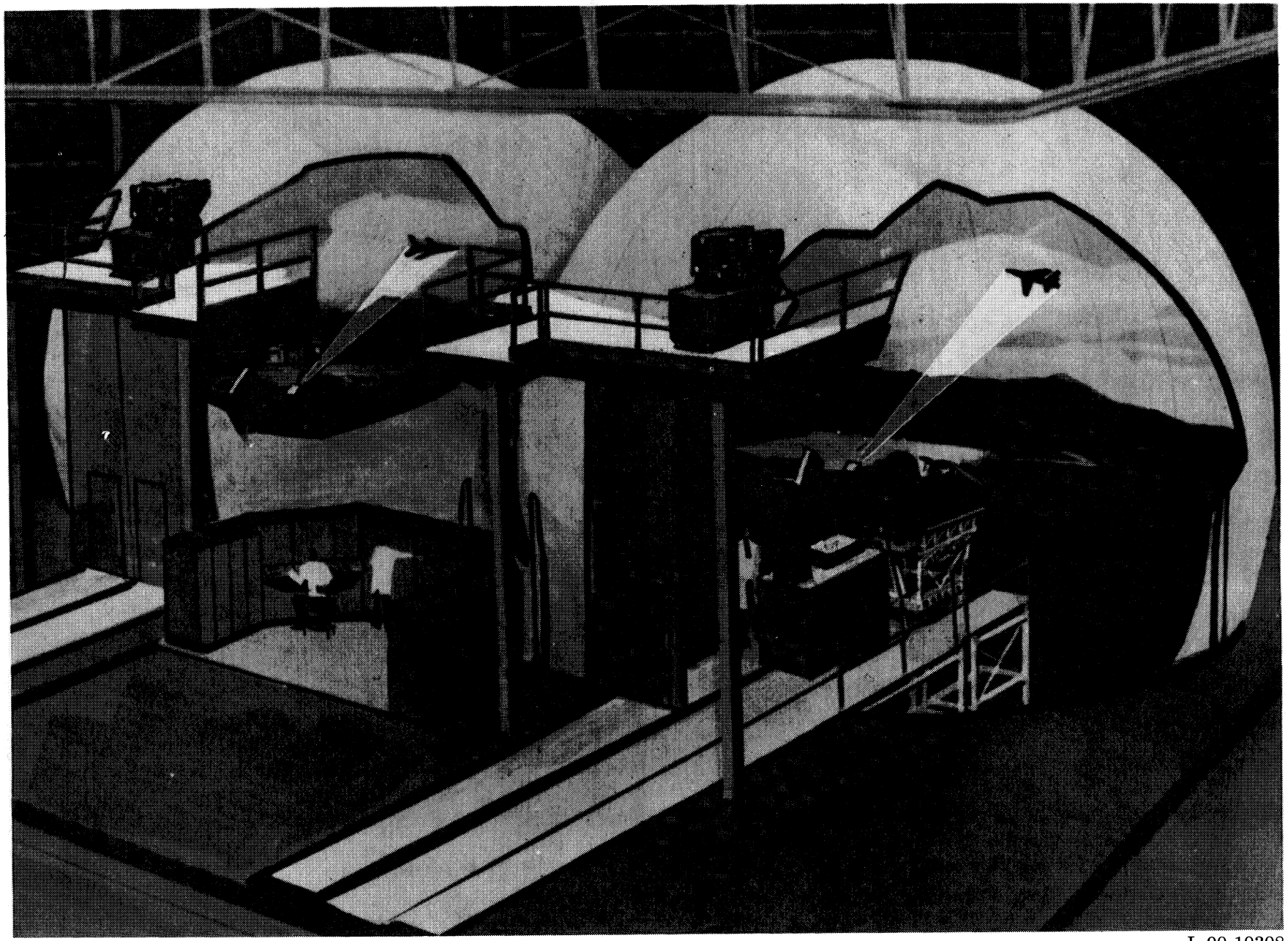

L-90-10308

Figure 3. Differential Maneuvering Simulator (DMS).

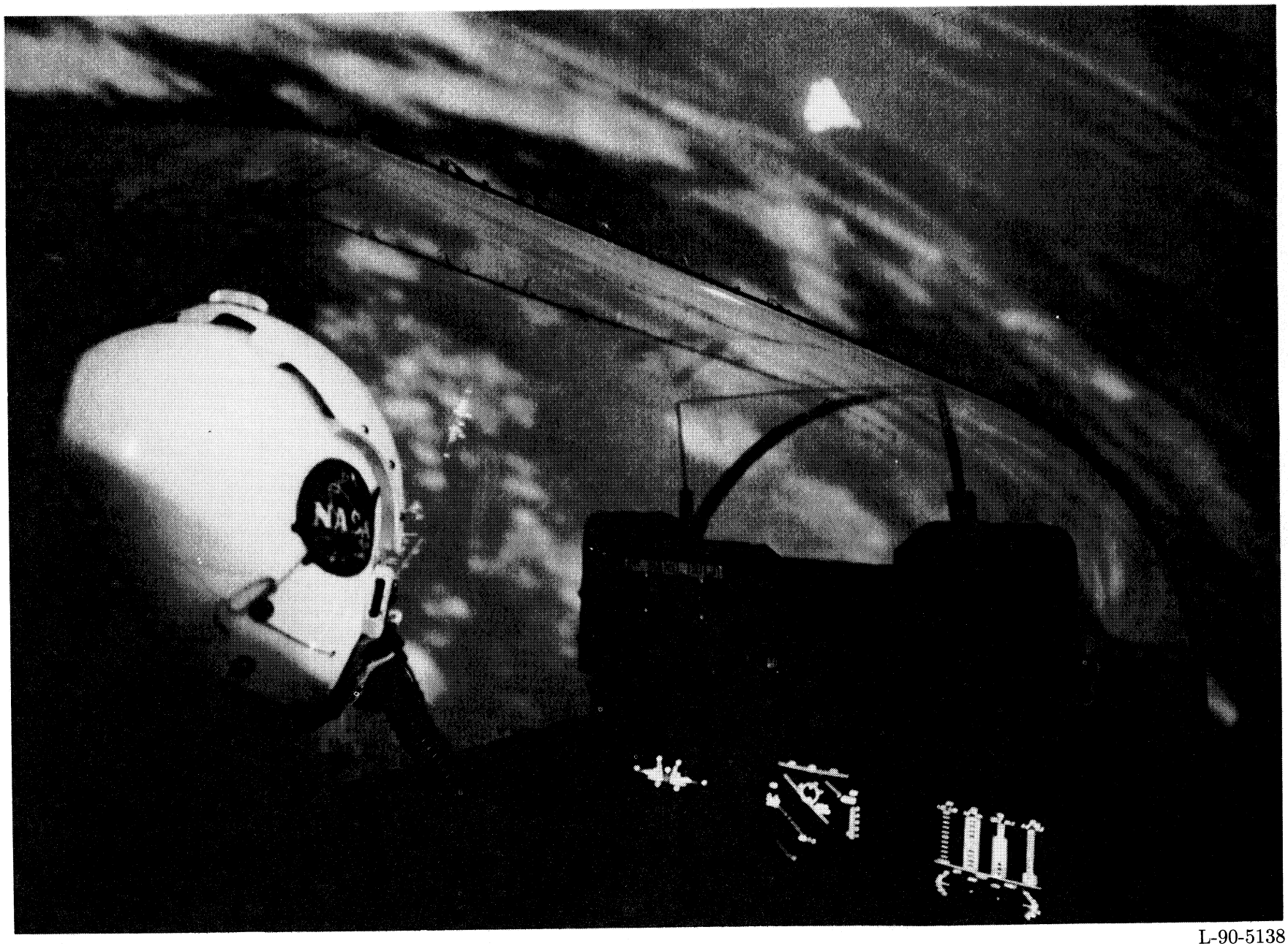


L-90-5138

Figure 4. Differential Maneuvering Simulator cockpit.

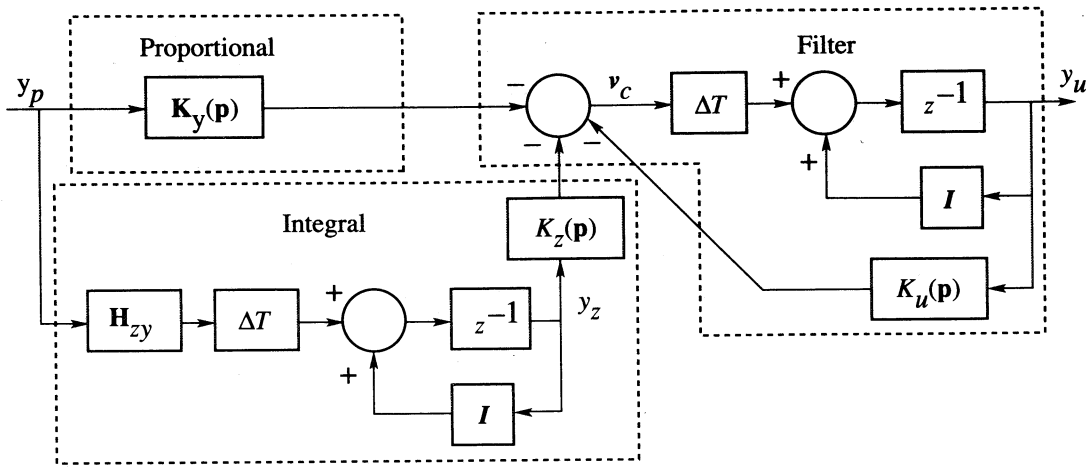


Figure 5. Feedback control structure for design and linear analysis.

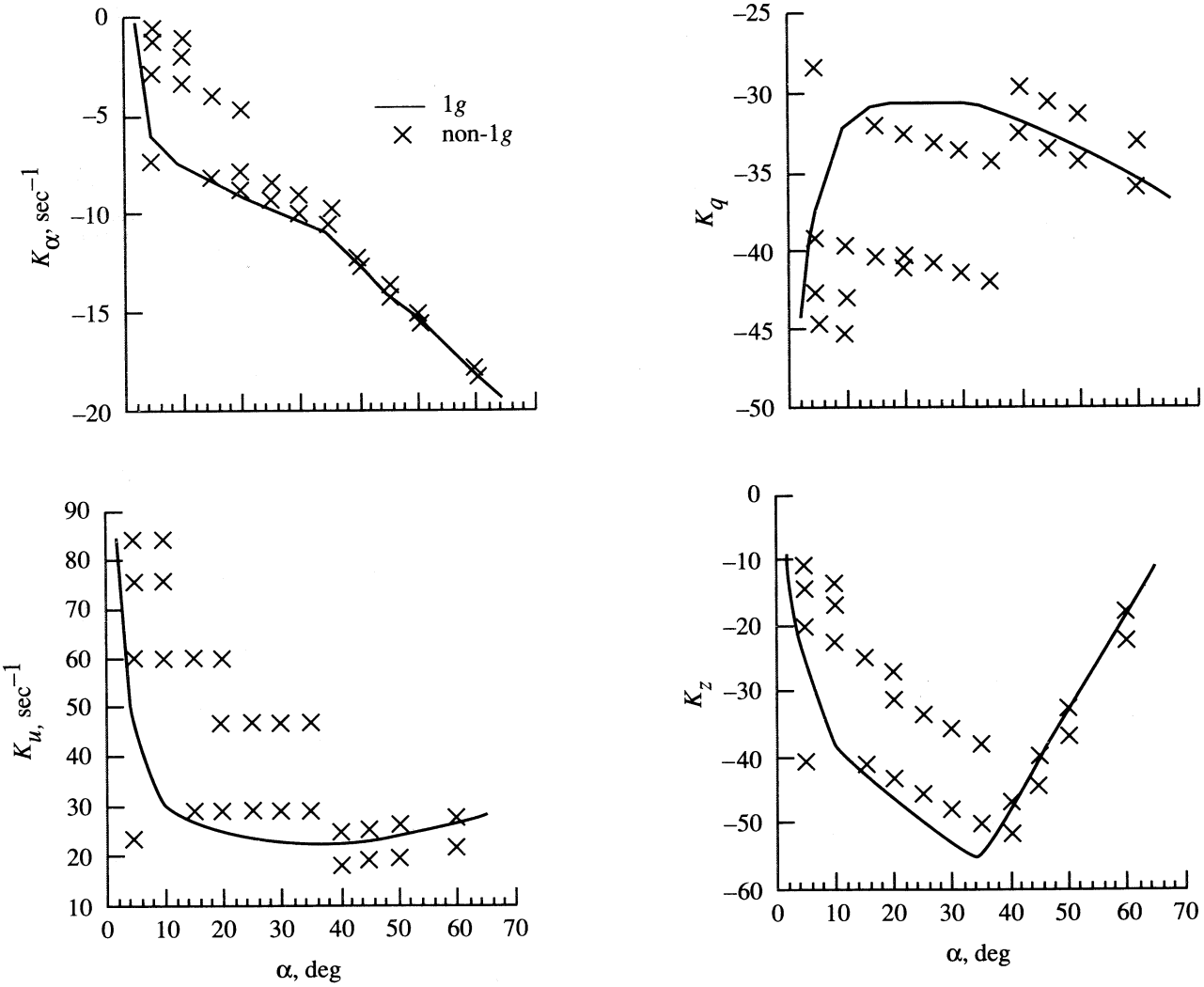


Figure 6. Feedback gains at 25 000 ft.

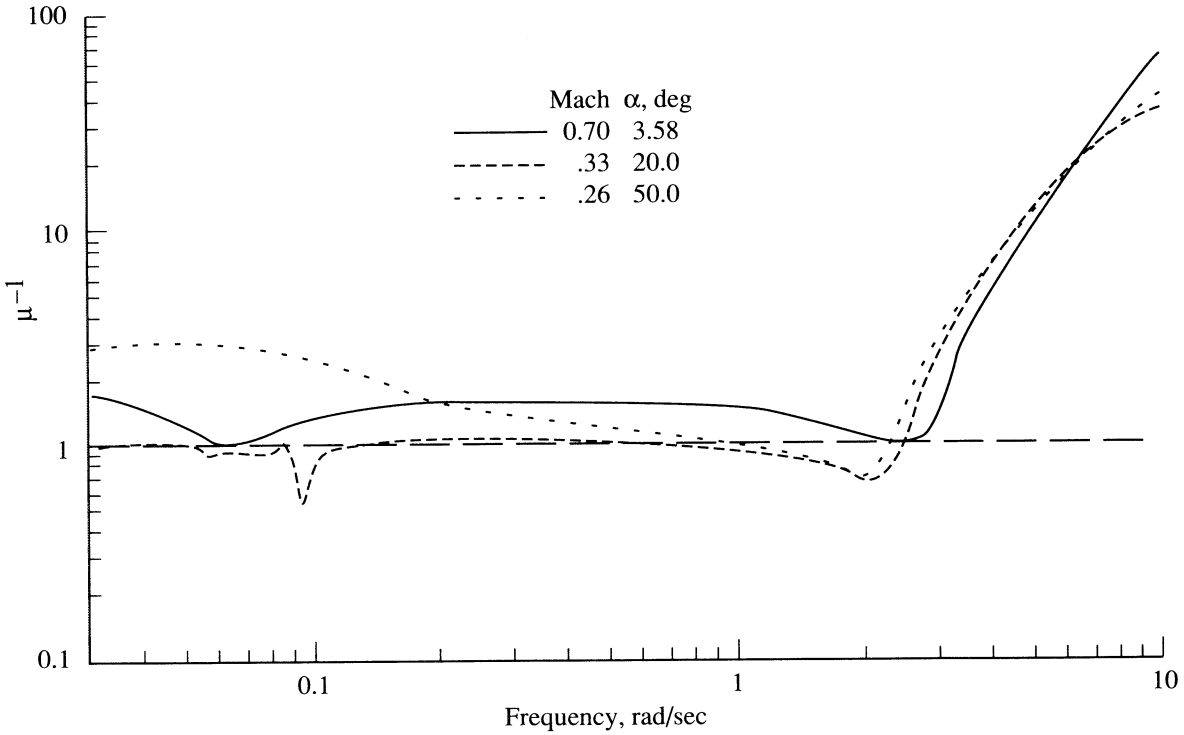


Figure 7. Results of real-$\mu$ analysis at plant output. $h = 25\,000$ ft; $1g$ trim.

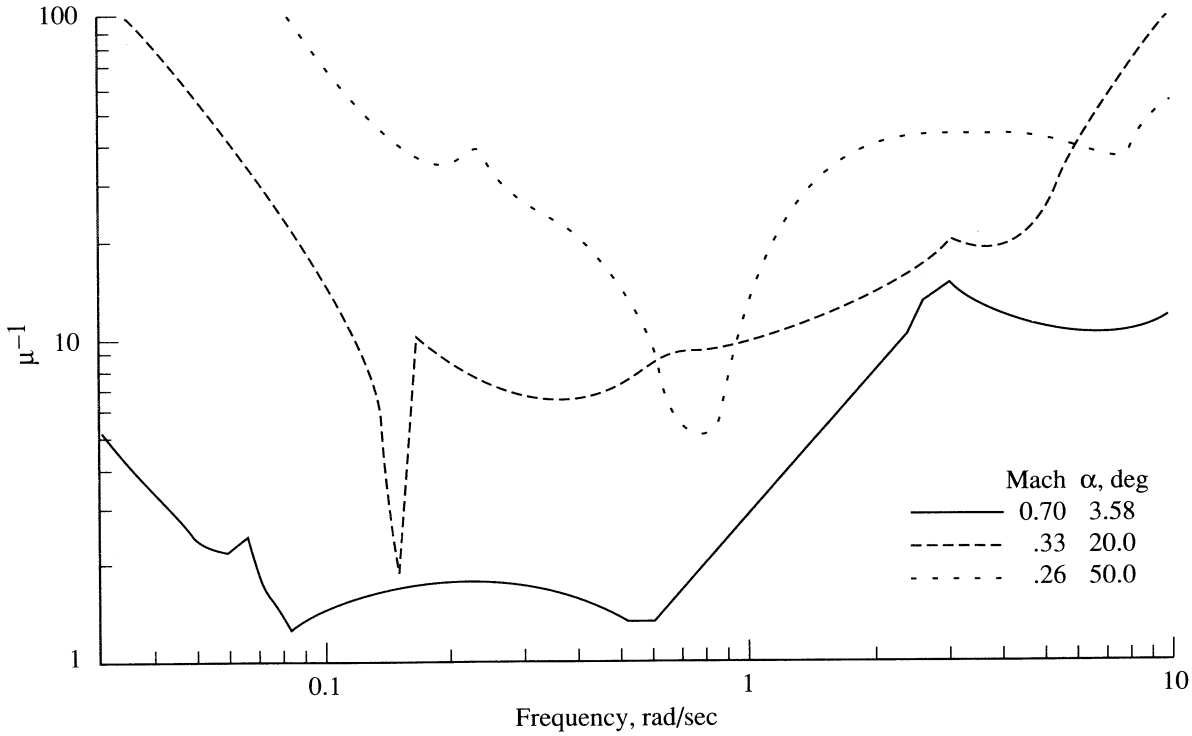


Figure 8. Results of real-$\mu$ stability derivative sensitivity analysis. $h = 25\,000$ ft; $1g$ trim.

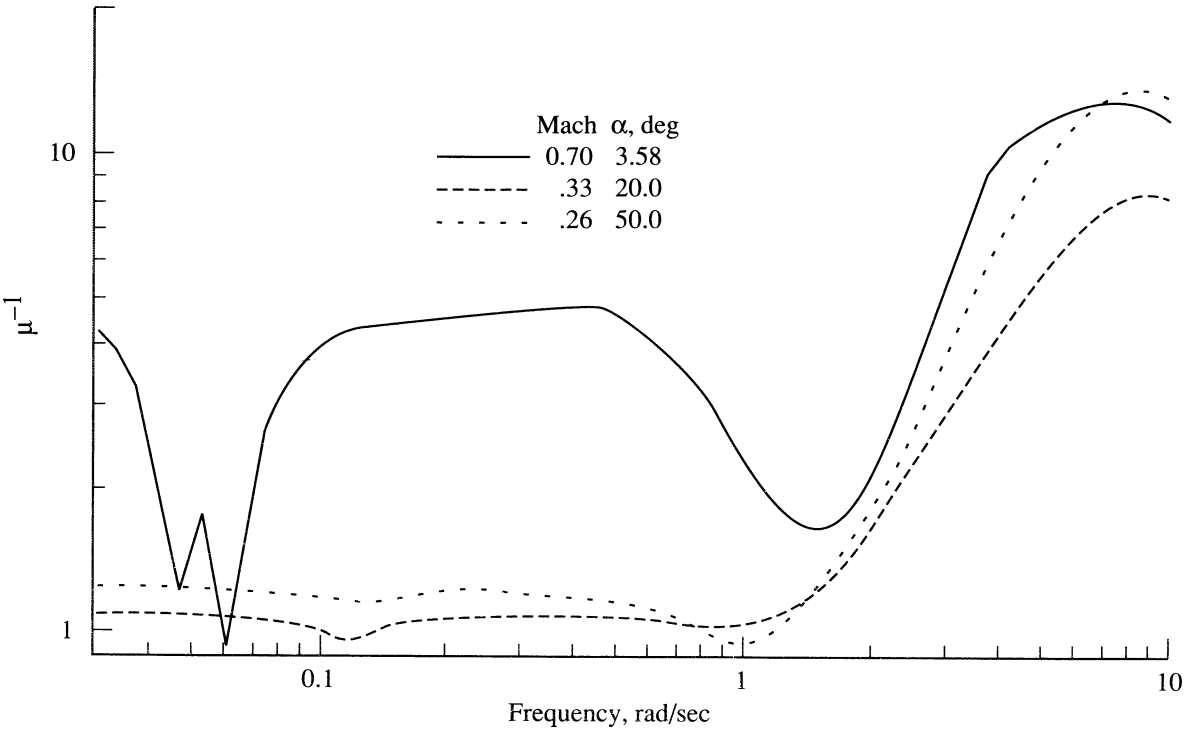


Figure 9. Results of real-$\mu$ control derivative sensitivity analysis. $h = 25\,000$ ft; $1g$ trim.

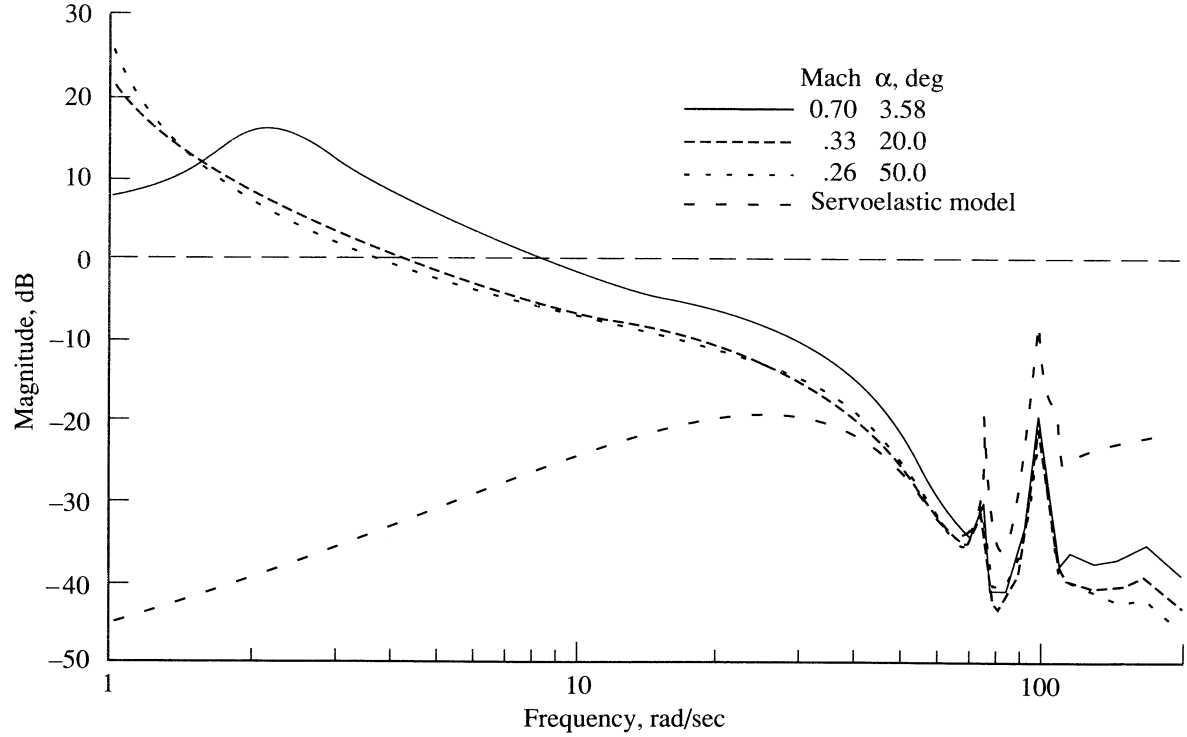


Figure 10. Singular value loop transfer at plant input for servoelastic analysis.

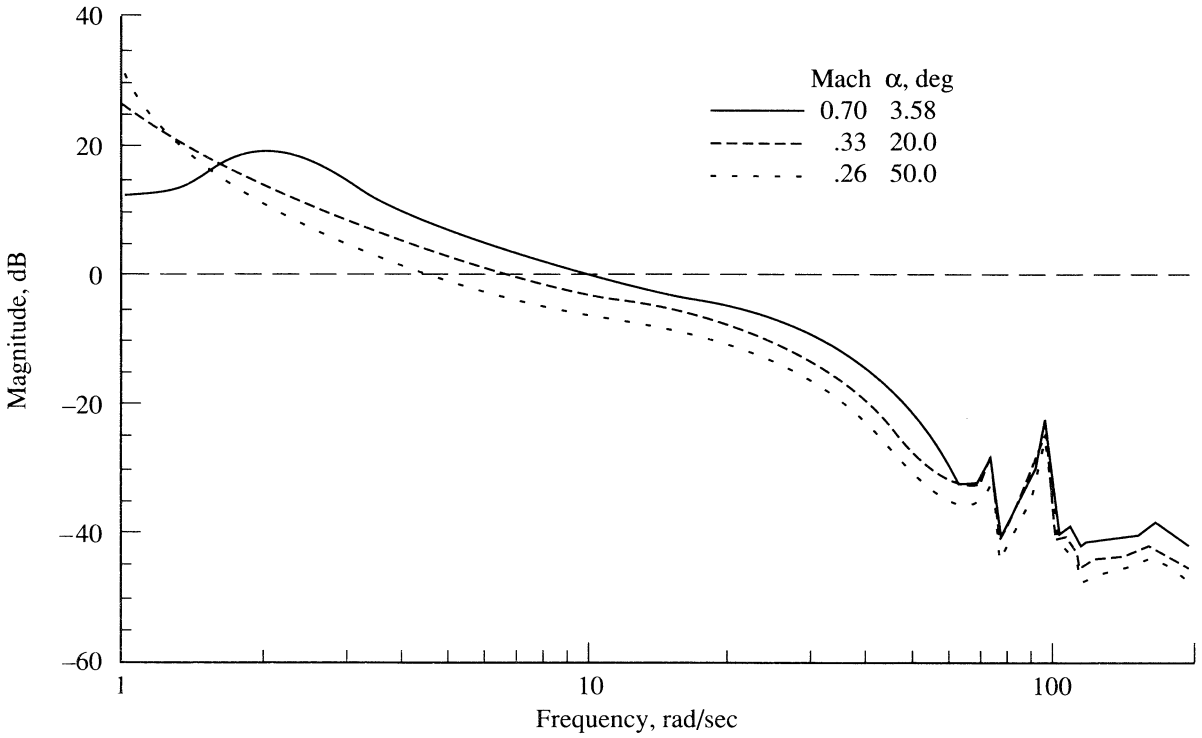


Figure 11. Singular value loop transfer at plant output for servoelastic analysis.

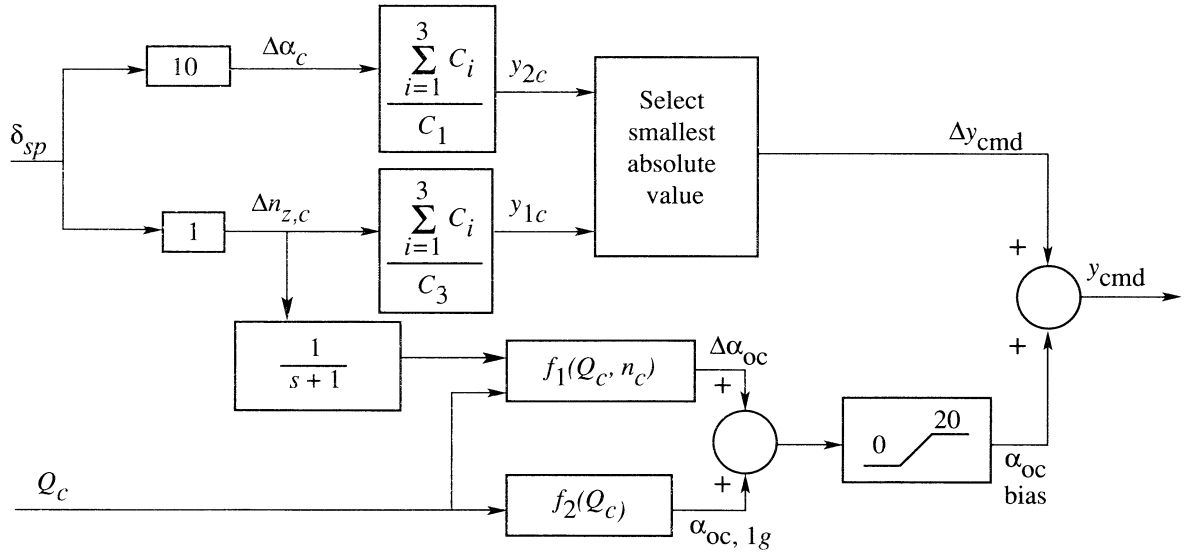


Figure 12. Block diagram of FFCG.

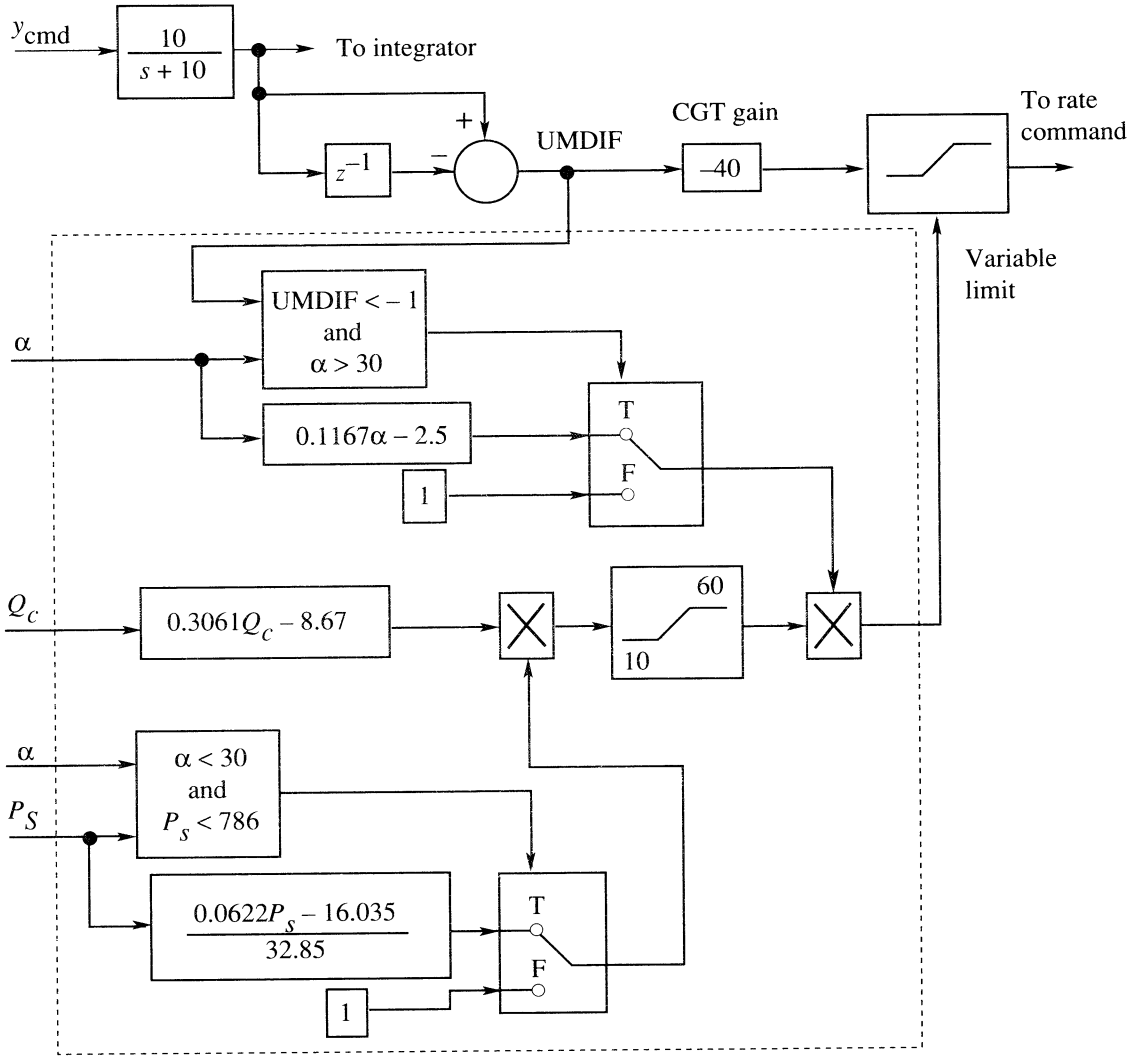


Figure 13. CGT feed-forward control with variable limit.

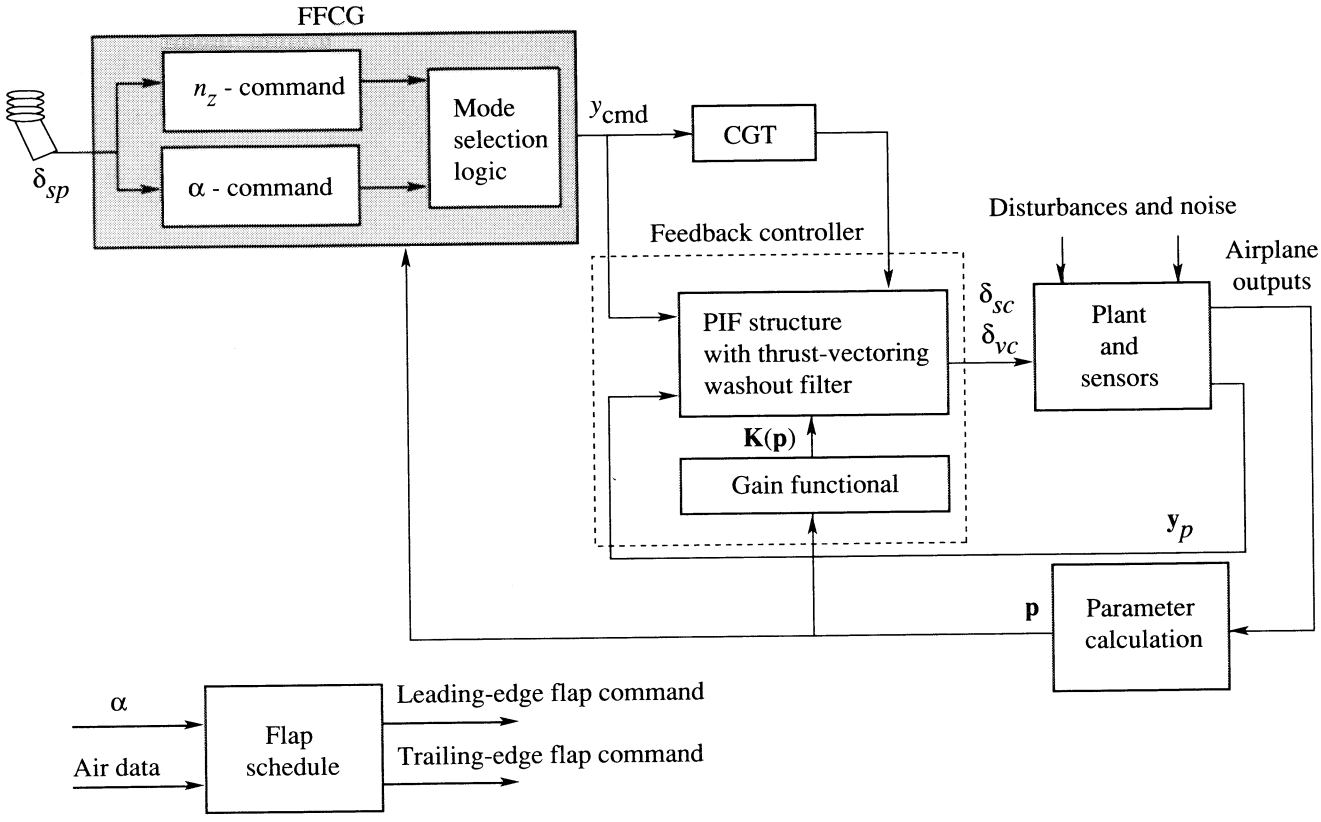


Figure 14. Block diagram of HARV longitudinal controller.

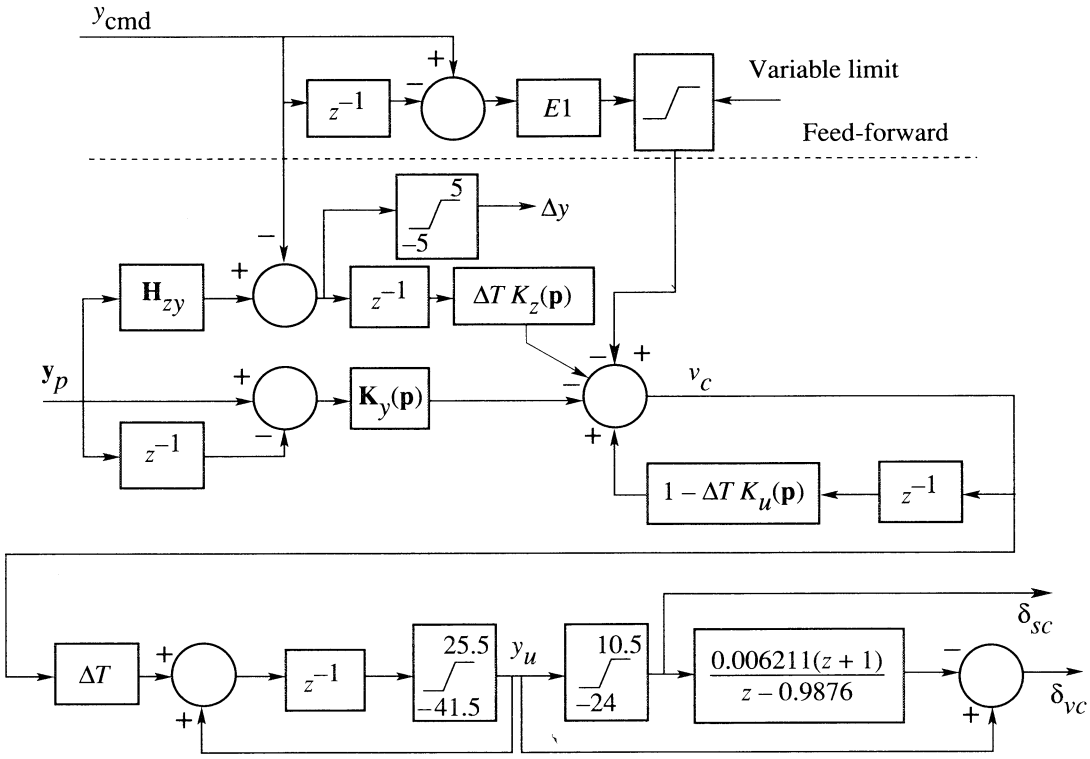


Figure 15. Feedback controller incremental form for HARV implementation.

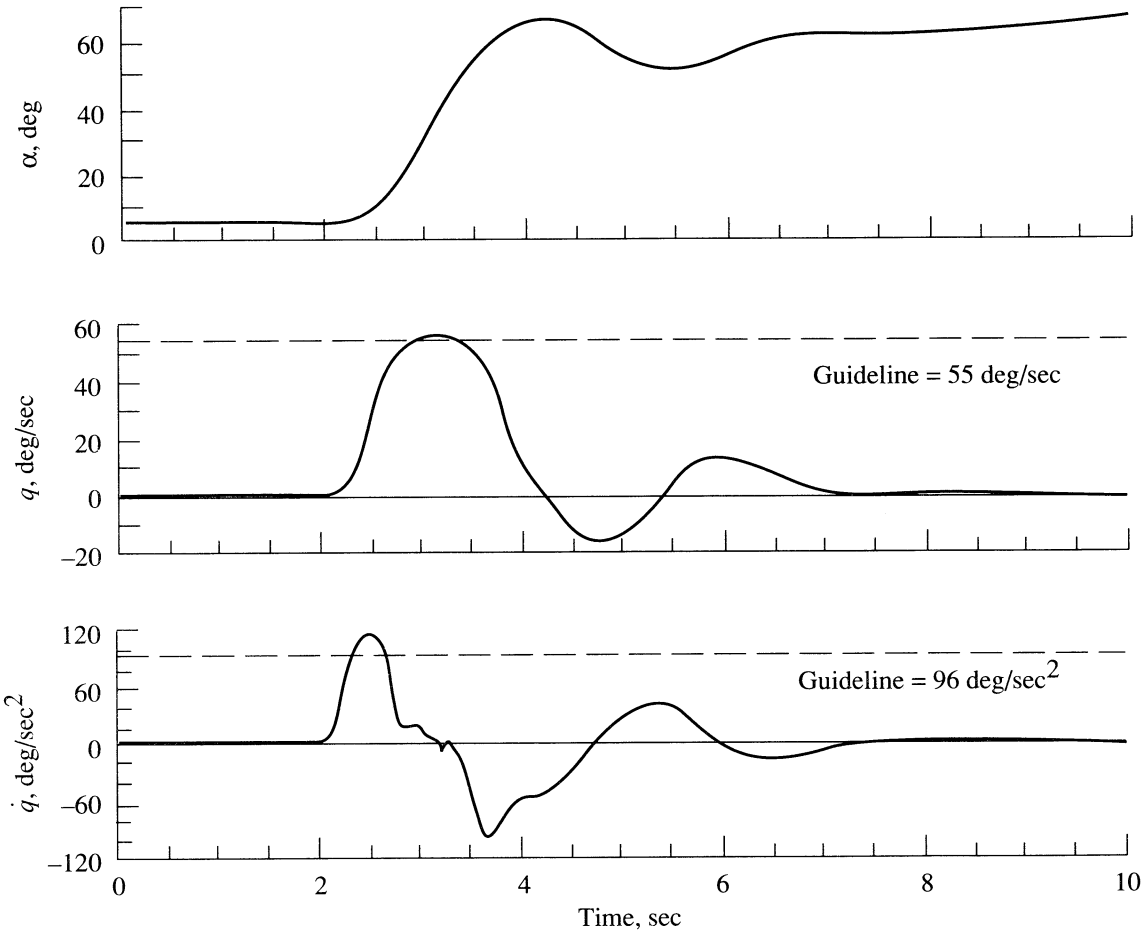


Figure 16. Pitch-up response with maximum aft stick at 25 000 ft.

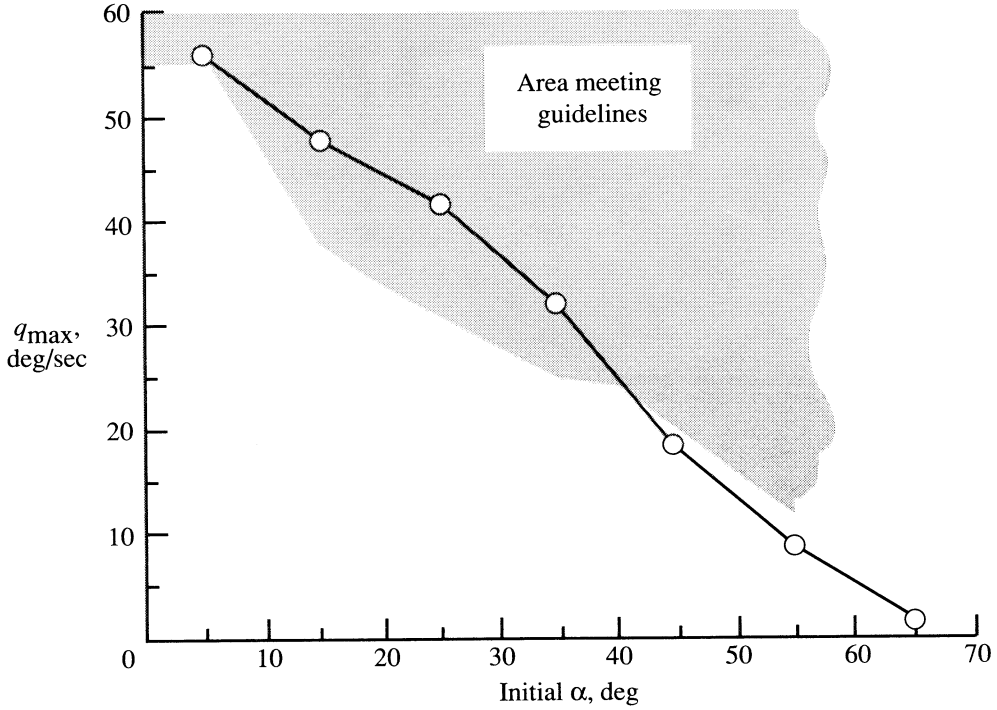


Figure 17. Maximum pitch rate achieved with maximum aft stick pull-up from 1$g$ at 25 000 ft.

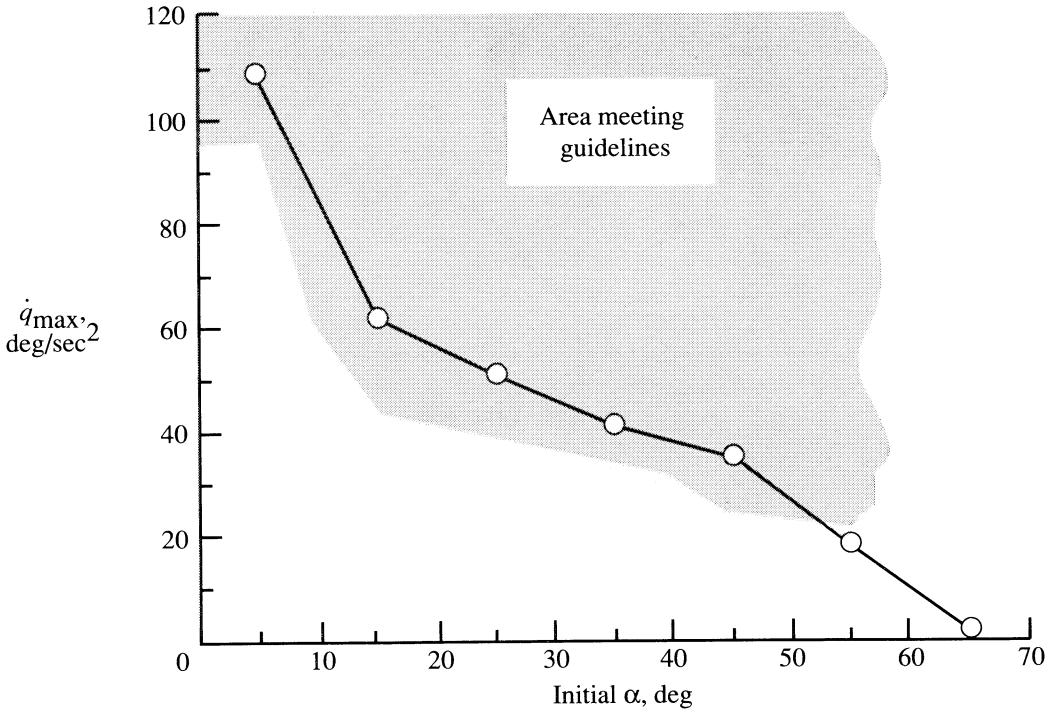


Figure 18. Maximum pitch acceleration achieved with maximum aft stick pull-up from 1$g$ at 25 000 ft.

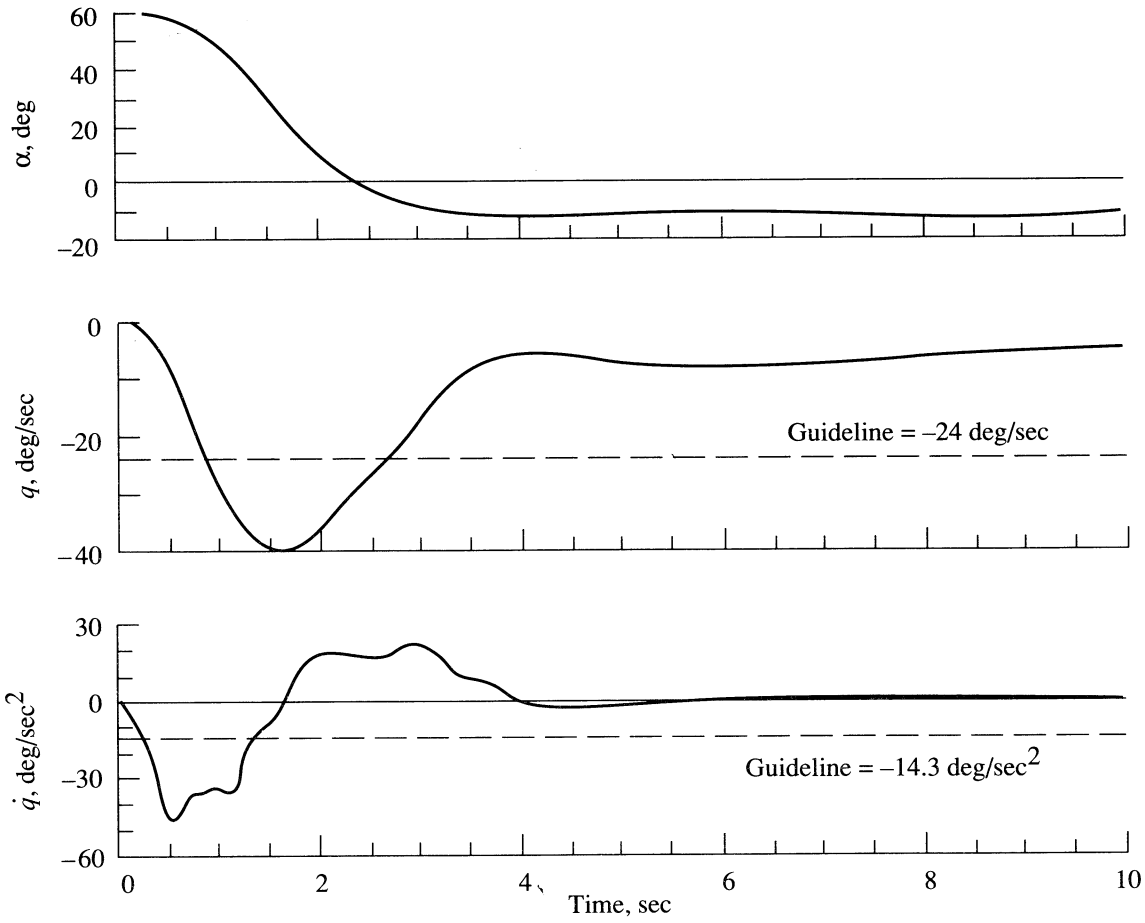


Figure 19. Pitch-down response with full-forward stick at 25 000 ft.

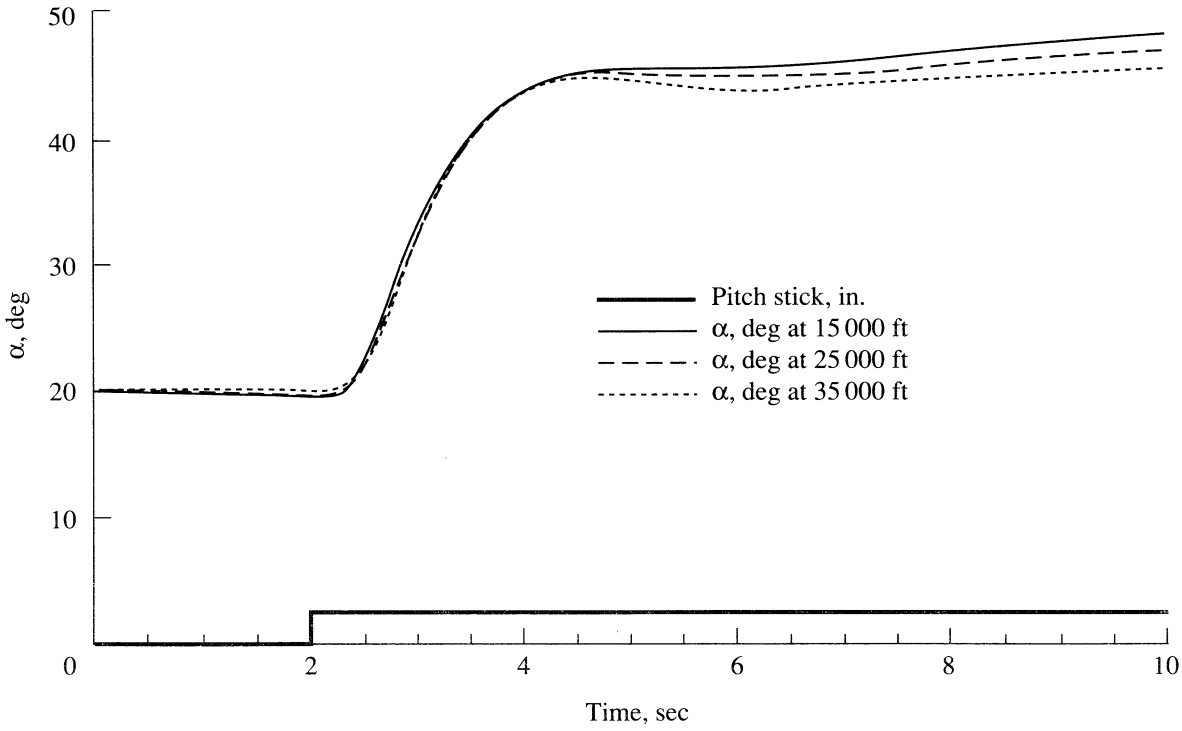


Figure 20. Alpha captures of 20° to 45° for three altitudes.

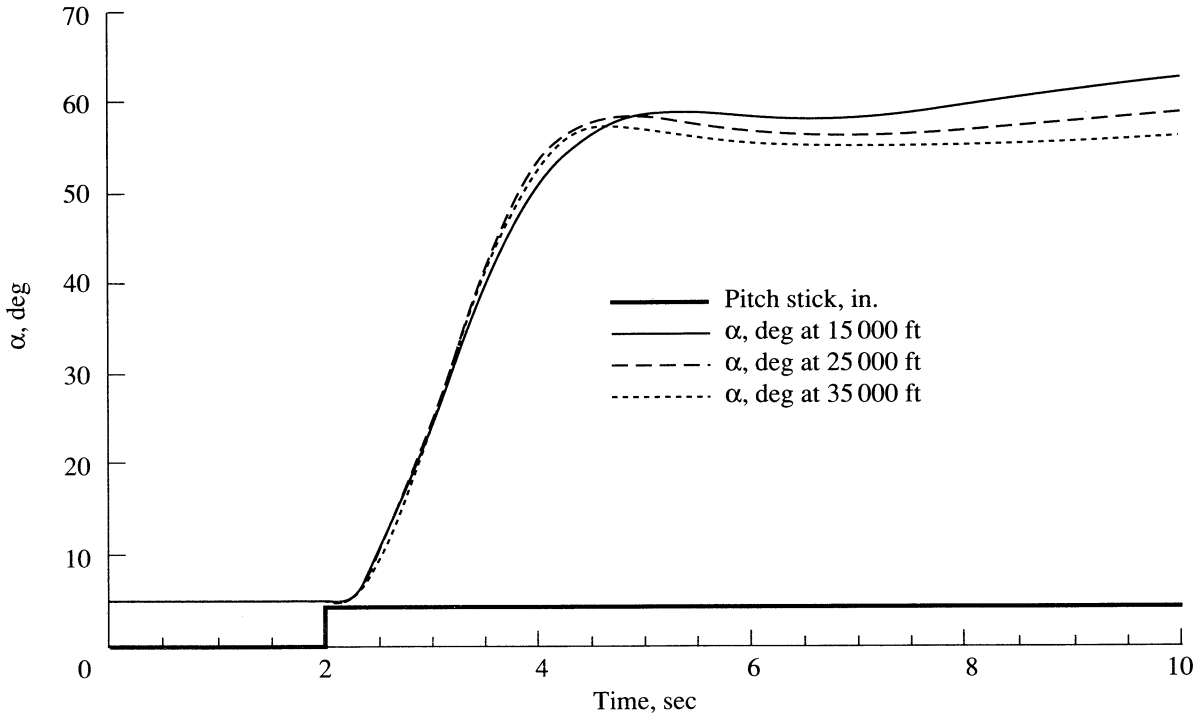


Figure 21. Alpha captures of 5° to 60° for three altitudes.

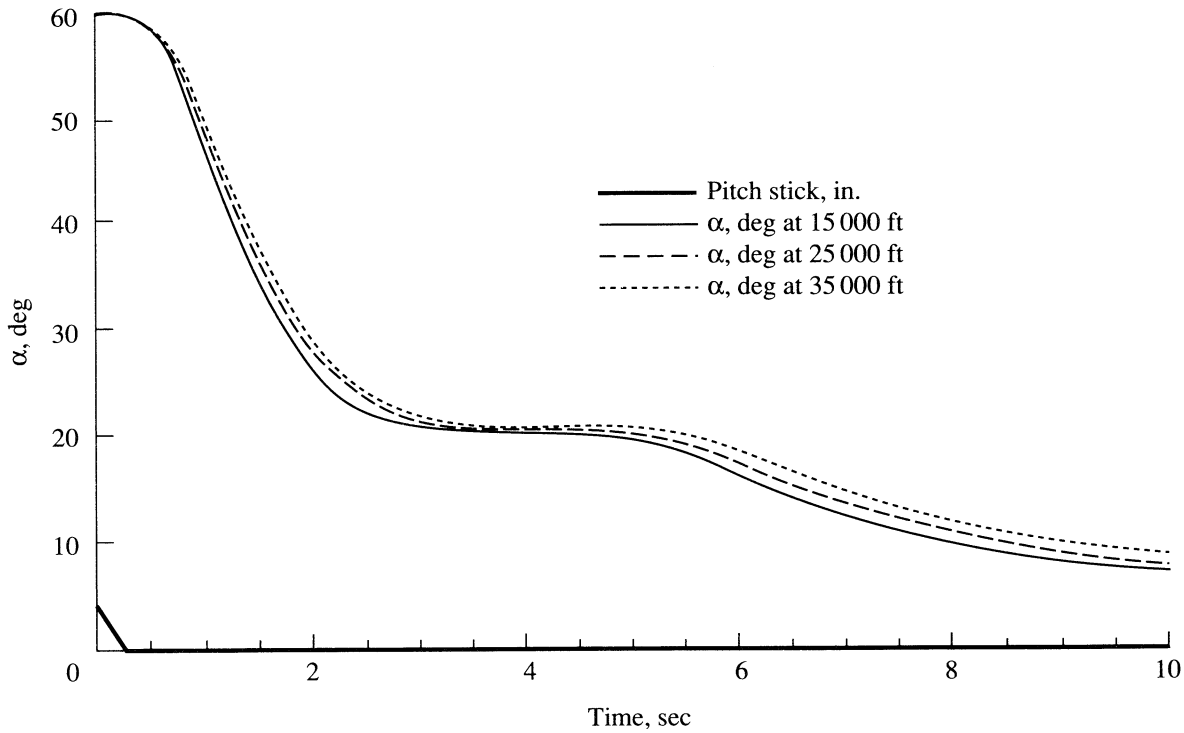


Figure 22. Alpha captures of 60° to 20° for three altitudes.

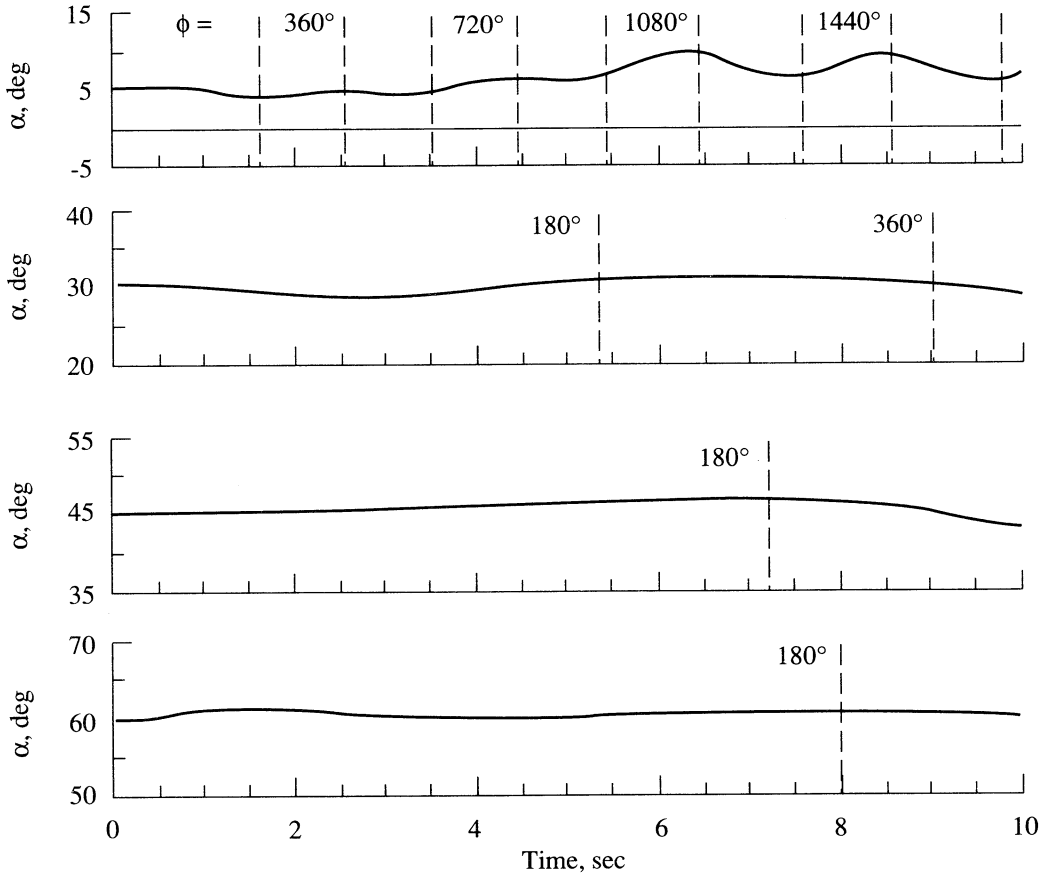


Figure 23. Angle-of-attack regulation for trims of 5°, 30°, 45°, and 60° during full-lateral stick rolls at 25 000 ft.

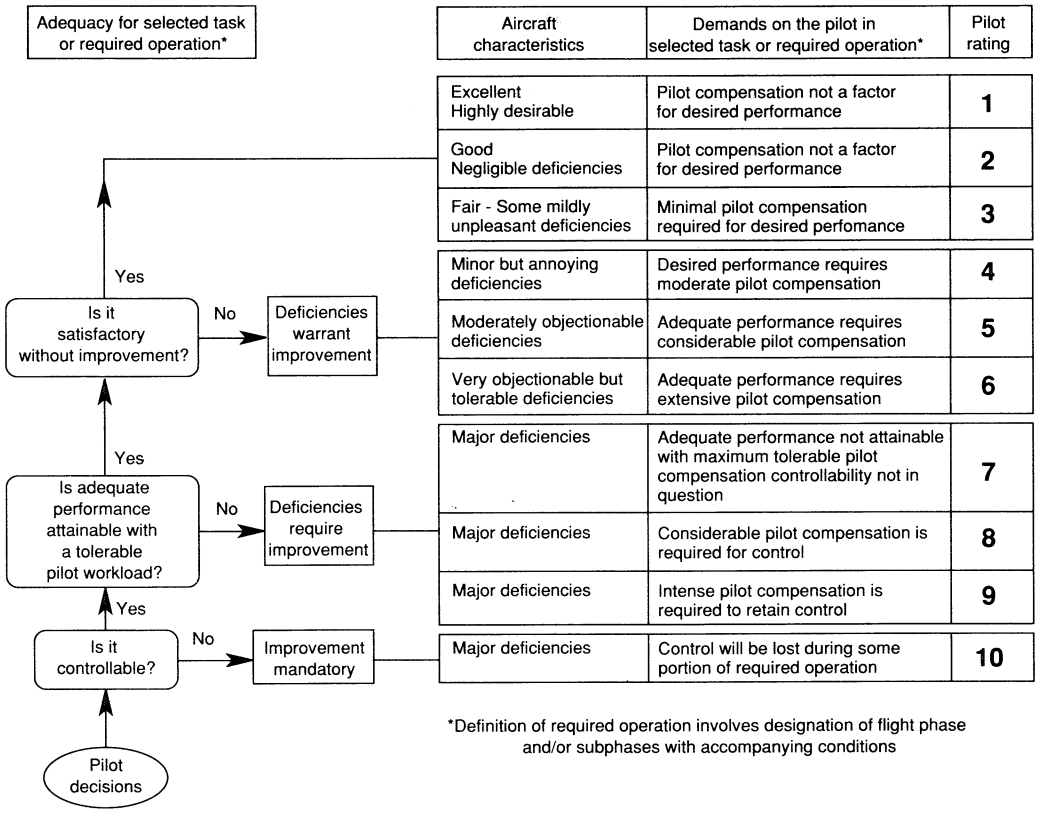


Figure 24. Cooper-Harper handling qualities rating scale (from ref. 24).

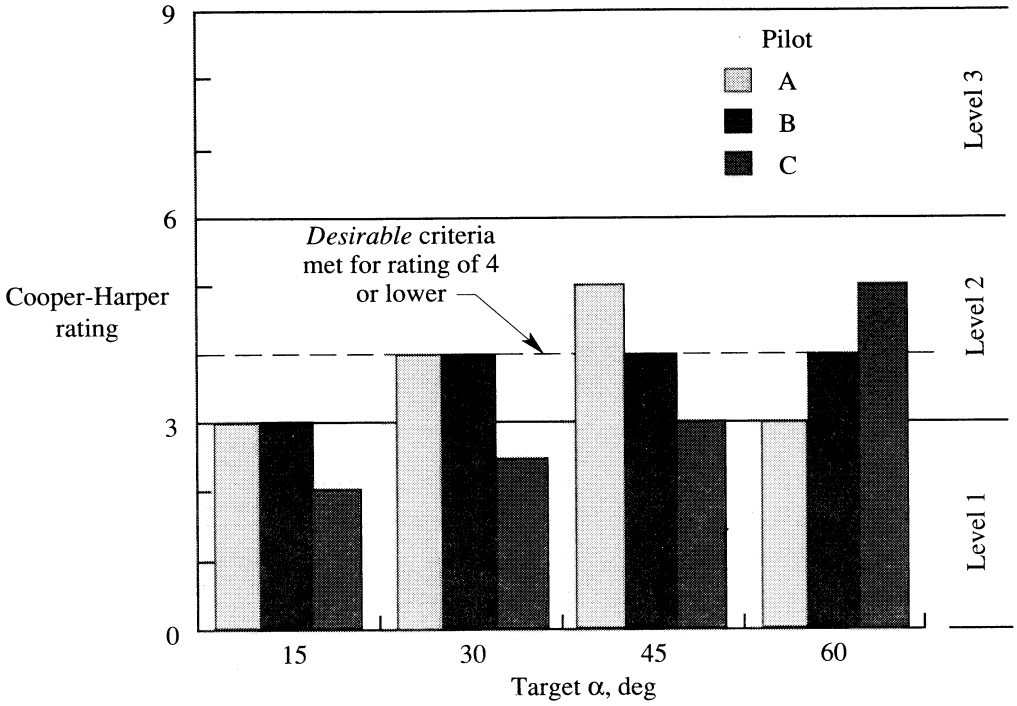


Figure 25. Nose-up angle-of-attack captures from Mach 0.6 at 25 000 ft.

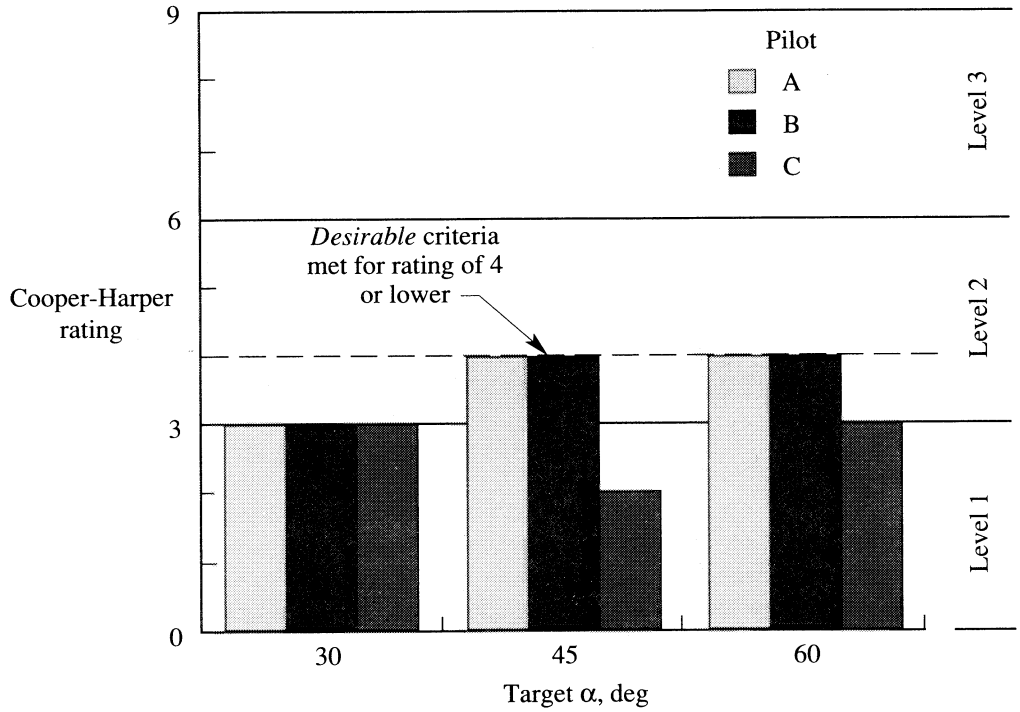


Figure 26. Nose-up angle-of-attack captures from $\alpha = 20°$ at 25 000 ft.

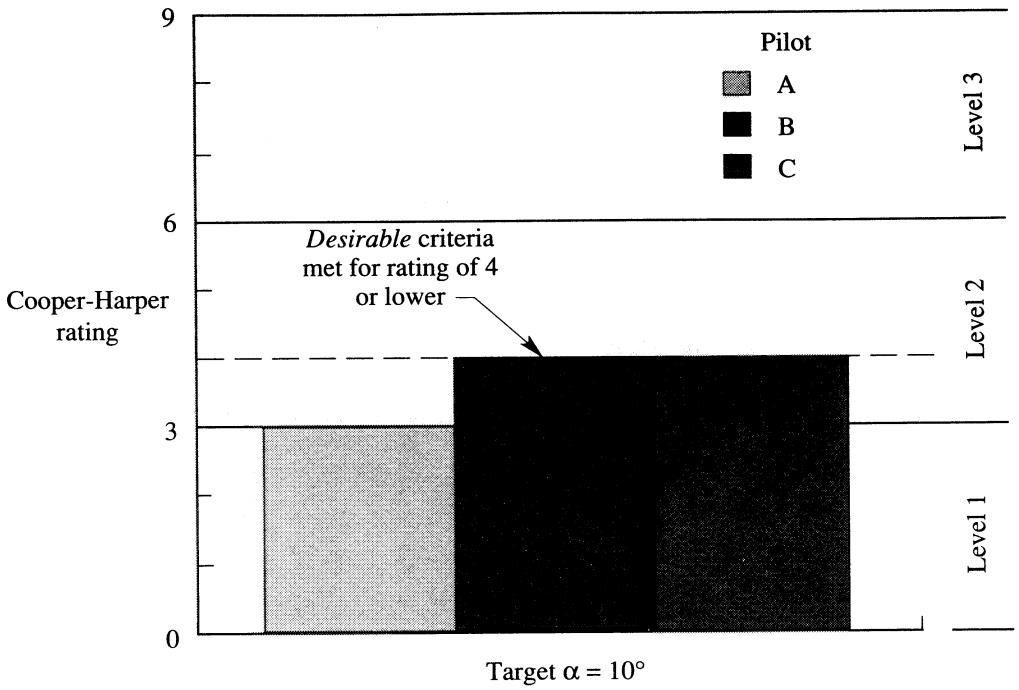


Figure 27. Nose-down angle-of-attack capture from $\alpha = 60°$ at 25 000 ft.

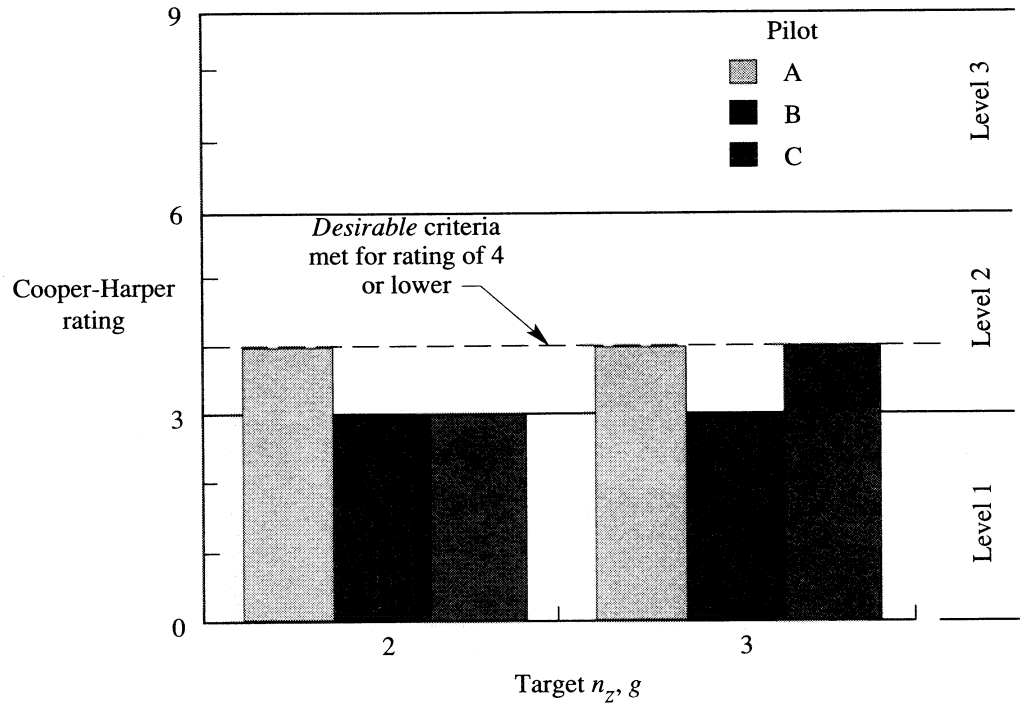


Figure 28. Target $n_z$ capture from Mach 0.6 at 25 000 ft.

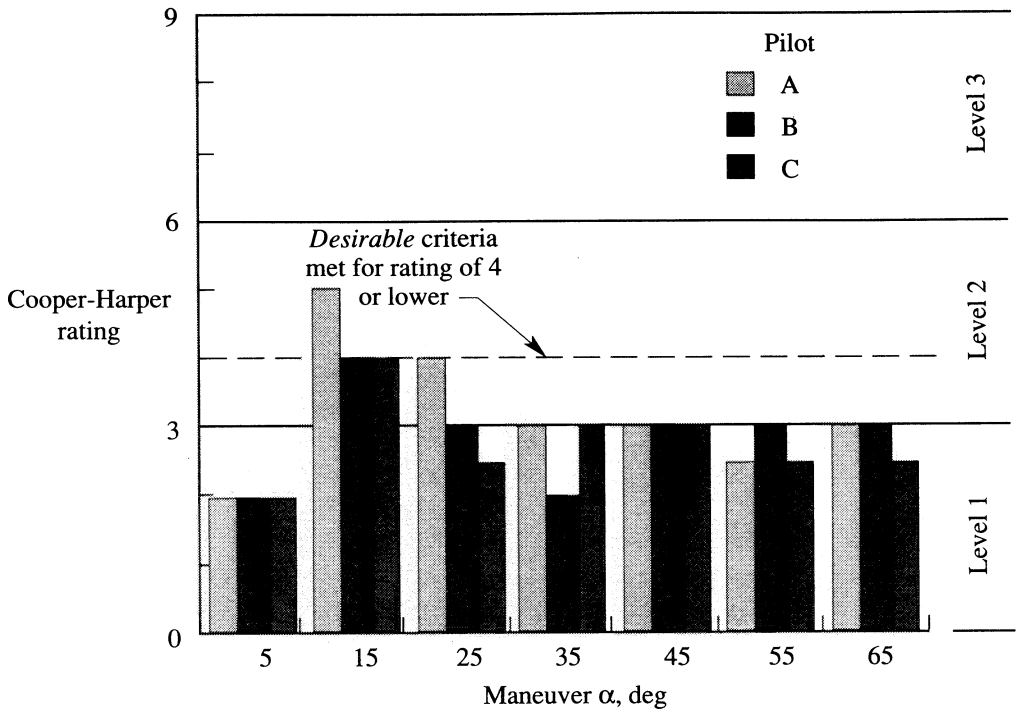


Figure 29. Angle-of-attack regulation during 1$g$ rolls at 25 000 ft.

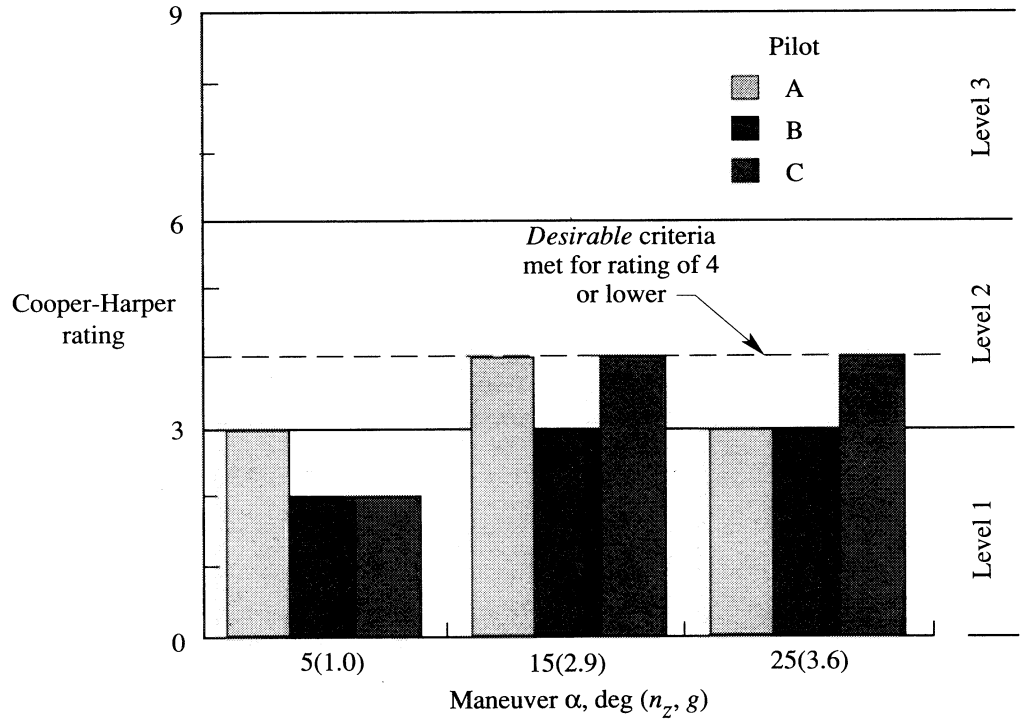


Figure 30. Angle-of-attack regulation during loaded rolls at Mach 0.6 and 25 000 ft.

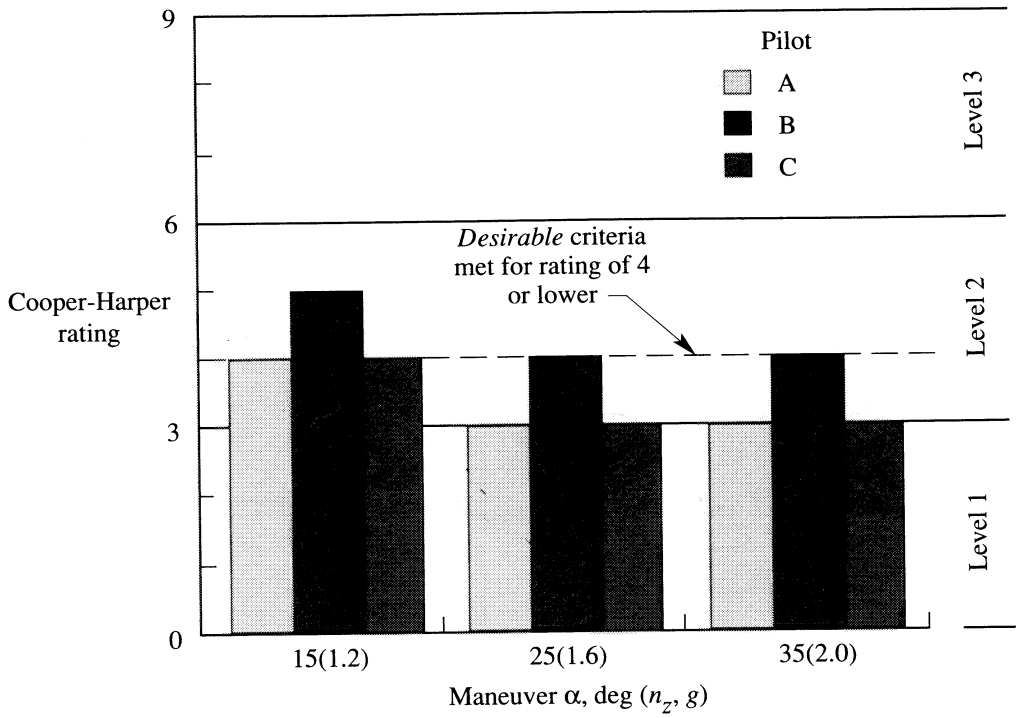


Figure 31. Angle-of-attack regulation during loaded rolls at Mach 0.4 and 25 000 ft.

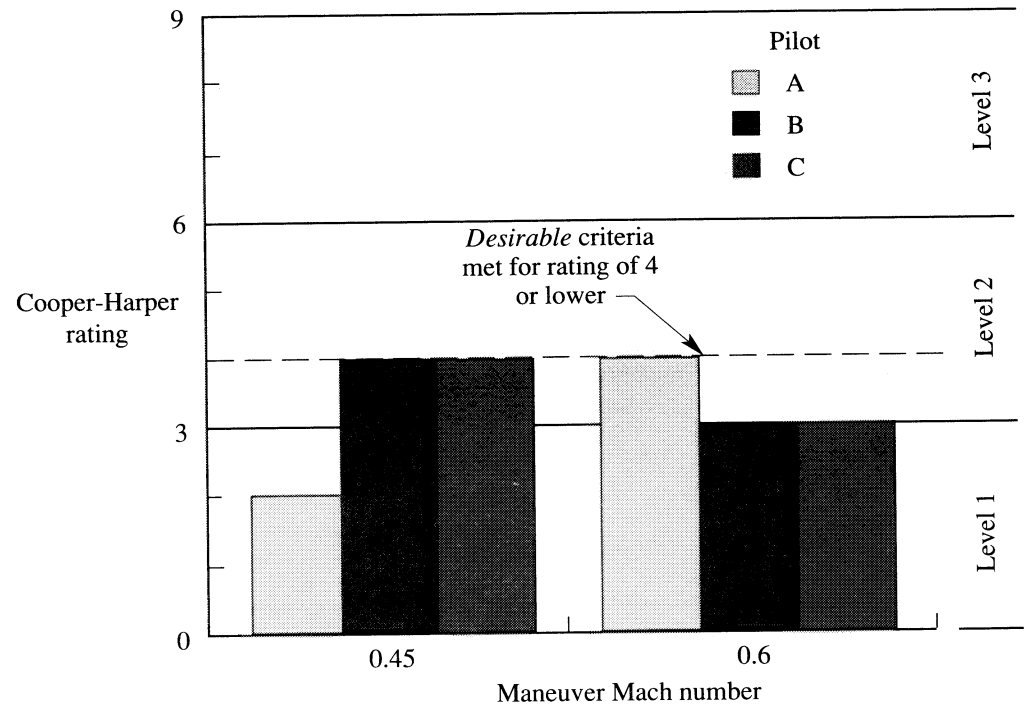


Figure 32. Longitudinal tracking at $3g$ and 25 000 ft.

# REPORT DOCUMENTATION PAGE

*Form Approved*
*OMB No. 0704-0188*



| 1. AGENCY USE ONLY *(Leave blank)* | 2. REPORT DATE | 3. REPORT TYPE AND DATES COVERED |
|---|---|---|
| | July 1994 | Technical Paper |

**4. TITLE AND SUBTITLE**
High-Alpha Research Vehicle (HARV) Longitudinal Controller: Design, Analyses, and Simulation Results

**5. FUNDING NUMBERS**
WU 505-68-30-05

**6. AUTHOR(S)**
Aaron J. Ostroff, Keith D. Hoffler, and Melissa S. Proffitt

**7. PERFORMING ORGANIZATION NAME(S) AND ADDRESS(ES)**
NASA Langley Research Center
Hampton, VA 23681-0001

**8. PERFORMING ORGANIZATION REPORT NUMBER**
L-17323

**9. SPONSORING/MONITORING AGENCY NAME(S) AND ADDRESS(ES)**
National Aeronautics and Space Administration
Washington, DC 20546-0001

**10. SPONSORING/MONITORING AGENCY REPORT NUMBER**
NASA TP-3446

**11. SUPPLEMENTARY NOTES**
Ostroff: Langley Research Center, Hampton, VA; Hoffler: ViGYAN Inc., Hampton, VA; Proffitt: Lockheed Engineering & Sciences Company, Hampton, VA.

**12a. DISTRIBUTION/AVAILABILITY STATEMENT**
Unclassified–Unlimited

Subject Category 08

**12b. DISTRIBUTION CODE**

**13. ABSTRACT** *(Maximum 200 words)*
This paper describes the design, analysis, and nonlinear simulation results (batch and piloted) for a longitudinal controller which is scheduled to be flight-tested on the High-Alpha Research Vehicle (HARV). The HARV is an F-18 airplane modified for and equipped with multiaxis thrust vectoring. The paper includes a description of the facilities, a detailed review of the feedback controller design, linear analysis results of the feedback controller, a description of the feed-forward controller design, nonlinear batch simulation results, and piloted simulation results. Batch simulation results include maximum pitch stick agility responses, angle of attack $\alpha$ captures, and $\alpha$ regulation for full lateral stick rolls at several $\alpha$'s. Piloted simulation results include task descriptions for several types of maneuvers, task guidelines, the corresponding Cooper-Harper ratings from three test pilots, and some pilot comments. The ratings show that *desirable* criteria are achieved for almost all of the piloted simulation tasks.

**14. SUBJECT TERMS**
Longitudinal control; High-$\alpha$; HARV; Variable gain; Feedback control; Feed-forward control; Airplane control

**15. NUMBER OF PAGES**
62

**16. PRICE CODE**
A04

| 17. SECURITY CLASSIFICATION OF REPORT | 18. SECURITY CLASSIFICATION OF THIS PAGE | 19. SECURITY CLASSIFICATION OF ABSTRACT | 20. LIMITATION OF ABSTRACT |
|---|---|---|---|
| Unclassified | Unclassified | Unclassified | |